HOST UNIVERSITY: The University of Queensland, Ghent University

FACULTY: Civil Engineering

Academic Year 2013-2014

Evaluation of the burning behaviour of wood products in the context of structural fire design

Arne Inghelbrecht

Promoters: Prof. José Torero, Prof. Bart Merci

Master thesis submitted in the Erasmus Mundus Study Programme

International Master of Science in Fire Safety Engineering

Disclaimer

This thesis is submitted in partial fulfilment of the requirements for the degree of The International Master of Science in Fire Safety Engineering (IMFSE). This thesis has never been submitted for any degree or examination to any other University/programme. The author(s) declare(s) that this thesis is original work except where stated. This declaration constitutes an assertion that full and accurate references and citations have been included for all material, directly included and indirectly contributing to the thesis. The author(s) gives (give) permission to make this master thesis available for consultation and to copy parts of this master thesis for personal use. In the case of any other use, the limitations of the copyright have to be respected, in particular with regard to the obligation to state expressly the source when quoting results from this master thesis. The thesis supervisor must be informed when data or results are used.

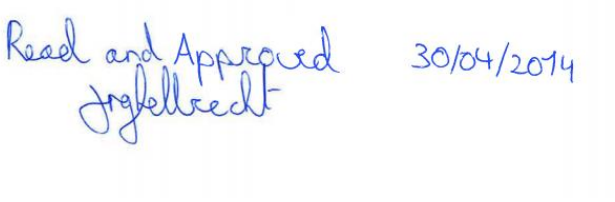

Acknowledgements

Working on my thesis was a great experience, thanks to Professor José Luis Torero for giving me the great opportunity to conduct my thesis at The University of Queensland (UQ). It was a real honour to work with someone so knowledgeable and respected in the Fire Safety Engineering community. Moreover a special thanks to my promoter Professor Bart Merci for all the support, feedback and even bringing a visit down-under.

I also want to thank all the Fire Engineering researchers I have met the last couple of months at UQ. With special thanks to Juan Hidalgo Medina, Rick Emberley, Dr Luis Yerman Martinez, Jeronimo Carrascal Tirado and Dr Dilum Fernando for their technical and academical support.

Also Thanks to Henri Bailleres from the Australian Government *Department of Agriculture, Fisheries and Forestry* (DAFF) for providing the wood test samples. Birgit Ostman (SP), Sven Thelandersson (Lund University) are thanked for providing me with some very helpful literature in the field of structural fire design.

A special thanks to the whole IMFSE board for creating such a wonderful Fire Engineering program. It was an absolute pleasure to have spent a semester at each partner University. IMFSE is a great and unforgettable learning experience, both academically and non-academically.

Thanks to everyone I have met during my travels the last two years, you were all awesome.

Most importantly I would like to thank Anneleen, for keeping up with a boyfriend who travelled almost non-stop the last two years.

Abstract

The possibility of 40+ storey buildings made mostly out of timber is being studied by many structural engineering firms as a sustainable form of tall building construction. However building codes and laws require tall buildings to be made out of non-combustible materials which inevitably force all timber members to be covered by non-combustible materials, mainly plaster boards. This approach takes away the environmental benefit of timber buildings. A framework is introduced in order to demonstrate how an improved understanding of the fire behaviour of timber might lead to an adequate structural design of fire exposed members. A literature review is given in order to demonstrate the discrepancy between common design practice and the state-of-the art. This review beckons the question what happens with structural timber elements near extinction of the contents of a fire. Do the structural elements really sustain burning beyond the combustion of the building contents, as is commonly assumed for structural design? To provide an answer, bench-scale tests are conducted on novel timber products. It is found that for structural applications wood products usually self-extinguish. However specifically for CLT elements ply delamination implies a potential for significant fire contribution and structural failure well before self-extinguishment becomes relevant.

Abstract Nederlands

Hoogbouw tot 40+ verdiepingen voornamelijk bestaande uit hout wordt onderzocht door talloze ingenieursbureaus als een duurzaam alternatief voor klassieke staal en beton hoogbouw. De opkomst van gelamineerde houtproducten zoals Cross Laminated Timber (CLT) zorgen ervoor dat men aanzienlijk hoger kan bouwen met hout. Een enorme beperking voor het structureel ontwerp van dergelijke gebouwen zijn de brandeisen. In de meeste gevallen moet het hout beschermd worden door gipsplaten, wat het duurzame karakter deels wegneemt. In deze thesis is een methode vooropgesteld die demonstreert hoe een beter begrip van het brandgedrag van hout kan leiden tot een efficiënter structureel ontwerp onder brandcondities. Na het uitvoeren van een literatuurstudie i.v.m. het brandgedrag van hout, blijkt dat de huidige structurele ontwerpmethode impliciet aanneemt dat hout onverminderd en constant blijft verkolen gedurende alle fases van een brand. Het is echter niet duidelijk of houten structurele elementen consistent blijven verkolen of uitdoven, wanneer de eigenlijke brandhaard uitdooft. Een reeks bench-scale proeven zijn uitgevoerd om het brandgedrag van gelamineerde houten producten (zoals CLT) nader te onderzoeken. Hieruit blijkt dat hout een zeer goed en positief uitdovingsgedrag vertoont. Anderzijds wordt ook geobserveerd dat het delamineren van de houten elementen een kritisch bezwijkcriterium is dat plaatsvindt aanzienlijk voor uitdoving.

Summary

In the first chapter of this thesis an introduction is given on the structural design for wood buildings, more specifically the structural design for tall wood buildings under fire conditions. First the mechanical properties of wood and novel timber products are discussed. Next a framework is introduced in order to demonstrate how to adequately design structural timber elements for tall buildings under fire conditions. This design method will be referred to as the performance based approach, and is founded upon the criteria that structural elements should be designed so that structural collapse is prevented until full fire burnout. Next the performance based design method is opposed to the standard design method (e.g. *EN 1995-1-2*). By introducing the concept of self-extinguishment within the performance based method, it will be demonstrated that uncovered structural timber elements can potentially be designed much more efficiently than what is common practice. In the context of the performance based framework, two key topics need to be further elaborated before the concept of self-extinguishment can be properly introduced.

The first key topic is to correctly define the imposed heat load onto a structural element during a fire. Chapter two describes the heating conditions in a compartment fire in terms of imposed heat flux and exposure time. Next the heating conditions in a furnace test are discussed, the furnace test is the prescribed test method for achieving standard fire resistance requirements. It will be demonstrated that the heating conditions for a structural wood element in a furnace are very onerous compared the conditions expected in a 'real' compartment fire. The main goal of chapter two is to quantify a bound on the heat flux and coupled expected exposure times for full burnout of a compartment fire.

The second key topic that needs to be further elaborated for the performance based framework, is the heat transfer and burning behaviour of the structural wood element itself. The burning behaviour of wood is further elaborated in chapter three. The burning behaviour of wood is discussed in terms of the general pyrolysis reactions, a simple 1D heat transfer model and a discussion on charring models. The main goal of this chapter is to demonstrate that relatively simple heat transfer mechanisms dominate the burning behaviour of wood and that simple charring models can accurately describe the burning behaviour of wood in the context of structural applications.

In chapter four the topic of self-extinguishment is introduced. From a literature review, evidence will be given that in the absence of external heating wood ceases to char. This self-extinguishment evidence combined with data obtained in the previous chapters enables an experimental setup to be devised. The experimental setup and procedure is elaborately described in chapter four.

Chapter five presents the results and discussion of the experiments. It is basically found that timber elements demonstrate good self-extinguishment behaviour within the tested heat flux and exposure ranges. This evidence can potentially lead to more adequately designed structural timber elements. However delamination of the wood layers also showed to be a major concern and indicate a potential failure mode well before the point self-extinction even becomes relevant.

In order to support some of the statements in this thesis, four documents are added in annex:

- An illustration of the potential advantage of taking into account the extinguishment conditions versus standard fire design is given in annex A.
- Annex B contains a calculation to demonstrate the thermal behaviour of structural timber elements.
- Annex C contains an overview of the main experimental data.
- In annex D the thermal properties of wood at elevated temperatures are discussed.

Nomenclature

A	Pre-exponential factor(s^{-1})
E	Energy (J) or Activation Energy (J/mol)
K	Reaction rate coefficient (s^{-1})
L	Thermal penetration depth (m), characteristic length scale (m)
MC	Moisture content (kg_{water}/kg_{wood})
R	Universal gas constant (J/(mol.K))
T	Temperature (K)
ΔH_p	Heat of pyrolysis (J/kg)
$\dot{m}''$	Mass loss rate (kg/(m^2.s))
$\dot{q}''$	Heat flux (W/m^2)
c_p	Specific heat (J/(kg.K))
h	Heat transfer coefficient (W/(m^2.K))
k	Thermal conductivity (W/(m.K))
l	Mean beam length (m)
m	mass (kg)
t	time (s)
w	Speed (m/s)

Greek symbols

α	Thermal diffusivity (m^2/s)
ϵ	Surface Emmissivity
κ	Absorption coefficient (m^{-1})
ρ	Density (kg/m^3)
σ	Stefan-Boltzmann consant (5.67 10^{-8} W/(m^2.K^4))
ν	Kinematic viscosity (m^2/s)

Subscripts

o	Ambient
c	Convective
e	External

f	Flame or burning
g	Gas
s	Solid, surface
w	Wood or compartment walls

Abbreviations

ABS	Australian Building Code
CLT	Cross Laminated Timber
EC	EuroCode
Glulam	Glued and laminated timber
HF	Heat Flux
IBC	International Building Code
LVL	Laminated Veneer Lumber
MC	Moisture Content
NDS	National Design Standard

Contents

1 Introduction

A century ago around only 20% of people lived in an urban area. Yet a decade ago 40% of people already lived in an urban area, but by 2010 this figure has been estimated to be more than 50%. Moreover the Global Health Observatory forecasts that by 2050 this fraction will even further increase to 70% [1], [2]. In order to accommodate this increase there will be a significant demand for new tall buildings. So building tall will be necessary in order to accommodate the predicted urban growth.

Traditionally steel and concrete are the predominant structural elements in a tall building. Recent building projects such as Tall Timber Tower Research Project[3], Tall Wood [4] Murray Grove [5], demonstrate that the building industry wants to promote wood as a construction material for tall buildings. Structural engineering firms want to push the limits of timber as a material in order to provide a sustainable alternative to concrete and steel. A parameter that is often considered when making statements on the sustainability of buildings is the Embodied Energy (EE). The EE represents the sum of energy needed to go from extraction, harvesting, transporting, to eventually maintaining materials/products in the building. The issue with concrete and steel is that they require lots of energy to produce, so structures built with these materials will embody a high amount of energy. Although discussion might exist on the exact quantification, it is generally accepted that wood buildings are more ecological advantageous than comparable concrete and steel structures [6],[7].

Building codes and fire safety laws require tall buildings to be made out of non-combustible materials which inevitably force all timber members to be covered by non-combustible materials, mainly plaster boards. This approach takes away the environmental benefit of timber buildings. However within the framework of performance based fire codes tall timber buildings well above six stories are becoming a reality. Nonetheless lack of understanding of the fire behaviour of timber still limits the effective use of timber and its full potential as a building material.

The main objective of this chapter is to introduce a framework for the adequate structural fire design of uncovered timber elements for tall buildings. Before presenting the framework in *Section 1.2* a short introduction is given to the structural design of tall wood buildings in *Section 1.1*.

1.1 Structural design for tall timber buildings

In general most structural design codes (North America the IBC, Europe the EC and Australia the ABC) are all based upon the same design procedure. Namely a structural design must be made so that several limit states are met. These limit states represent different events on the building, from extreme weather or fire to normal day use. Any state that may have an effect on costs, safety and environment can be of interest and used as a limit state. The limit states are implemented via load and resistance factor design, so that the effect of the loads on the building must be lower than the resistance of the construction itself [8].

The structural design philosophy is in essence the same for low and tall buildings. Yet, when building taller there are some key effects should be considered [9]. The most logical effect is that the loads (dead-, live-, wind- and seismic-loads) will increase as the height of the building increases. The deadweight and life loads imposed on the structure increase linearly with height, which results in a linear curve for the normal forces. However, the increase of wind loads on tall buildings follows nonlinear behaviour, resulting in a more than linear increase of the lateral loads with height. This way wind loading becomes very important for designing tall buildings.

However besides obvious increased loads, other effects that should be considered are:

- Increased potential for shrinkage and differential movement between building elements
- Extra attention for sound transmission issues
- Increased fire resistance requirements

These effects are applicable to any tall building made out of any material.

The next obvious question is then: why is timber not commonly used for building tall? At first glance the mechanical properties of wood might thought to be low compared to other common building materials like concrete and steel.

Table 1-1 represents an overview of the characteristic mechanical properties of commonly used timber (C24), concrete (C55) and steel (S355) grades.

Table 1-1: Characteristic mechanical properties of common wood (C24), concrete (C55) and steel (S355) grades

	Softwood *C24*	***Concrete*** *C55*	***Steel*** *S355*
Density [kg/m^3]	530	2400	7850
Strength properties [N/mm^2]			
Bending	24	27	(Yield) 355 (Tensile) 470
Tension parallel	14	4.2	
Tension perpendicular	0.5		
Compression parallel	21	55	
Compression perpendicular	2.5		
Stiffness properties [kN/mm^2]			
Mean modulus of elasticity	11	29	200

When looking at the strength properties of wood, it is important to note that wood is especially weak in the direction of the grain[1]. When comparing steel to timber, the strength of timber is in the order of 5-10% of the yield strength of steel, whilst steel is about 20 times stiffer. When comparing wood to concrete on the other hand, it is noticeable that wood is especially strong in tension and achieves about 40% of the compressive strength of concrete, whilst concrete is around 3 times stiffer than wood.

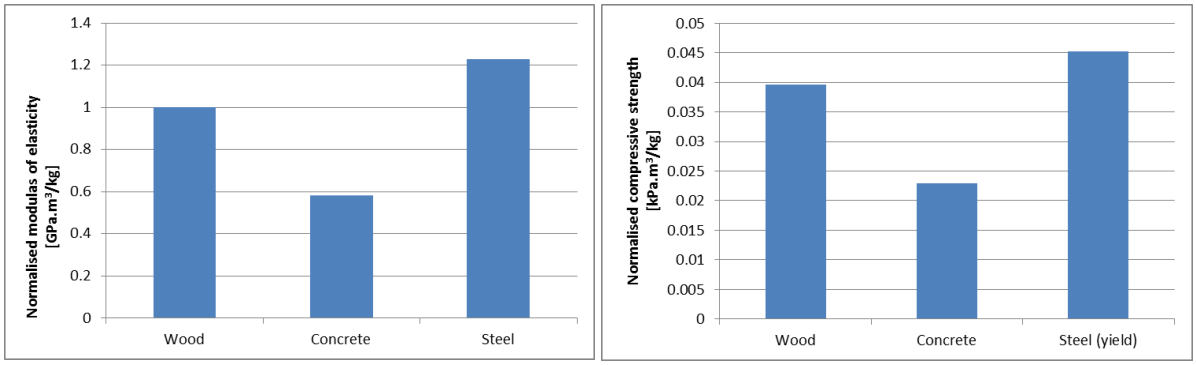

Figure 1: Wood, concrete and steel properties normalised over their density

When considering the density of each material, wood is about 4 times lighter than concrete and 16 times lighter than steel. In *Figure 1* the material properties of *Table 1-1* are expressed in values normalised over the density of the material. From *Figure 1*it can be observed that from a strength over weight perspective, wood is superior to concrete and almost comparable to steel.

[1] For an explanation of the different grain directions in a timber board, see *Figure 2*.

Wood can be a competitive building material to concrete and steel, at least if the design allows for increased member cross sections and also if the loads are distributed in such way that consideration is made of the weaknesses of wood (e.g. the weak behaviour in loading perpendicular to the grain).

Figure 2: Left: Grain directions of wood members; Right: visual failure around local defects of loaded timber elements, both taken from [10]

It is important to remark that in comparison with other common building materials, the properties of wood are not designed according to some fixed procedure. Sawn timber is besides an anisotropic material also a non-homogeneous material and can contain defects such as knots or zones with different grain orientation. These defects can have a deteriorating effect on the mechanical properties of wood (*Figure 2*). Due to the large variability in strength and stiffness of wood the mechanical properties cannot be simply derived from a prototypical clear wood sample. So the material properties of timber vary from piece to piece and even within each piece there are variances. Note that variable material properties within elements is not only an issue for timber, this is true in fact for all building materials. What is characteristic for timber is the relatively large spread on these properties compared to concrete and steel [11].

In order to resolve issues related the inhomogeneity and anisotropy of wood Engineered Wood Products (EWP[2]) were developed. EWP products are typically produced by taking small wood fractions which are bonded together again in order to create a more structurally effective product. A first advantage is that the strength reducing effects of knots and other defects can be neutralised. The second advantage is that the fibres of the wood can be orientated in such way that they provide an orientation that leads to the highest mechanical strength. So structural elements can be designed to be stronger and most importantly have a significantly lower spread on the material properties [10] (see *Figure 3*). Yet, the most important advantage of all is that EWP products allow much greater dimensions to be achieved, resulting in large cross-sections of well-graded and affordable wood.

Three main types of EWP are commonly used in construction, namely LVL, Glulam and CLT (see *Figure 3*).

[2] For future reference in this thesis, EWP products such as CLT and Glulam will be referred to as novel timber products.

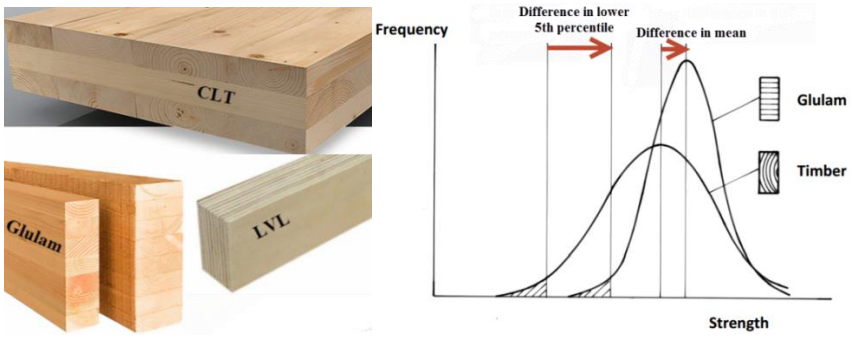

Figure 3: Left: EWP Products CLT, Glulam and LVL; Right: Probability distribution for sawn timber versus an EWP product taken from [10]

CLT is an EWP typically consisting of three to seven or more layers of orientated lumber in which each layer is orientated crosswise. Different types of orientation and a wide range of dimensions are possible. Commonly wall panels are orientated with the grain of the outer layers parallel to the vertical loads. Floor and roof application will have the outer layers parallel to the span or dominant load carrying direction.

LVL stands for Laminated Veneer Lumber and is produced from laminating several thin (usually 2-3mm) wood veneers. Glulam is another type of EWP products with mechanical strength properties similar to LVL. It was found that strength to weight ratios equivalent to steel can be achieved [12]. As opposed to LVL, Glulam is made from bigger pieces of wood.

Clearly products such as CLT provide a structural material that will enable taller buildings to be made due to the possibility of producing large sections of homogenous wood at a relatively cheap price. Recent building projects (e.g. Murray Grove London) demonstrated novel timber products such as CLT allow tall buildings to be made. However further research should be made in order to verify the claims of the EWP timber industry. Also further research is needed in order to provide answers for structural design issues such as timber connections and building stiffness issues [13].

Because of the controlled production process of EWP products, the spread on the material properties of these products is much smaller than the spread of properties on a similarly graded solid wood. This way the characteristic strength values for an EWP product will be relatively higher than the corresponding solid wood product (see *Table 1-2*). As indicated before, the main advantage of EWP products is obviously that large sections of wood can be produced in a well-controlled way at a relatively low cost.

Table 1-2: Comparison of the characteristic strength properties of similarly graded wood (C24) and glulam (GL24H)

Grade	*C24*	*GL24*
Strength properties [N/mm^2]		
Bending	24	24
Tension parallel	14	16.5
Tension perpendicular	0.5	-
Compression parallel	21	24
Compression perpendicular	2.5	-
Stiffness properties [kN/mm^2]		
Mean modulus of elasticity	11	11.6

1.2 Fire resistance requirements

Fire safety concerns are a common factor that seem to drive a distinction between low rise and high rise buildings [14]. Experiences of historic fires, like the Windsor Tower or World Trade Centre, contributed

to the development of specific safety provisions in codes and standards for tall buildings such as the *Society of Fire Protection Engineers (SFPE) Guideline for Very Tall Buildings* [15]. From these guidelines several characteristic fire safety issues for tall buildings are identified:

- The height is potentially beyond what fire department ladders can reach
- Building evacuation might be prolonged due to the evacuation height
- The stack effect might become a pronounced smoke spread phenomena
- Water supply limitations for fire fighting
- Challenges because of mixed occupancy of the building
- Iconic nature

As indicated above the fire safety characteristics for tall buildings are different from low rise buildings but they do not directly discriminate any material. Yet fire safety aspects are the main regulatory limitations of using timber in buildings [16], [13].

These fire regulation restrictions basically exist because timber is classified as a combustible material. Inevitably most building codes force all structural timber members to be covered by non-combustible materials, taking away the environmental benefit.

Now so far it has been established that when one designs strictly according to the prescriptive requirements, a tall building must be made out of non-combustible materials. So in order to achieve compliance, timber elements should be protected by plasterboards but from an environmental point of view this solution is non-desirable.

The next step is to further research what is exactly possible with uncovered timber elements whilst keeping in mind standard design methods. The most obvious way to meet the intent of the code is to simply allow combustible materials to be used in tall buildings and design them according to the standard methods, e.g. *EN1995-1-2* or the NDS.

When a fire design is made according to standard fire resistance calculations, the heat load onto the structural element is basically determined by the furnace used for standard testing. Given the heating conditions imposed on a wooden element in a standard furnace tests, the wood elements chars over the entire exposure time at an almost constant rate. Due to the specific burning and thermal behaviour of wood, the remaining load bearing capacity of the furnace/fire exposed timber element can easily be determined from an effective cross section method.

The effective cross section method indicates that the remaining load bearing capacity of wood can be obtained by reducing the original cross section of wood with charring thickness and a small heat affected compensation layer. In other words, structural wood elements under fire conditions are designed in such way so that a specific section of the wood can be sacrificed to fire. The longer the fire exposure, the bigger the sacrificial cross section will need to be.

The issue with standard requirements for tall buildings is that they demand up to several hours of exposure in the context of tall buildings. As will be quantified in Annex A the original cross section of timber elements must be increased by almost impractical amounts in order to meet tall building requirements for unprotected timber elements.

In order to build tall timber buildings with uncovered timber element, the actual intent or physical criteria behind the regulatory requirements must be understood.

Frangi et al. [13] give an extensive overview of the main fire design issues for tall buildings. It is commonly suggested that fire safety design for tall buildings should be based on the scenario that occupants located in the upper part of the building cannot leave the building [15] (see *Table 1-3*)

Table 1-3: Main differences in fire design for high versus low-rise buildings, reproduced from [13]

Height of building	**Evacuation during fire event**	**Fire spread to other parts of the building**	**Collapse**
Low and medium-rise	Feasible	Accepted after defined period of time	Accepted after defined period of time
High-rise	Might require to stay in a safe place until fire burn-out	Not acceptable	Not acceptable

This way it is critical to design building elements for tall buildings respecting following guidelines:

- Separating building elements should be designed in a way to allow full burnout, thus preventing uncontrolled fire spread to other parts of the building during the complete fire event
- Load-bearing building elements should be designed in a way to prevent structural collapse for a full burnout without any fire brigade intervention.

So if a structural fire design is conducted for tall buildings, the main physical characteristics imposed on the design are preventing fire spread and collapse until full-burnout of the compartment fire. In other words, a load-bearing element is adequately designed if it can withstand a complete fire till burnout without causing collapse.

Above performance criteria basically represent how failure or success of a design is identified. The next logical step of structural fire design is to provide a calculation mechanism by which the fire resistance be checked. In *Figure 4* a framework is presented for the Performance-based fire resistance calculation of a structural timber element. The flowchart in the middle of the figure illustrates the general steps that should be adopted during a fire resistance calculation from the design fire to the structural model, as described by *Buchanan* [17]. Basically following three simple steps, the structural fire resistance of a structural element can be calculated:

- A design fire must be selected depending on the fire design application. From a design fire the heat load imposed onto the structural elements inside the fire compartment can be calculated. This topic will be elaborately discussed in chapter two.
- Once the heat load onto the structural element is known, it must be understood how the structural element behaves under this heat load. In other words the heat transfer through the material must be understood. Note that for example in the case of a combustible material like wood, the element will combust under a certain amount of external heating. So in order to make a sound heat transfer calculation also the complex burning behaviour of the material itself must be understood. This topic will be discussed in detail in chapter three.
- When it is established how the element is heated, considering the thermo-mechanical properties of the heated element, the load bearing capacity under fire conditions can be calculated.

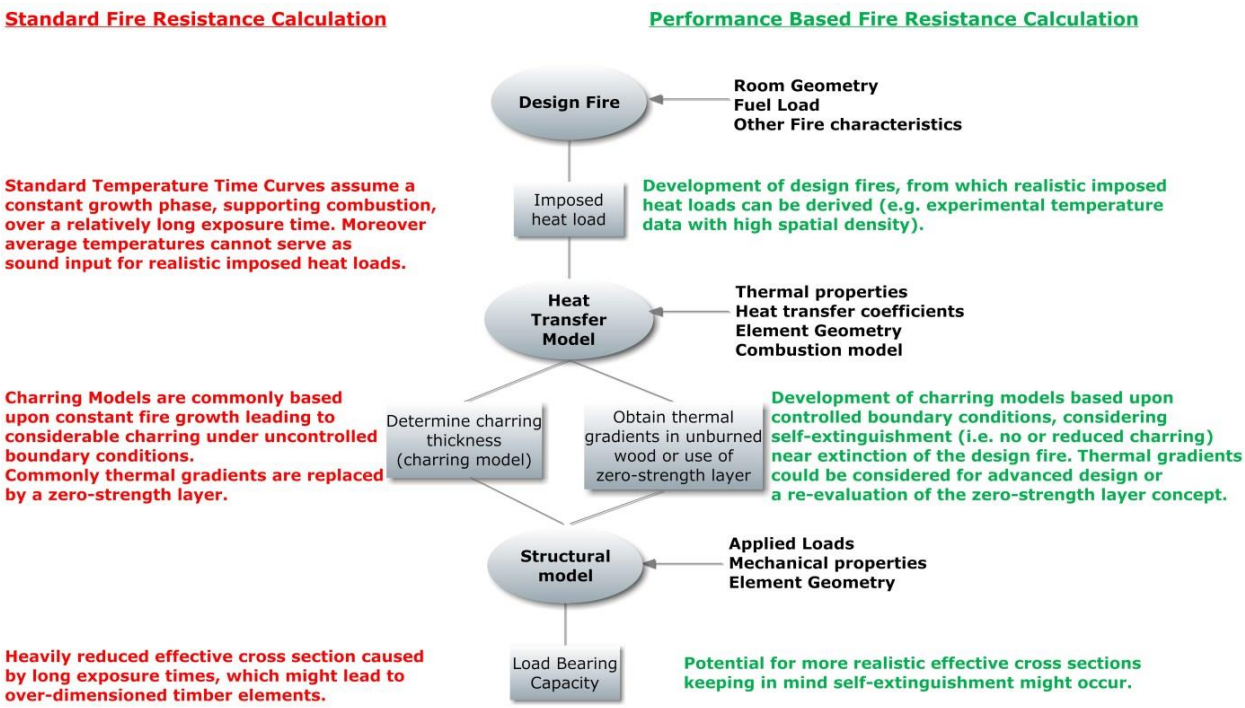

Figure 4: Framework for the adequate fire resistance design of a structural timber element

At the right hand side of the flowchart in *Figure 4*, comments are presented in order to demonstrate how a sound application of all steps in the flow chart will lead to an adequate structural design compared to the standard method.

As is indicated on the left side of *Figure 4* the standard method of calculating the fire resistance of unprotected timber elements becomes inadequate for tall buildings.

The goal of chapter two is to demonstrate what heat loads are expected during full-burn out of a compartment fire. It will be demonstrated that unlike furnace tests, compartment fires tend to extinguish within relatively short time-frames compared the ones demanded for standard fire resistance ratings. In other words the standard fire resistance requirements do not make much physical sense in respect to the timescales associated to full burnout.

The burning and heat transfer behaviour of wood is elaborately discussed in chapter three.

In the context of heat transfer and charring of wood the discrepancies between realistic conditions and the ones required for standard design, beckon a very important question in the context of structural design: What exactly happens with the timber elements, near extinction of the contents of the compartment fire, do the elements continue to burn or do they simply self-extinguish?

The concept of self-extinguishment is introduced in chapter four. In order to research the topic of self-extinguishment and further study the burning behaviour of wood experimental bench-scale tests are conducted.

Note that the third step of the framework, namely the structural models will not be further elaborated in this thesis. However, it cannot be stressed enough that the topic of self-extinction is very relevant in the

context of structural applications. As can be seen from *Figure 4*, taking into account self-extinction means charring would cease within the relatively[3] small time scales associated to compartment burn-out. If charring does not sustain for a long time, also the associated sacrificial wood section will be relatively small. Thus if the concept of self-extinction is valid, it is expected that wood elements designed for relatively long standard exposure times are seriously over-dimensioned for what is adequate to meet the performance criteria of preventing structural collapse or fire spread until full burnout.

[3] With relatively small timescales, indicating small compared to the exposure times demanded by standard requirements.

2 Imposed heat load

As per the framework (*Figure 4*) introduced in the *Introduction*, this chapter aims at defining the imposed heat load onto a structural element.

The objective of this chapter is to quantify the evolution of the external heat load imposed onto a structural element during a 'real' compartment fire until burnout (*Section 2.1)*. For further reference the imposed heat load in a standard furnace test is briefly discussed in *Section 2.2*.

2.1 Imposed heat load during a compartment fire

The external heat flux ($\dot{q}_e^{"}$) onto a structural element during a fire can be quantified as:

$$\dot{q}_e^{"} = \dot{q}_{cf}^{"} + \dot{q}_g^{"} + \dot{q}_w^{"} + \dot{q}_c^{"} \qquad \textbf{Equation 2-1}$$

With: $\dot{q}_{cf}^{"}$ the radiative heat flux from the compartment fire, $\dot{q}_g^{"}$ the radiative heat flux from the hot smoke gases, $\dot{q}_w^{"}$ the radiative heat flux from the compartment walls and $\dot{q}_c^{"}$ the convective terms.

An elaborate discussion of these heat transfer terms in their full complexity is given by *Jowsey* [18].

In *Section 2.1.1* the convective term ($\dot{q}_c^{"}$) is quantified, in *Section 2.1.2* the radiative terms ($\dot{q}_{cf}^{"}, \dot{q}_g^{"}, \dot{q}_w^{"}$) are further discussed.

2.1.1 Convective terms

Basically convection refers to the energy transfer due to bulk motion, for example air flowing over a solid surface. The air might be moving by itself, in which case the convection occurs naturally or freely, for example the movement of hot gases in a fire. Convection might also be driven by an external source, referred to as forced convection.

Generally the convective heat flux is expressed as:

$$\dot{q}_{conv}^{"} = h_c(T - T_s) \qquad \textbf{Equation 2-2}$$

The term h_c is the convective heat transfer coefficient and is basically defined by type of flow field. The convection towards an object in a fire compartment is known to occur under natural convection conditions and is pretty much constant during the fire [19]. Since the flow conditions are turbulent natural convection, the Nusselt number can be used to approximate the convective heat transfer coefficient. Furthermore for a simple flat slab orientation under natural convection the Nusselt number can be related to the Rayleigh number [19]:

$$Nu = \frac{h_c L}{k} \approx 0.13 Ra^{1/3} \qquad \textbf{Equation 2-3}$$

$$Ra = \frac{g(T - T_0)l^3}{T\nu^2} Pr \qquad \textbf{Equation 2-4}$$

$$Pr = \frac{\upsilon}{\alpha} = \frac{\rho c \upsilon}{k} \qquad \textbf{Equation 2-5}$$

Through *Equations 2-3 to 2-5* the underlying parameters affecting the convective heat transfer are exposed. Three parameters are of importance, namely the gas properties, the gas velocity and the characteristic length scale. Note that the gas properties in its turn are all temperature dependent properties. Yet it is found that at temperatures in excess of 20°C there is very little temperature dependence. The Prandtl number has a bound of 0.71 to 0.68 in the range of 300 to 1000 k, therefore it is commonly taken to be 0.7 for combustion gases [19].

Jowsey [18]demonstrated the influence of the length scale on h_c and noted that for length scales smaller than 0.1m there is a significant effect increase in the convective coefficient. For length scales beyond 0.1m h_c stagnates. Considering the properties of air in the range of 300-100 k and relative large length scales the Nusselt number gives h_c values in the order of 25W/(m^2.K) for simple plate geometries. This heat transfer coefficient value is also in line with the prescribed value by *EN1991-1-2* [20].

Experimentally it has been demonstrated that in compartment fires h_c values are in the order of 10 W/(m^2.K) up to 40 W/(m^2.K) [21]. These heat transfer coefficients are also in line with [22] which showed that for fully developed fire experiments the convective heat flux accounted for approximately 25% of the total heat flux. In both of these experiments the prescribed h_c value of 25 W/(m^2.K) was found to be on the low side of the spectrum. These higher convective heat flux values were attributed due to high local velocities disturbing the flow field.

Clearly using a fixed convective heat transfer coefficient for fire design should be handled with care and the quantification should depend on the exact application. Convection heat transfer is commonly downplayed in structural fire design applications. Ignoring the convective terms can only be justified if radiation dominates the burning, the length scales are well beyond 1 m and if the occurring velocities are relatively low. However convective heat transfer should especially be evaluated in following cases:

- Fully developed fires where high velocities can be expected (i.e. forced flows, or non-uniform temperature fields with high velocity peaks).
- Scaling effects around length scales smaller than 0.1m (e.g. small beams or around flanges).

In order to address the variety of h_c in terms of lengths scale and velocity *Jowsey* [18] created a convective heat flux coefficient bound (*Figure 5*) for simple plate geometries.

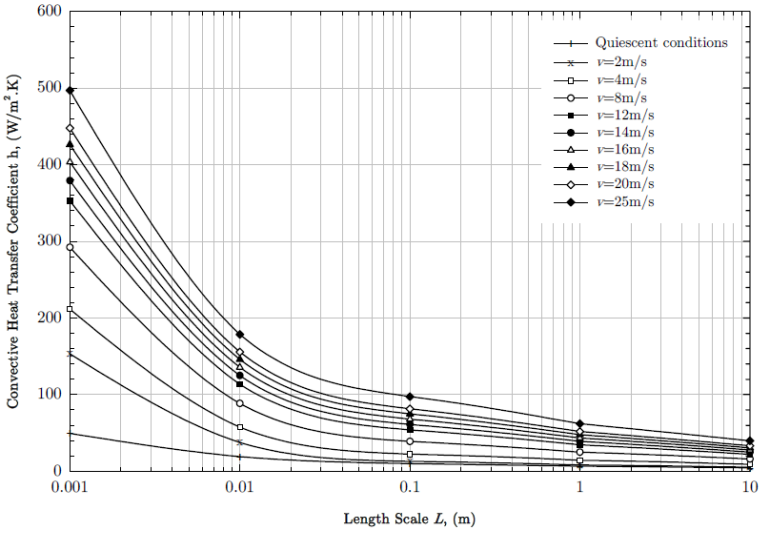

Figure 5: h_c as function of length-scale and velocity, taken from [23, p. 120]

2.1.2 Radiative terms

In compartment fires, radiation is often considered to be the dominant mode of heat transfer. The principles behind radiation are a topic in its own, a very complete overview of the full complexity of this

mode of heat transfer can be found in [24]. Only the main concepts related to radiation encountered in compartment fires will be discussed here.

As any flux for that matter, the radiative heat flux is a directional property. So in essence a radiative heat flux can only be quantified when a clear relationship between sender and receiver is known. Moreover radiative heat transfer occurs at different wavelengths, so a bound of wavelengths should also be quantified. However for fire engineering applications one is interested in a very wide range of objects and emitted wavelengths. Therefore the concept of emissive power is often used. The total emissive power is the summation of the emitted power at all possible wavelengths and in all possible directions:

$$E = \varepsilon\sigma T^4 \qquad \textbf{Equation 2-6}$$

In simplified form the radiant heat transfer on a surface from a remote emitter can then found by the use of the so called configuration factor ϕ which takes into account the directionality:

$$\dot{q}''_{rad} = E\phi = \varepsilon\sigma T^4\phi \qquad \textbf{Equation 2-7}$$

From *Equation 2-7* it can be seen that radiative heat transfer is highly temperature dependent (T^4). Moreover also the emissivity of the radiating object is a function of the temperature $\varepsilon(T)$. In other words correctly defining the temperatures in a fire compartment is crucial in order to quantify the radiative heat flux.

Within the flame and smoke regions such as encountered at the fully developed stage of the fire, a grey gas approximation is commonly made [19]. In current design practice the radiation between the fire and the structural elements is often approximated by a lumped one-dimensional model. As the density of the smoke increases the emissivity of the smoke will also increase. The absorption coefficient of the smoke can consequently be coupled to the emissivity:

$$\varepsilon_g = 1 - e^{-\kappa l} \qquad \textbf{Equation 2-8}$$

The mean beam length l is considered to be the thickness of the smoke layer. The absorption coefficient is found to be dependent on the wavelength and soot volume fraction:

$$\kappa = Cf_vT_g \qquad \textbf{Equation 2-9}$$

With: C a constant and f_v the soot volume fraction

Furthermore the radiation can be determined by a local gas conditions if the atmosphere around this element can be considered as optically thick. The product of a given path length l and the absorption coefficient is indicative for the optical thickness [23]:

$$\kappa l \gg 1 \; Optically\ thick$$

$$\kappa l \ll 1 \; Optically\ thin$$

So the smoke conditions during a fully developed fire can be linked to an absorption coefficient, for example a reasonable approximation of the absorption coefficient for fully developed fire is $\kappa = 1m^{-1}$[19]. Because of the high absorptivity of the smoke, the exact radiative inputs from the compartment fire ($\dot{q}''_f$) or the other walls($\dot{q}''_w$) are absorbed by the smoke. Thus exactly quantifying the other radiative contributions than $\dot{q}''_g$ becomes of secondary importance in relationship to structural design in fully developed fires.

Qualitatively the radiative heat flux can now be linked to the different stages of fire growth:

- Growth phase: Low radiative heat flux, which will quickly grow as the smoke layer builds and the temperature and absorption/emissivity of the smoke layer increases. This increase will be quick given the low thermal inertia of the gases.
- Fully developed phase: maximum stable temperatures are achieved and the compartment is fully filled with dense smoke ($\varepsilon_g \approx 1$). The radiative heat fluxes are expected to peak and remain stable during the fully developed phase.
- Cooling phase: Smoke temperatures and densities drop as the gases cool, quickly ε_g drops. However the heat flux will gradually drop because of internal re-radiation of the heated compartment.

In order to quantify the radiative heat flux and link it the local gas conditions, some important assumptions are commonly made in structural fire design [25],[20]:

1. There is no radiative exchange between the soot particles and the gas, in other words the smoke is considered as one entity. By making this assumption the gas temperatures can be used to establish the radiative heat fluxes.
2. The smoke in the compartment is considered as an optically dense layer compared to the compartment geometry. Thus radiation is treated as a local phenomenon.
3. The compartment fire temperature is homogeneous, so the temperature time curve is a valid representation of the smoke temperature.

T_g is consequently coupled to the temperature time curve. The total radiative power emitted to the structural element is then expressed as:

$$E = \varepsilon_g \sigma T_g^4 = (1 - e^{-\kappa x_g}) \sigma T_g^4 \approx \sigma T_g^4 \qquad \textbf{Equation 2-10}$$

With T_g commonly assumed to be prescribed by a temperature time curve describing an average compartment temperature. However up to this date no sound experimental data supports the homogenous temperature assumption, at least not for structural design purposes [26],[27], [28]. During well-instrumented full scale fire tests, the temperatures are found to be not homogenous at all [29]. Especially considering that the temperature dependence is to the power of four when calculating the radiative heat flux, the discussion on non-uniform temperatures becomes very critical.

2.1.3 Total external heat flux

From the previous sections it has been demonstrated that:

- Because of the turbulent nature of compartment fires consideration should be made of the spatial and temporal variability of temperatures. Radiative heat transfer is a highly temperature dependent phenomena thus temperature heterogeneity should be taken into account.
- Consideration should be made of the length scales of the considered structural element and the possibility of high flow fields around it, in order to correctly address the convective heat transfer terms.

For the purpose of structural fire design a well-established method is relating a temperature time curve to the opening factor and fuel load of a building. The methodology is based on solving an energy balance for the compartment fire in order to create a temperature time curve related to the compartment geometry and fuel load. Keeping in mind this method results in a single curve that represents a single homogenous compartment temperature, it becomes apparent from the above discussion that these curves simply cannot serve as sound input for radiation calculations. In order to have an idea of the imposed heat flux and relevant time scales during 'real' fires, one must resort to high spatial density heat flux or temperature measurements. Test data from two fire tests will be used for this purpose, namely the Dalmarnock fire tests and the Cardington fire tests. Data from a number of full scale natural fire tests will be used to bound the time scales associated to full compartment burnout.

The Dalmarnock fire tests were conducted in a high-rise building in the UK [30]. These tests were conducted by the BRE Centre for Fire Safety Engineering and the University of Edinburgh in 2006. The goal of the test was to recreate a realistic residential/office fire scenario and collect a comprehensive dataset in order to use the data for validation purposes. More specifically '*Post-Flashover Fire Test* One' is selected, simply because the second test was manually suppressed before flashover.

The total heat fluxes at the rear wall (*Figure 6*) and the ceiling (*Figure 7*) of the compartment were determined. The results represent the total external heat flux, thus take account of both radiation and convective terms.

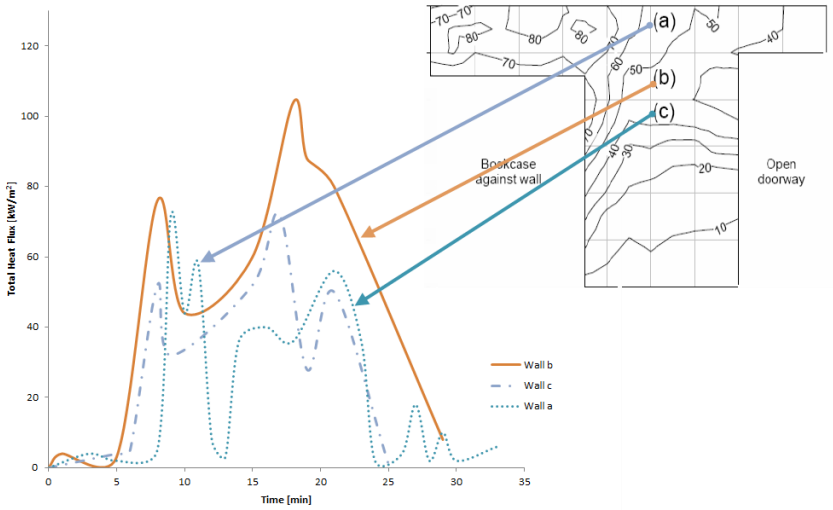

Figure 6: Total Heat Flux History at the Rear Wall (Dalmarnock Fire Tests) [23]

The total average heat flux at the ceiling (averaged from time to ignition till fire brigade intervention including all 20 heat flux sensors) is found to be 41 kW/m^2.

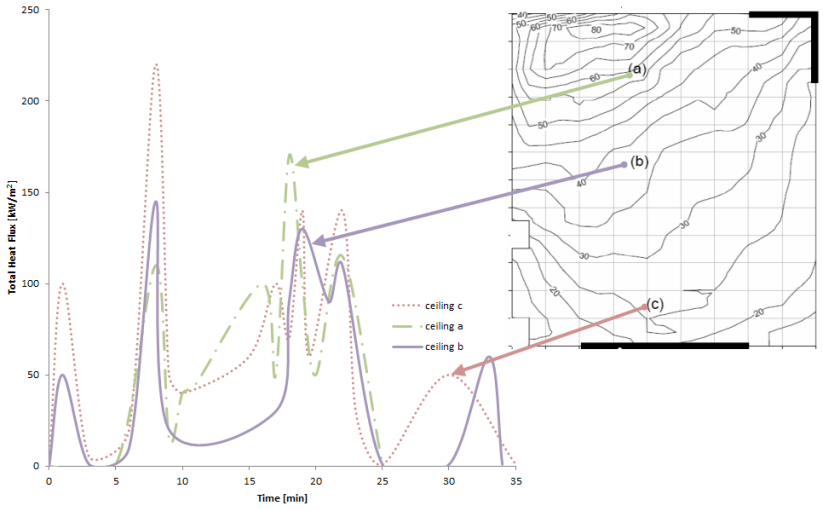

Figure 7: Total Heat Flux History at the Ceiling (Dalmarnock Fire Tests)[23]

The total average heat flux at the ceiling (averaged from time to ignition till fire brigade intervention including all 9 heat flux sensors) is found to be 46 kW/m^2.

Although the Dalmarnock fire tests were manually extinguished, the tests were finished only shortly before full burn-out of the compartment contents. Therefore a representative burnout exposure time of roughly 20 to 30 minutes can be coupled to these tests.

An overview of the expected heat flux levels in the Dalmarnock tests, considering all heat flux sensors, is given in *Figure 8*. Moreover in Figure 8 a bound is placed on the expected heat fluxes in a compartment fire, more specifically three average bounds are used: a peak or high bound corresponding to 80kW/m^2, an average bound corresponding to 44kW/m^2 and a low bound corresponding to 30kW/m^2.

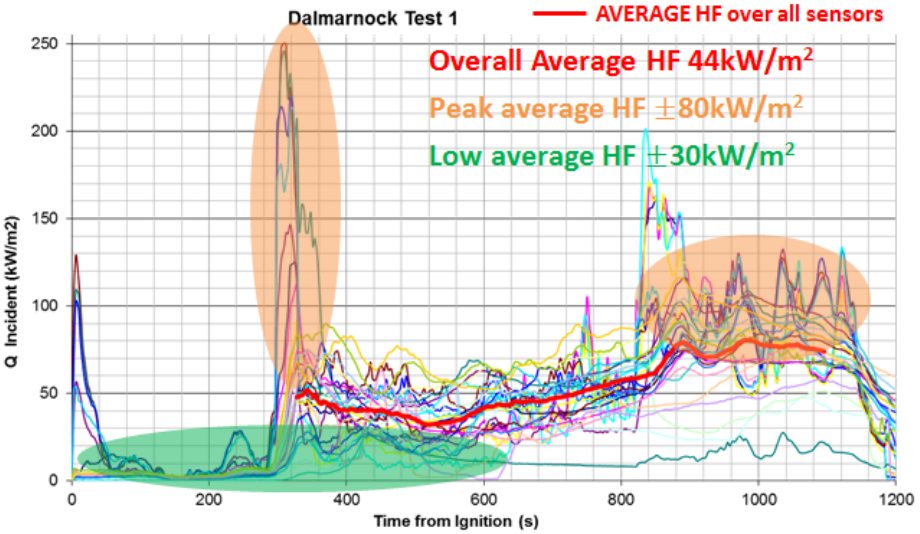

Figure 8: Average Heat Flux History over all heat flux sensors (Dalmarnock Fire Test 1)

The second data set is based upon the Cardington fire tests. These tests were a series of large scale fire tests conducted in a steel-framed structure. The tests were also conducted by the BRE Centre for Fire Safety Engineering. In the test data presented in *Figure 9,* billets 5 to 6 represent the ceiling heat fluxes and billets 7 to 8 the wall heat fluxes. The data presented includes both radiation and convection terms. Note that the heat flux bound for the Cardington tests is significantly higher than for the Dalmarnock tests. It must be understood that the measurement density in the Cardington tests was a lot lower and the locations were more biased towards the upper layer of the compartment. Moreover the Dalmarnock test were conducted using a realistic fuel load for an office, whilst the Cardington tests were using a relatively high fuel load that was ignited all at once (no fire spread). This way the Dalmarnock data can be considered to represent a realistic bound, whilst the Cardington data can be considered as an upper bound.

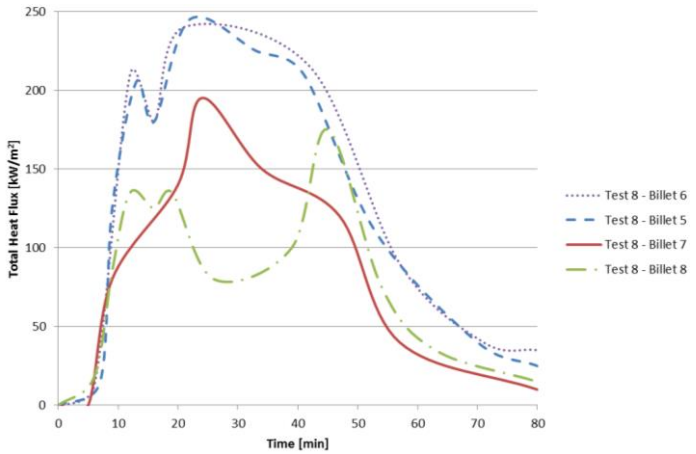

Figure 9: Total Heat Flux Cardington Fire Tests [18]

A summary of expected exposure times for a full burnout scenario are given in *Table 2-1*. Note that these time scales are not intended to represent accurate times, but just serve as rough approximations made after consulting data of several full scale fire tests.

Table 2-1: Summary of the relevant time scales associated to full compartment burnout fire scenarios

Bound	Design Fire Scenario	Expected time duration	Data obtained from:
Lower	Relatively rapid sprinkler activation, resulting in almost no fire spread.	±10 min	Full scale CLT compartment [31]
	Full burnout of a single item (e.g. sofa),so no significant fire spread due to spacing of items, sprinkler activation, etc.		Upholstered furniture room fires, ISO room [32]
Average /Realistic	Expected fire burnout for average fire load motel/hotel room fire.	20 to 30 min	Representative hotel room [33]
	Expected near fire burnout for office configuration.		Dalmarnock fire tests, as discussed before
Upper	Burnout wood crib fires representing bedroom configurations with high fire load density.	+60 min	Full scale 3 storey XLam building [34]
	Wood crib fires for large compartment fires with high fuel loads		Fire test conducted in large steel structures [35]

2.2 Furnace test

In this section the heat transfer to a structural element in the standard furnace test is discussed. The standard furnace test is the prescribed test method to determine the standard fire resistance rating of an element.

The standard furnace test has been around for almost a century since it was first introduced in 1916 [25]. So far the basic concept has largely remained unchanged for all these years. However throughout many years of research and despite major advances in the fire safety science field the test method is seriously questioned [36], [37], [38]. A fundamental issue with the standard fire resistance test is the poor repeatability which is caused by the inability to quantify the thermal loading on the test element. The key control parameter in a furnace test is the fire curve, which only dictates the gas temperature inside the furnace. However the received thermal loading on an exposed element is dependent on many other factors that are not prescribed in the test method, hence the inability to quantify the thermal loading correctly. Other influencing parameters on this thermal load are the characteristics and conditions of the furnace and most importantly the thermal properties of the test subject itself.

Attention should be given to the convective heat flux, especially considering scaling effects, as the convective heat flux increases as the characteristic length scales decrease. Depending on the scale and type of heater the convective heat flux can become an essential part of the heat transfer in a furnace.

As in the compartment fire, the radiative component is generally the dominant form of heat transfer in the full-scale standard furnace [39]. However the quantification and evolution of the radiative heat flux is where the large difference lies between compartment and furnace fires.

In the compartment fire case the radiative heat flux can be coupled to a local gas phase condition. This connection is possible because the hot gases in the compartment are considered to be optically thick. The contributions of other walls or the compartment fire itself thus become unimportant due to the optical thickness of the smoke. However in the furnace test an almost opposite situation is created. The hot gases in the furnace test have a relative low absorptivity (depending on the type of fuel burned) [40], and the medium will therefore be optically thin. The interactions between the furnace walls will become the dominant mode of radiative heat transfer. So the type of fuel used and the type of furnace linings will have a major effect on the imposed heat flux. In general $\varepsilon_g \approx 0$ can serve as a rough approximation [39].

Due to soot deposits and the expected high furnace temperatures, the furnace walls will have a high surface emissivity ($\varepsilon_w \approx 1$). So the heat flux becomes coupled to the temperature of the furnace walls. Because the furnace linings are prescribed to have a low thermal conductivity and low density, it is a common assumption to make that the surface temperature of the linings follows the gas phase temperature [41]. In its turn the gas temperature inside the furnace is prescribed by a constantly growing temperature time curve (ISO or ASTM). But as discussed before, only prescribing a gas phase temperature is not sufficient in order to define the thermal boundary conditions on an element.

Given that in a full-scale furnace test the convection coefficient can be approximated to be constant, the convective heat transfer will be linearly dependent on the furnace temperature. Due to the constant heating, the walls of the furnace quickly heat up following the standard fire curve. However because of the temperature to the power of four relationship (see *Equation 2-6*), the radiative terms will undergo a more than linear increase with temperature and consequently time.

Keltner [42] measured the total heat flux in different furnace tests. *Figure 10* for example demonstrates the heat flux in different types of horizontal furnaces where the temperature is controlled by different types of sensors.

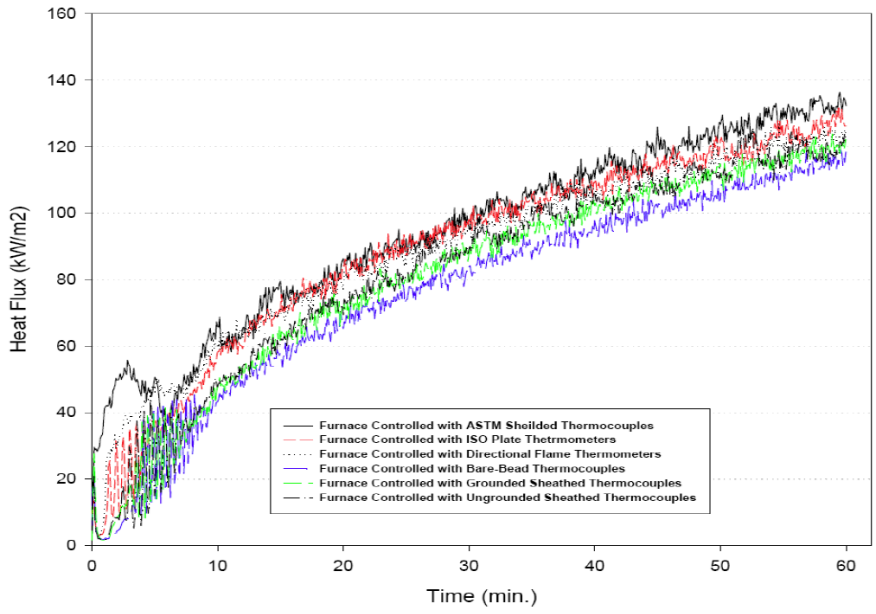

Figure 10: Heat flux measured by cooled heat flux gauges in different types of furnaces, taken from [42]

The heat fluxes presented in *Figure 10* are measured by cooled heat flux meters. This is an important observation to make because the expected net heat flux towards a wood element will be distinctly lower, given that the wood surface temperature will rise as the wood combusts.

For example the surface linings of the furnace [41], insulative materials or concrete elements will quickly obtain surface temperatures within the same range as the gas phase temperatures of the furnace, thus very little net het flux will be absorbed by these type of elements. However for wood elements a similar but lower heat flux trend as in *Figure 9* is expected, as the surface temperature of the wood will be significantly lower than the furnace temperature. Furnace temperatures quickly go within a range

beyond1000˚C, whilst the surface temperature of the wood elements can be expected to be relatively stable within the pyrolysis range (i.e. around 600˚C[4]).

Compared to the heat flux range found in compartment fires (*Figures 6 to 9),* the furnace heat fluxes might seem to be relatively small, moreover as indicated before the heat fluxes presented in *Figure 9* represent an upper bound.

However what is of importance for the furnace is not so much the quantification of the heat flux, but rather the received thermal load by the timber element. With the received thermal load being the integral over time of the heat flux, so basically representing the multiplication of the heat flux and the required exposure time. This remark is of importance because the furnace conditions are such, so that the wood is consistently and continuously charring over the whole exposure time[43].

Consider for example the required exposure times for a prototypical 42-storey tall timber building such as the one designed by SOM [3]. Within the Chicago Building Code a required *ASTM E119* exposure of 4 hours is demanded for most structural elements. Note that this required time rating is very onerous compared to the burnout times presented in *Table 2-1*.

2.3 Conclusions

Through a series of approximations and assumption it is possible to simplify the radiative heat transfer to an element so it can be easily quantified by a local gas phase temperature. Moreover also the convective heat flux terms can be approximated by some relatively easy to use formulations. The main problem is that the local gas phase temperatures are not correctly defined in a temperature time curve, whilst these curves are commonly used for design. In other words, currently fire designers lack a sound method/framework to define an imposed heat flux on a structural element derived from a certain design fire, further research in this field is recommended.

In order to correctly quantify a heat load bound onto a structural element, for a full burnout scenario, data sets obtained in full scale fire tests were used. Especially the Dalmarnock fire tests were used to serve as input for a heat flux bound. Data from several other large scale fire tests was used in order to quantify a bound on full-burnout associated time scales.

A summary of the data is given in *Figure 11*, where the ‘real’ fire conditions are put into perspective with the heat flux trend which is expected in a furnace test. *Figure 11* basically combines the heat flux bounds proposed in *Figure 8* with the timescale bounds indicated in *Table 2-1*, these data sets represent the bounds on a ‘real’ fire and are indicated in green in the figure. The dashed red line in *Figure 11* is an indication of the expected heat flux trend in a furnace. The furnace trend demonstrates the onerous nature of the required exposure times for fire resistance ratings in the context of tall buildings. It important to remark that the actual heat flux received in a furnace by an unprotected wood element will be lower than what is indicated with the curve. However what is of importance here is that during the whole exposure time the furnace conditions are such so that the timber element continues to burn. This way, the total heat load onto a wood element in a furnace is expected to be relatively large compared to the ‘real’ fire especially because of the long exposure times required for elements in tall buildings.

The heat flux and exposure bounds indicated in green will further be used in order to devise an experimental setup in *Chapter 4*.

[4] See section 5.1 concerning a TGA analysis of different wood species.

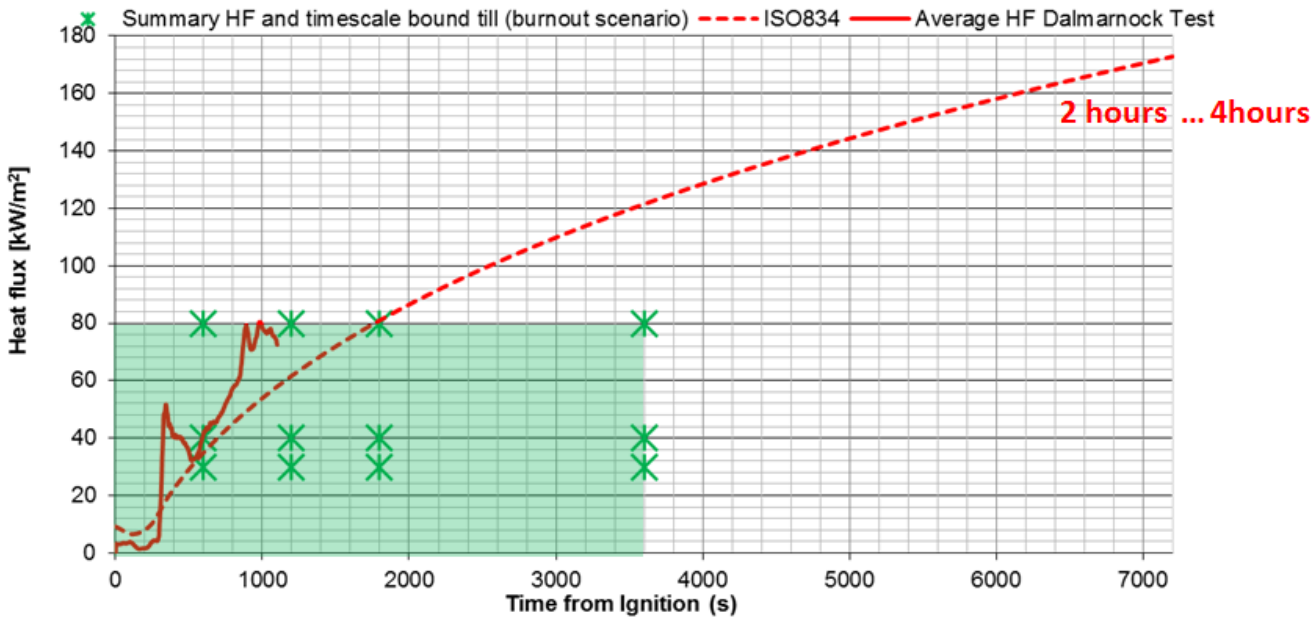

Figure 11: Heat flux and exposure time bounds for full burnout scenarios versus standard requirements

3 The combustion behaviour of wood

This chapter starts with a general overview on the material wood, with focus on the material composition.

The first objective of this chapter is to give an overview of the combustion behaviour of wood (*Section 3.2*). The general combustion behaviour of wood is split up into the pyrolysis behaviour of wood (*Section 3.2.1*) on the one hand and the thermal oxidation (*Section 3.2.2*) on the other.

The second objective of this chapter is to describe a simple heat transfer model (*Section 3.3*). This simple heat transfer model will further used in *Chapter 5* in order to support the experimental findings.

In *Section 3.4* charring models are discussed. Charring models are crucial in the context of structural applications because these models provide an easy method to accurately model the combustion behaviour of wood. Charring models for both solid wood and novel timber products are discussed.

3.1 Material composition

Excluding moisture, wood consists out of three main building blocks (i.e. polymers) namely cellulose (40-50%), hemicellulose (21-35%) and lignin (22-34%) [25]. Cellulose is made up from long linear carbon chains and it makes up the cell walls, it is also the most abundant component of wood. For example the tensile strength of wood is mostly provided by cellulose. Hemicellulose is essentially quite similar to cellulose and grows around the cellulose fibres. Hemicellulose serves as the interface between cellulose and lignin. Lignin is considered as being the glue/cement of wood and it gives rigidity to wood. The compressive and shear strength of wood is provided by lignin [44].

Aside from the three main polymers wood consists out of other small organic compounds, called extractives (examples of extractives are fatty acids or terpenes).

Defining the properties of wood is not as simple as considering these three main polymer properties in isolation. Wood properties at ambient temperature depend on the complex and variable internal structure which is determined by the species, age, moisture content, environmental factors and position of localised defects [44].

In general tree species are subdivided in two major classes, softwoods and hardwoods. Most hardwoods have broad leaves and shed them at the end of each growing season. As opposed to softwoods of which most species are evergreen.

A tree log shows three distinct zones, the bark, sapwood just beneath the bark and an inner zone called the heartwood. Sapwood allows for sap conduction and food storage, a young tree is composed mainly out of sapwood. As the tree grows the inner sapwood stops conducting sap and deposits start to form in the cells, thus softwood becomes heart wood. These deposits in the cells make heartwood more durable than sapwood. However once dry there is no consistent difference between heartwood and sapwood in weight or strength. Within the different growth rings of wood another two zones can be identified, early or springwood and late or summerwood. Springwood is light coloured compared to summerwood because it contains large cavities. In its turn springwood contains large cavities because it grew quickly. Summerwood or latewood contains more solid wood substances, and has grown slower. Since the growth rate has an effect on the structure of wood, it has also an important effect on the structural properties of wood.

Wood contains water in two distinct forms, it can be either ‘free water’ in the cell cavities or it can be ‘absorbed water’ in the capillaries of the cells. When wood loses moisture first the free water evaporates, the cell walls initially remain saturated. At the point when the free water has been evaporated and the cells start to lose moisture is referred to as the Fibre Saturation Point (FSP). This point is roughly 25 to 30 percent for most species. The moisture content of wood used in construction will vary depending on the environmental conditions (temperature, humidity). In general moisture contents above the fibre

saturation point will not have a significant influence on strength or volume of wood. However once wood dries below the fibre saturation point in general it starts to shrink and strength increases. Wood shrinks mostly in the tangential direction, in the radial direction there can also be significant shrinkage. In the longitudinal direction wood will shrink very little.

3.2 Burning behaviour

When timber is exposed to a heat-flux from a fire it will gradually heat up, creating temperature gradients inside the wood. It is the propagation of this heat by conduction that will dictate how a structural timber element fails [45]. There are two main causes by which timber elements can fail during a fire. The first is a loss in mechanical resistance due to degrading wood properties at elevated temperature. This failure is especially important to consider in the design of connections, since failure can occur at temperatures as low as 50°C, so well below the charring temperature [46]. Secondly timber elements can also fail due too much charring and consequently loss of cross-section. In this failure the amount of cross section that remains uncharred after burning simply cannot support the loads. This can be explained because the uncharred layer remains at almost full strength however the char layer losses all of its strength [43].

When exposed to high enough heat loads wood will start to degrade due to physical and chemical changes inside the material. Wood is weakened by both temperature and moisture increases [44], so in general the material properties of wood go down as moisture content and temperature increase (*Figure 12*).

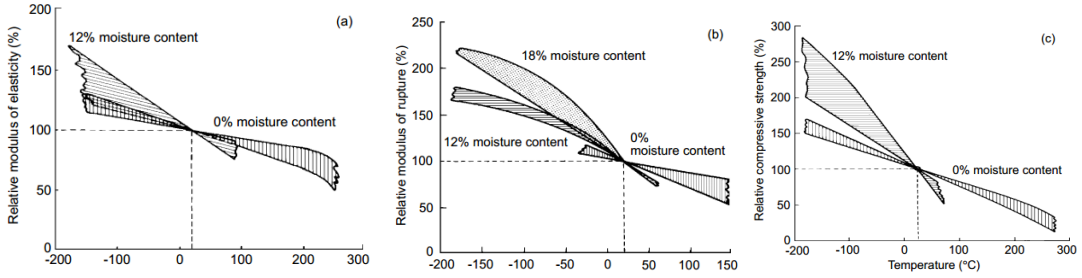

Figure 12: Effect of temperature and two moisture content compared to the ambient value with (a) modulus of elasticity parallel to grain, (b) modulus of rupture in bending, (c) compressive strength parallel to grain taken from [47, pp. 4–36]

Since wood is a combustible material at some heating point it will start to combust. However before the onset of pyrolysis some important changes inside the material occur. Initially the free water inside the wood will start to evaporate which generates a pressure build up. In its turn the pressure build-up will enable a flow of vapour and water away from the heated zone. Some part of this moisture may escape to the outside; another part may increase the moisture content in the colder zones of the wood.

One of the most referenced papers on the temperatures associated to wood decomposition is published by *Browne* [48]. In this paper, *Browne* proposed several temperature ranges and the occurring decomposition events in that range.

Table 3-1: Key temperature ranges associated to wood pyrolysis and combustion, adopted from [49]

Temperature range	Main decomposition events:
>100°C	Evaporation of free water.
160-200°C	Hemicellulose and the other polymers start to decompose. Volatiles formed are not combustible.
200-225°C	Slow wood pyrolysis, most gases produced are still non-combustible.
225-275°C	Main pyrolysis reactions start to occur. Flaming combustion only possible with aid of piloted ignition.
280-500°C	Volatile gases are being produced. Rapid char formation as wood gets consumed.

>500°C	Char continues to smoulder and further oxidises into CO, CO_2 and H_2O.

*Table 3-1*is just a rough outline of temperature ranges. As *Babrauskas* [50] noted, researcher have presented a very wide range of temperature data related to wood pyrolysis. Yet for structural design purposes an indicative value of 300°C has become the widely accepted value for the onset of charring [51].

The initial mass losses when species are heated will occur at temperatures of 100-150°C, caused by the endothermic reactions of water evaporation. Beyond 150°C the polymers inside the wood start decomposing in an exothermic way. The decomposition of wood can take two forms: flaming and smouldering combustion [52]. These are two distinct processes based on different decomposition mechanisms. In this chapter the main aspects of both of these decompositions processes are discussed.

During flaming combustion there is a transport of gaseous volatiles produced by the solid wood into the flame reaction zone which is present just outside the solid material. Due to the presence of this flaming zone the diffusion of oxygen to the surface layer of the solid is prevented. So during stable flaming conditions the combustion of wood is mainly determined by thermal decomposition of the wood (pyrolysis). An overview of this pyrolysis process is given in *Section 3.2.1*

Only once a char layer has formed and in the absence of stable flaming combustion the char layer will be able to interact with the oxygen and thus smouldering combustion might occur. The oxidation reaction of char is a complex inhomogeneous exothermic reaction. An overview of this process is given *Section 3.2.2*

3.2.1 Pyrolysis

Timber pyrolysis is typically represented as the decomposition of the main polymer materials it consists out of. As opposed to some other polymer materials, timber decomposition is particularly complex due to its charring (carbonising) behaviour and inherent variability in the material itself.

Depending if the chemical reactions or the heat transfer phenomena limit the pyrolysis behaviour, two different regimes can be identified:

- *Kinetic regime* where the pyrolysis is controlled by the chemical behaviour of the wood, the heat transfer time scales are assumed to be non-limiting.
- *Heat transfer regime* where the time scales associated to chemical reactions are assumed to be a lot smaller than the ones associated to heat transfer. Thus the heat rate of the wood is a lot slower than the occurrence of the main chemical reactions. This regime that normally occurs under fire conditions for structural elements [53]. In this case large temperature gradients are created and pyrolysis can be assumed to occur over a relatively narrow zone. Because the heat transfer regime is mainly dominant for structural design, the pyrolysis behaviour of wood is commonly modelled as a conductive heat transfer problem [54].

The chemical process of decomposition is usually further subdivided into two types of reactions:

- Primary reactions of the virgin wood
- Secondary reactions of the decomposition products created by the primary reactions

Thus far the primary reactions of wood have been quite well researched. The secondary reactions however have received much less attention and up to this date the mechanisms are not fully understood yet. A thorough overview of the modelling attempts and mechanisms of these primary reactions is given by *Di Blasi* [55]. Basically the combustion behaviour of wood is commonly understood form the combustion behaviour of its three main components. Each of these three polymers have a distinct burning behaviour, for example the temperature range in which they create volatiles is different [25]:

- Hemicellulose 200-260°C
- Cellulose 240-350°C
- Lignin 280-500°C

The main polymers of wood further decompose into three type groups of products:

- Gaseous products, of which a part are volatile combustible gases and a part inert. This group represents the low molecular weight products.
- Liquid like tar products which might be gaseous during combustion but will be condensing at low temperatures. Tar products are generally high in molecular weight and volatile.
- Solid char which represent a group of carbon rich and non-volatile residue.

The most common approach in understanding the pyrolysis behaviour is to consider some kind of reaction scheme and representing the chemical kinetics by one or more reaction rates (see *Figure 13*). Presenting a multi-reaction model gives an insight into the understanding of the pyrolysis behaviour. However this is still just an approximation and for modelling purposes often a one or two stage model is adopted [56].

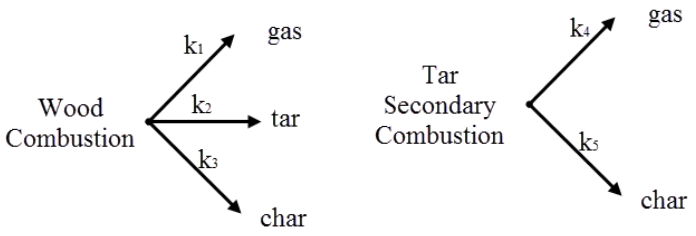

Figure 13: Primary pyrolysis reaction scheme of wood and secondary reaction scheme of tar

In general the mass loss of a reaction is given as:

$$\dot{m} = \frac{\partial m}{\partial t} = -m_0 \sum K_i \qquad \textbf{Equation 3-1}$$

Depending on the model different reaction rates are used. Simple pyrolysis models assume a single reaction rate, whilst others might use many to describe to decomposition of the different polymers. The reaction rate is assumed to be governed by the Arrhenius law:

$$K_i = Ae^{-E/RT} \qquad \textbf{Equation 3-2}$$

A and E are also referred to as the kinetic parameters and are dependent on the specific reaction being considered. *Long Shi et al.*[54] give an extensive overview of the different kinetic parameters found for modelling purposes. Be aware that the parameters cited in literature will vary from sample to sample and are also dependent on the test methods used to obtain them. The best known pyrolysis reaction at the moment is the one of cellulose [57]. The amount of research on the kinetic parameters of lignin and hemicellulose is still very low compared to cellulose. It is understood that the combustion of hemicellulose is highly dependent on the amorphous state and the presence of inorganic pollutants[54]. Hemicellulose has a lower thermal stability compared to cellulose, making even harder to define the kinetic parameters. The same holds for the kinetic parameters of lignin, an up to date overview of the thermal degradation of lignin is given by [58].

The reaction products formed in the primary reaction undergo further thermal degradation, referred to as the secondary pyrolysis reactions. However these secondary reactions have received much less attention simply due to their inherent complexity. Up to this date these mechanisms are not even fully understood [52]. The main secondary reactions considered in literature are the further oxidation of the tar products. Again some models approximate the pyrolysis reaction of tar by an Arrhenius expression. However as

before in the primary reactions, the reaction constants cited in literature have a huge spread, for example *Di Blasi et al.* [55] reports a spread of more than 100%.

In general the spread on the kinetic data is mostly due to a difference in:

- Lumping together pyrolysis products into groups (char, tar, gas) rather than the exact constituents.
- Experimental boundary conditions (temperature, pressure, air flow, heating rate, exposure time).
- Chemical composition, more specifically the polymer content and presence of inorganic products.
- Physical conditions, such as the particle size and moisture content.

Described above is the solid phase pyrolysis, however presenting the full complexity of the problem also involves other processes: the gas phase combustion processes, the moisture migration inside the wood element which will have an effect on the chemical reactions. Moreover it is also well known that the extractives in wood also have a big influence on the burning behaviour of wood [59].

The volatiles produced by the thermal degradation of wood as just described will interact with air and under the right conditions create a flammable mixture. Subsequently ignition can be caused by an external source (e.g. ignition spark or flame) or due to a thermal runaway reaction of the product itself (i.e. auto-ignition).When ignition is caused by an external source the flaming combustion might be a short flash, so the flames are immediately quenched after the flash has occurred. This point is commonly referred to as the `flashpoint` and occurs because the fuel vapours deplete too soon in order to sustain flaming combustion. If on the other hand the generation rate of volatiles is high enough flaming will sustain after ignition, this is commonly referred to as the `fire point`[25]. External parameters such as oxygen content, orientation of the fuel (effect of gravity) and flow conditions especially come into play into the gas phase process. However gas phase combustion is not really fully considered in most research.

It is generally acknowledged that the fundamental process of heat transfer controls the combustion process of wood. So for structural applications a conductive heat transfer model has the potential to accurately represent wood pyrolysis.

3.2.2 Thermal oxidation

After pyrolysis has occurred, timber further decomposes in the presence of oxygen. Flaming combustion was described to occur as a pure thermal decomposition process. Thermal oxidation on the other hand is an even more complicated process, due to the strong exothermic character and heterogeneous reaction properties. The chemical reactions during this oxidation were found to be mainly controlled by the oxygen diffusion in the char layer [52]. As in the pyrolysis of wood the oxidation rate can be described by an Arrhenius law.

It must be understood that both thermal oxidation and pyrolysis are in reality occurring at the same time. It is the external heat exposure which affects one of these two mechanisms dominates [60].

3.3 Heat transfer

From the previous sections it has been demonstrated that approaching the pyrolysis behaviour of wood from a pure fundamental level is practically impossible. However due to the fact that the conductive heat transfer is dominant over the chemical reaction rates, heat and mass transfer models can be used to adequately approximate the pyrolysis behaviour of wood.

Heat transfer through a solid is dominated by conduction, more specifically for timber the conduction behaviour will be thermally thick. The thermal behaviour of a simple 1D wood block is quantified in annex B.

Non-steady state 1D conduction through a solid (assuming a constant thermal conductivity k) can generally be described by a differential equation:

$$\rho c_p \frac{\partial T}{\partial t} = k \frac{\partial^2 T}{\partial x^2} \qquad \textbf{Equation 3-3}$$

So in order to define the heat transfer, the thermal properties of the wood and char must be known.

It is important to stress that thermal properties cited in literature may represent the physically correct values obtained from direct measurements whilst other may be determined by test calibration. However most thermal properties found in literature are experiment specific. For example the thermal properties as described in *EN1995-1-2* are obtained under standard fire exposure, and are found to be only valid under these conditions [61].

Moreover in dense solids the heat is mainly transferred by pure conduction. However wood and char are porous materials, so fundamentally heat transfer through wood is governed by all modes of heat transfer (see *Figure 14*). Apart from the obvious conductive heat flux, considerable convective heat fluxes account for the mass transport of vapour and pyrolysis gases. Furthermore due to the formation of cracks and fissures in the char layer radiation and convection heat fluxes increase. These effects of mass transport (e.g. moisture/vapour and pyrolysis gases) and other modes of heat transfer are indirectly taken into account by using effective thermal properties rather than the physically correct ones.

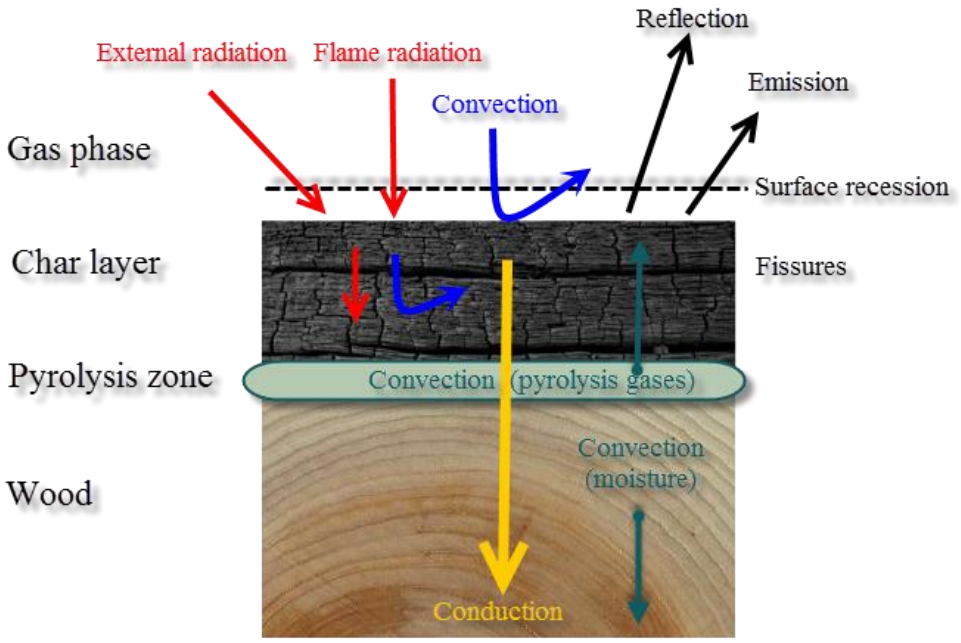

Figure 14: Heat flux components in a fire exposed semi-infinite wood slab

In the next section a simple heat transfer model is presented that basically only takes into account conductive heat transfer. Note that this model will only be used to support the experimental findings and it is not designed to be used for modelling purposes. Phenomena like moisture migration or crack formation definitely play an important role in heat transfer, but are not considered at all in this model.

3.3.1 Simple 1D heat transfer model

As indicated before, conceptually the burning behaviour of wood is modelled by setting up some partial differential equations describing the heat transfer inside the wood. Pyrolysis is modelled as an infinitely fast and isothermal process occurring at a pyrolysis temperature T_p (e.g. 300°C). Subsequently the partial

differential equations are solved by setting out the initial and boundary conditions. These boundary and initial conditions basically represent the heat transfer to the element and thermal decomposition of wood.

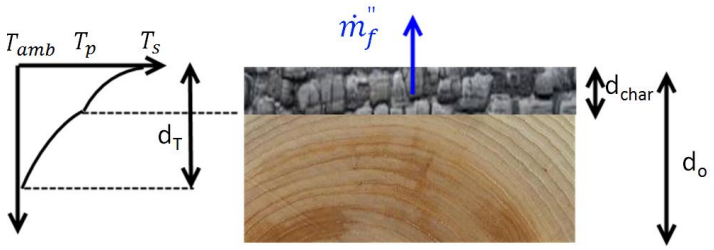

Figure 15: Expected thermal gradients inside a decomposing semi-infinite wood slab

A simple example of a burning block is given in *Figure 15*. The conductive heat transfer inside the wood can be modelled by solving a partial differential heat conduction equation, as proposed by *Bamford et al.* [62]:

$$\rho c_p \frac{\partial T}{\partial t} = k \frac{\partial^2 T}{\partial x^2} - \Delta H_p \dot{m}_f'' \qquad \textbf{Equation 3-4}$$

The heat of pyrolysis of wood (ΔH_p) represents the energy released by a certain mass flux of gases $\dot{m}_f''$. For example for wood specific values from $2 \cdot 10^5 J/kg$ up to $7 \cdot 10^6 J/kg$ are reported in literature [25]. It was found that this spread is partly due to differences and/or a lack of accurately defining the concept of heat of pyrolysis, more specifically at which temperature the value is measured is a vital parameter that is often not well-identified[63].

Given that wood decomposes and forms char which has distinct material properties from virgin wood [64] at least two partial differential equations should be considered to solve for *Equation 3-4*. For this reason the burning timber sample is broken down into three distinct zones (see *Figure 16*). First there is the zone over which the wood has charred. The thickness of this zone is d_{char} and the temperature gradient inside this material goes from a certain surface temperature T_s to the pyrolysis temperature T_p. The boundary of this charred zone is linked to the other zones and moves at a speed referred to as the charring speed (w).

$$w = \frac{d}{dt} d_{char} \qquad \textbf{Equation 3-5}$$

The second zone is where the pyrolysis of virgin wood is occurring and will be referred to as the interface. The interface is considered to be at a temperature T_p and the thickness is assumed to be small. As in [63] the pyrolysis can be represented as an infinitely fast, irreversible, endothermic and isothermal process, taking place at the pyrolysis temperature over an infinitely thin zone. It is assumed that in this zone the main pyrolysis reactions occur. The interface is effectively the coupled boundary condition between the partial differential equations valid in zone one (char) and three (wood).

The third and last zone is the virgin wood itself. Assumed is a thermally thick material so within the virgin wood there will be a moving heating front with thickness (d_T-d_{char}).

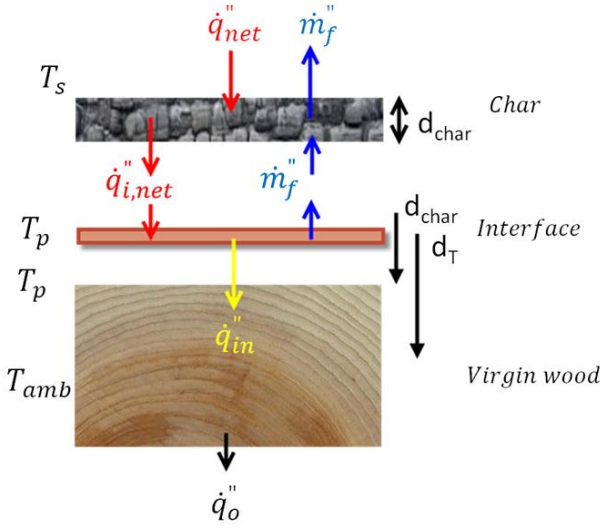

Figure 16: Semi-infinite wood slab heat transfer components, subdivided into char, interface and virgin wood layers

3.3.1.1 The char zone:

The partial differential equation for the char zone:

$$\rho_{char} c_{p\,char} \frac{\partial T}{\partial t} = k_{char} \frac{\partial^2 T}{\partial x^2} \qquad \textbf{Equation 3-6}$$

The thermal properties of the char are further discussed in *Annex D.*

The surface of the char layer will have a certain surface temperature T_s. At the surface of the char layer the boundary condition can be specified:

$$\dot{q}''_{net} + \dot{q}''_{ox} = -k_{char} \frac{\partial T}{\partial x}\bigg|_{x=0} \qquad \textbf{Equation 3-7}$$

With $\dot{q}''_{ox}$ a heat flux term representing the heat created by further oxidation of the char layer.

The net heat flux at the surface can be found by taking into account the total external heat flux (both convective and radiative parts), the flux received by the flames of the burning wood itself and the surface losses (reflection and emission):

$$\dot{q}''_{net} = \dot{q}''_e + \dot{q}''_{fl} - \dot{q}''_l \qquad \textbf{Equation 3-8}$$

Furthermore the flame heat flux is broken down into a radiative and convective part. The radiative flux from the flame, approximated as a grey gas, can be calculated as:

$$\dot{q}''_{fl,rad} = \sigma T_f (1 - e^{-\kappa l}) \qquad \textbf{Equation 3-9}$$

The average absorption coefficient of wood flames is approximately $0.7 m^{-1}$ [65], although this value will be very susceptible to the burning conditions. Furthermore Parker[66] measured flame temperatures of burning wood to be around 1200°C. Furthermore the mean beam length is approximated to be in the order of 10 mm [64]. With these values a radiative flame flux of 2 kW/m^2 is calculated, of this heat flux about half will reach the exposed surface of the specimen. *Janssens* [64] noted that the magnitude of the flame radiative heat flux is of that order, although it might be at the low side in situations where a lot of CO_2 and H_2O gains are expected. Either way the radiative component of the flame is relatively low given that is quite transparent the external radiative heat fluxes are dominant. Consequently the flame heat flux

can be represented in the convective heat flux adopting the gas temperature to a value related to the flame temperature:

$$\dot{q}''_{fl} = h_c(T_f - T_s) \qquad \textbf{Equation 3-10}$$

Detailed measurements in the cone Calorimeter were made by Parker [66] where it was found that the convective heat flux will be in the order of 25W/(m^2.K). In similar experiments flame heat fluxes were both measured and predicted from the burning rates and demonstrated the value depends if burning is along or across the grain and the wood type. The range of values found for $\dot{q}''_{fl}$ was around 30-45 kW/m^2 [67].

In *Chapter 4* the external heat flux was approximated by *Equation 2-10*, so now net heat flux is can be further approximated as:

$$\dot{q}''_{net} = h\left(T_g - T_s\right) + \sigma\left(\varepsilon_g T_g^4 - \varepsilon_{char} T_s^4\right) \qquad \textbf{Equation 3-11}$$

3.3.1.2 The interface

The net heat flux at the interface surface can be approximated by the thermal gradient in the char layer:

$$\dot{q}''_{i,net} = -k_{char} \left.\frac{\partial T}{\partial x}\right|_{x=d_{char}^-} \qquad \textbf{Equation 3-12}$$

The heat flux going into the wood layer can be approximated using the thermal gradient in the wood layer:

$$\dot{q}''_{in} = -k_{wood} \left.\frac{\partial T}{\partial x}\right|_{x=d_{char}^+} \qquad \textbf{Equation 3-13}$$

The boundary condition at the interface layer is then given by:

$$-k_{char} \left.\frac{\partial T}{\partial x}\right|_{x=d_{char}^-} + k_{wood} \left.\frac{\partial T}{\partial x}\right|_{x=d_{char}^+} = \Delta H_{p,wood} \dot{m}''_{f,wood} \qquad \textbf{Equation 3-14}$$

Equation 3-14 will be used in *Chapter 5*, in the light of a discussion on temperature measurements inside wood samples, under more or less steady state conditions, evaluated just at the moment the external heat flux from a burning block of wood is removed. The discussion in *Chapter 5* is made in order to approximate the thermal conditions at the pyrolysis front in the context of flaming extinction (i.e. self-extinguishment).

It is thus of importance to look a bit closer at the different terms in *Equation 3-14* and see what the different terms exactly represent and how these terms can be approximated.

The terms on the right hand side of *Equation 3-14,* basically represent what heat fluxes are coming in and out of the pyrolysis zone. The heat flux gains or what comes into the pyrolysis zone is basically determined by the thermal gradient inside the char layer times the thermal conductivity of the char (*Eq. 3-12*). These heat gains will be caused by char oxidation and the heat received near the surface as discussed in *Section 3.3.1.1*. The heat losses near the pyrolysis front correspond the thermal gradient inside the unburned wood times the thermal conductivity of wood (*Eq. 3-13*). In other words, the heat losses near the pyrolysis front correspond to the heat flux which is absorbed by the unburned wood.

The difference between the heat gains and the heat losses near the interface determine the pyrolysis rate of the wood. If the heat gains are greater than the losses, pyrolysis occurs. If the heat losses are greater

than the gains there will be no heat to support pyrolysis. As the mass loss rate drops lower, eventually a critical mass loss rate for flame extinction will be reached, so the flames will quench [67].

So it can be stated that the net heat through conduction received at the burning wood surface is distributed into two terms, one part will serve as in-depth conduction into the wood and the other part will be used to support pyrolysis.

In other words, if the in-depth conduction term into the unburned wood is too large or the heat from the char is too small, the net heat gain at the interface is too small to support pyrolysis and flame quenching is expected to occur. So in a sense *Equation 3-14* could serve to simplistically determine extinction by evaluating the thermal gradients in the char and wood layer at the pyrolysis interface.

Note that in the experiments discussed in *Chapter 5,* extinction occurs after removal of the external heat flux. Before removal of the heat flux steady state conditions might have been achieved, but this does not imply the conditions are still steady state after removal of the heat flux when extinction occurs. However the use *Equation 3-14* for approximating the energy balance near the pyrolysis front at extinction can be motivated. It is expected that the response time of in-depth conduction[5] is orders of magnitude slower than the chemical times associated to flame quenching [68]. Thus is expected that the wood does not have time to reduce the steady state in-depth gradient before flame quenching physically occurs. This way the steady state assumption might still be somehow appropriate.

In the experimental discussion in *Chapter 5* the thermal gradient inside the unburned wood at the pyrolysis interface will be approximated. Combined with an assessment of the thermal conductivity of the wood (see *Annex D*), the heat absorbed by the unburned wood near the pyrolysis front can be calculated. This absorbed heat flux is useful to assess because it represents the lower bound of what heat is minimally needed to be conducted through the char to further support pyrolysis.

As indicated before, the heat transferred inside the char can only be adequately determined by solving the energy balance near the char surface. Unfortunately this evaluation is outside of the scope of this thesis.

3.3.1.3 Virgin wood

The partial differential equation for the virgin wood:

$$\rho_{wood} c_{p_{wood}} \frac{\partial T}{\partial t} = k_{wood} \frac{\partial^2 T}{\partial x^2} \qquad \textbf{Equation 3-15}$$

At the back surface the boundary conditions can be described as:

$$\dot{q}_0^{''} = k_{wood} \frac{\partial T}{\partial x}\Big|_{x=d_0} \qquad \textbf{Equation 3-16}$$

[5] See calculation of the characteristic heating time of wood conduction in Annex B, this analysis lead to a characteristic time in the order of 5 seconds.

3.4 Charring models

3.4.1 Solid wood

As understood before, timber members which are exposed during a fire event will at a certain point undergo charring (unless the member is sufficiently protected). In order to calculate the mechanical resistance of a charred timber element, the original cross-section should be reduced by the charring depth. Charring can be calculated by the use of simple charring models.

The mechanical strength of the remaining part of uncharred wood can be calculated in two different ways.

The first method is to calculate the mechanical properties of the uncharred section by taking into account reduced properties. This method takes into account a reduction of mechanical properties depending on the loading mode, cross-section and temperature distribution inside the uncharred wood. In other words a full thermo-mechanical analysis of the uncharred wood is made in order to calculate the remaining load bearing capacity of a burned piece of wood.

As described before the thermo-mechanical behaviour of wood is very complex. For timber structures the thermal analysis is therefore normally simplified by the use of the reduced cross-section method (*EN 1995-1-2*). This way the problems related to heat transfer and combustion behaviour of wood are avoided and all considered into one empirical parameter, namely the charring rate. Given that determining the char rate is such an important factor, much research has gone into determining the charring rate under different conditions. The work of *White* [69] is up to this date one of the main references on the topic of charring behaviour of wood for structural applications. *White* [69] experimentally established a wide range of charring rates under standard fire exposure. However many different researcher established charring rates for other species or boundary conditions throughout the years [70], [48],[71],[72]. An extensive review of the different experimentally established charring rates and coupled external influencing factors is given by *Friquin* [73].

In Eurocode design (*EN 1995-1-2*) the charring rate is given a constant value, depending on the wood being hardwood, softwood, LVL or a timber panel. Within the hardwood and softwood charring rates two values are possible depending on the density. Keeping in mind the charring rate basically represents an analytical model for the full thermo-mechanical behaviour of wood, assuming constant charring rates might be a too simplified model. An overview of the different influence factors that should be considered in an adequate charring model are given in *Table 3-2*.

Table 3-2: Main charring rate influence factors, adopted from [73]

Internal influence factors	
Density	In general the charring rate decreases as density increases
Moisture	Increased moisture content leads to a decreased charring rate
Chemical composition	Depending on the polymer content and other chemicals present in the wood the charring rate will vary. Of the three constituting polymers lignin is the most influential on the charring yield.
Heat transfer direction	Charring along the grain is greater than across the grain due to the greater conductivity/permeability along the grain.
Char contraction	With increasing char contraction factor the charring rate has been found to reduce.
Char oxidation	Charring rate has been found to increase as the char oxidation increases
Scale effects	The scale effects have an effect on the heat transfer and thus charring rate.
External influence factors	
External heat Flux	Total charring rate tends to increases with increasing heat flux but on the other hand char yields tend to decrease with increasing heat flux
Oxygen concentration	The oxygen content and more general the air composition will have an influence on both burning rate and char yield

The charring rate can be measured based upon through thickness temperature measurements of the burning wood. In this case a pyrolysis front is tracked by assuming some kind of fixed pyrolysis temperature. A second method to determine the charring rate, which is adopted by *White* [69], is to determine the average charring rate w from the mass loss rate (*Equation 3-17*). Note that this method generally ignores mass loss rate in advance of the char front and assumes that the mass of the char is negligible.

$$w = \frac{\dot{m}_f''}{\rho_w} \qquad \textbf{Equation 3-17}$$

A general trend in the mass loss rates obtained from the different researchers can be observed. Following ignition, a peak mass loss rate occurs followed by a more or less exponential decay and almost steady-state burning period near the end of the tests. From this steady state mass loss rate the actual charring rates presented in literature are commonly derived.

The peak mass loss rate occurs at ignition and when no considerable char layer has formed. As the char layer increases in thickness the mass loss rate goes down because the char insulates the wood, until a certain steady-state seems to be reached and the charring rates become constant. Moreover in some studies [74], [64] a third phase is identified.

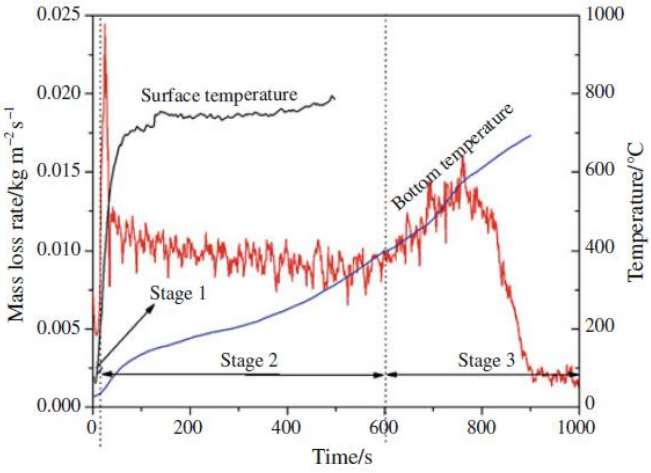

Figure 17: Mass loss rate of cherry wood under a constant external heat flux of 75 kW/m^2, taken from [74, p. 3]

This third phase (*Figure 17*) occurs when the whole block of wood reaches an almost uniform temperature of 300C. At this stage the whole sample of wood is assumed to be burning at once, thus the third stage is not really of interest in this discussion given it is more an anomaly caused by the small test samples.

3.4.2 Novel timber products

Note that the commonly used charring rates established by *White*[69] and *Schaffer* [70], were obtained by tests on both solid wood and glued laminated timber (Glulam). So for both solid wood and Glulam products the charring rates are identical.

However few experimental investigations are available on the charring rates for cross-laminated timber products [75], [76],[77]. The research by *Frangi et al.* [77] established the relationship between solid wood charring behaviour and that of CLT under standard fire exposure:

- If the charred laminated layer remains in place the charcoal protects the remaining uncharred layer and in this case the charring behaviour of solid timber and CLT is assumed to be identical.
- If the charred layer falls off after charring the fire isolative function of the char layer is lost. After delamination an increased charring rate is expected. This phenomenon was described to be similar to initially protected timber elements.

An example of a standard charring calculation method in the case of delaminating CLT is given in annex A. Yet no conditions have been established when delamination exactly occurs and further research in this field is needed. Most of the research so far has only looked into the problem of CLT delamination in the context of standard fire testing.

It is crucial to remark that ply delamination potentially implies more than only increased charring rate issues. Research by *McGregor* [78] indicated that delaminating CLT panels could potentially become a very significant source of fuel for compartment fires. In the test reported by *McGregor* [78] delamination basically occurred well before the delaminating parts had been completely charred. This way the heat release rate contribution of the delaminated CLT was found to be in the same order as the total fuel load of the compartment contents.

3.5 Conclusions

In this chapter the burning behaviour of wood is described. It was found that the pyrolysis behaviour of wood is usually determined by the pyrolysis behaviour of three polymers, namely cellulose, hemicellulose and lignin.

Due to the fact that the chemical combustion time scales are much smaller than the time scale associated to heat transfer through the solid, the pyrolysis behaviour of wood can be approximated by a heat transfer model.

Neglecting complex effects such as multi-dimensional heating, moisture migration, presence of local defects, etc. a simple 1D heat transfer model was developed.

It was also demonstrated that charring models for wood can basically replace complex thermo-mechanical models, at least in the context of structural fire design. So far it has been well-established that the charring rates for solid wood are also applicable to Glulam products. The charring rates for solid wood are also valid found to be valid for CLT products, but only under the condition that no ply delamination occurs.

Several issues concerning ply delamination in the context of structural applications were identified but are in need of further research:

- Establishing when ply delamination is expected, especially in the context of natural fire conditions
- When ply delamination occurs well before the ply itself has been completely charred or consumed, methods must be researched in order to prevent delamination. Delamination must be avoided in these cases because the delaminated parts are still fuel rich and might significantly contribute to the compartment fire.

4 Experimental determination of the burning behaviour

So far the first two steps of the performance based framework (*Figure 4*) have been elaborately discussed. In chapter three the main heat transfer mechanisms behind wood decomposition have been exposed and in chapter two bounds on typical fire heat fluxes and burnout times have been placed.

In this chapter the concept of self-extinguishment is introduced. Evidence will be given that a decrease in mass loss rate will result in flaming extinction. Next it will be demonstrated that glowing combustion is not of concern for structural applications, as the charring rates associated to smouldering are too low to be of any concern in the context reducing the load bearing cross section. This literature review will provide the evidence that self-extinction is expected to occur near extinction/burnout of the compartment fire.

If the concept of self-extinction is valid, it is implied that unprotected wood elements designed for relatively long standard exposure times might be over-dimensioned for what is adequate to meet the performance criteria of preventing structural collapse or fire spread until full burnout. The concept of self-extinguishment is thus crucial because it implies that structural wood elements only sustain charring until fire compartment burnout.

In *Section 4.2* of this chapter an experimental bench-scale test setup is described. This test rig will be used to further determine the burning behaviour of wood products. More specifically emphasis is put on obtaining more insight into the self-extinguishment capacity of wood.

4.1 Past Experimental work

4.1.1 Extinction conditions

Drysdale [25]states that it is common experience that solid blocks of wood will not continue to burn unless supported by an external radiative or convective heating source. These claims are supported by observations that the flame heat fluxes of combusting wood are almost equal or smaller than the associated heat losses[79], [80] . *Tewarson and Pion* [80] basically observed that for different species of wood $\dot{Q}_f^{"} < \dot{Q}_l^{"}$, demonstrating that the burning of wood depends on an imposed/external heat flux.

Throughout the years many different analytical models have been developed to predict the extinction conditions of a fire [67],[81], [82]. For example *Spearpoint et al.* [67] established a theory for flame extinction based upon flame temperature using an integral model. It was found that in general extinction is controlled by the complex chemical kinetics of oxidation and that the current models do not allow making accurate predictions. *Quintiere* [19] deduced the extinguishment conditions from a critical parameter for extinction, namely the Damköhler number. This number can be expressed as the ratio of thermal diffusion over chemical reaction time. This ratio compares heat loss time scales associated to conduction against the chemical reaction times associated to the burning rate.

$$Da = \frac{\Delta H_p \dot{m}_f^{"}}{kT/\delta} \qquad \textbf{Equation 4-1}$$

With: δ the layer thickness [m]

If the Damköhler number is large the reaction is fast enough and burning will be sustained. As the number gets smaller the reaction slows down up until a point when the heat losses are too large so that the combustion reaction quenches. The times scales associated in the Damköhler number must be deduced from an energy balance effectively creating a relationship between heat capacity of the medium, heat losses and the energy gains from combustion.

However solving the energy balance at the surface requires some kind of analytical model near the surface. Any such solution should be treated with care because first of all the analytical solutions must be based upon some assumed kinetic and secondly the full kinetics are not fully known (see *Section 3.2*).

Besides the analytical models also several empirical conditions have been established.When assuming that flaming is not extinguished by an external source (such as sprinklers, wind) *Drysdale* [25] describes that there are two principal aspects to the phenomenon of extinction. The first aspect is the extinction of the flame and the second aspect is a pyrolysis rate below the critical value. These two conditions are in line with *Beyler* [83]. *Beyler* empirically set-out different extinction conditions based on observations of the energy balance over the surface of a burning solid:

- Extinction occurs when the flame temperature decreases below a critical value
- Extinction occurs when the mass pyrolysis is less than a critical value

Delichatsios et al. [84] reported a critical mass pyrolysis rate at extinction for particle board to be 5g/(m^2.s) with an accuracy of 4%. The results were obtained at an external heat flux of 35kW/m^2. Furthermore the critical mass pyrolysis was linked to the gas phase conditions through the use of a B-number.

$$\dot{m}_f^{"} = \frac{h_c}{c_p}\ln(1+B) \qquad \textbf{Equation 4-2}$$

The B-number was first introduced by *Spalding* [85] to characterize the burning behaviour of liquid droplets. In essence the B-number physically relates the heat release rate to the heat losses associated to combustion. A large B-number thus relates to a relatively high exothermic combustion compared to the heat of gasification required to support the reaction. The B-number has been predominantly researched in order to characterise material flammability in space because it is possible to measure this parameter under earth gravity conditions [86]. *Rangwala* [86] reported a critical B-value for Douglas fir wood of approximately 0.5. Given the test-setup used in this work a convective heat flux coefficient of 10W/(m^2.K) was estimated, using above equation this relates to a critical mass flux around 4 g/(m^2.s).

Note that in principle the conditions of piloted ignition at the fire-point and flame extinction near a solid are related to the same conditions, with ignition at the fire-point being the first appearance of quasi steady-state burning of the solid, as described by *Drysdale* [25]. In this case it can be expected that the wood interface temperature at ignition and extinction can be approximated both approximated by the fire point [87].

However there is the very important practical difference that ignition criteria are related to supplying enough energy to the wood sample as opposed to flame extinction which evolves from the flames and interaction with the wood itself. Since ignition and extinction can be related to fire-point ignition, for the remainder of this section these ignition conditions will be discussed. Note this is just an assumption, since hysteresis at the gas phase level will definitely occur. Yet the occurrence of hysteresis in the gas phase temperatures is not really relevant in this case since the pyrolysis behaviour of wood will be driven by heat transfer in the solid wood phase (see *Section 3.2.1*).

4.1.2 Ignition conditions

Janssens [64] provided a comprehensive experimental overview on flaming ignition under radiant heating. A commonly used ignition criterion in literature is that of the ignition temperature[50]. Since the ignition temperature is an empirical quantity, extension of the concept outside of the experimental conditions is not straightforward. Moreover it was found that there is no basis physical basis to clearly support the concept of a certain critical ignition temperature and that the critical mass flux is a more correct ignition criterion [88].

The concept of a critical mass flux at ignition was first established by *Bamford et al.* [62]. In this work a critical mass flux was found to be approximately 2.5g/(m^2.s). *Koohyar et al.*[89] were one of the first to

thoroughly report critical mass loss rates for different kinds of wood. The critical value was found to range from 1 to 21.7 g/(m^2.s). Fire-point theory and associated first systematic investigation into the critical mass loss concept was done by *Rasbash et al.*[90]. Specifically for wood very few experimental measurements of this critical mass loss rate at ignition have been done. In literature a range of 0.5-5.5 g/(m^2.s) has been reported for a range of materials [90], [91]. A recent study by *McAllister et al.* [92] involved measuring the critical mass loss rate for ignition at different moisture content and external heat flux for popular.

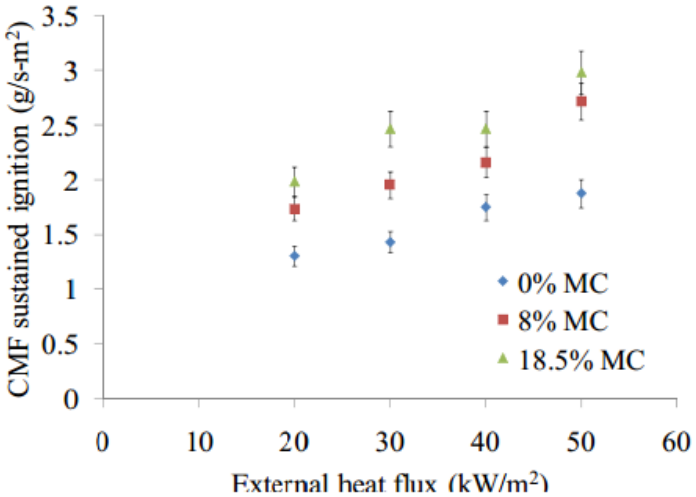

Figure 18: Critical mass flux for sustained flaming ignition in terms of applied external heat flux and sample MC, taken from[92]

From *Figure 18* it can be seen that as moisture content and external heat flux increase the critical mass loss rate also increases. *McAllister et al.* [92] suggested that as the heat flux increases the temperature gradient inside the material increases. Thus the wood will be at a high temperature only over a relatively small zone, thus more pyrolysis heat needs to be produced in order to heat the sample, consequently the critical mass loss rate is found to be higher.

Delichatsios [91] reported critical mass fluxes at ignition for plywood with change oxygen concentration.

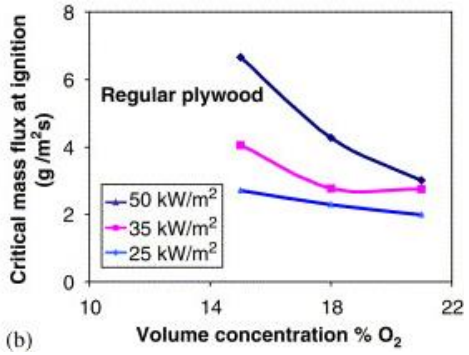

Figure 19: Critical mass flux for flaming ignition obtained under different heat flux levels and oxygen concentrations, taken from [91]

4.1.3 Smouldering/glowing combustion

Note that in the previous sections all extinction conditions that were discussed are within the context of flaming combustion. However besides flaming combustion, smouldering combustion of wood might lead to sustained charring after removal of the heat flux. The further thermal oxidation of char might cause sustained smouldering combustion[93].

For example certain cellulosic insulation materials have been found to sustain smouldering combustion under no external heat flux [94]. However specifically for solid wood it has been found that due to the relative low permeability and corresponding high density, smouldering will only sustain if the wood is subjected to an additional heat input of about 10 kW/m^2 [94], [95]. Compared to low density particles or fibres of wood where sustained smouldering is observed, the self-insulating capacity of the reaction zone of solid wood is too small for significant self-sustained smouldering.

4.1.4 Preliminary conclusions

So far the main heat transfer mechanisms of wood have been discussed in detail in chapter three. It was found that due to the charring characteristics of wood the mass loss rate after ignition naturally degrades due the insulation effect of the char layer. Subsequently in this chapter it has been demonstrated that there is a critical mass loss rate which results in flaming extinction. Further smouldering combustion of wood has not been considered thus far, yet there are suspicions that cellulosic materials can exhibit significant self-sustained smouldering. However evidence was presented that glowing or smouldering of solid wood will only sustain under additional heat input. In other words there is strong evidence that in the absence of the heat flux wood pyrolysis will cease.

Introducing the concept of self-extinguishment of wood is a vital step in the context of structural applications. Self-extinguishment near compartment burn-out means that wood will only sustain significant charring until burnout of the compartment fire. Structural wood elements will thus be adequately designed if they are designed for charring until compartment burnout.

Taking into account the heat flux and time scale bounds found in chapter two, an experimental procedure to further research the burning behaviour of novel timber products is given in *Section 4.2*.

4.2 Present experimental work

In this section the experimental setup is described.

Firstly an instrument description is given. Secondly the applied test conditions and sample characteristics are described. The experimental conditions are basically based upon the fire heat flux and burnout time bounds which were established in chapter two.

Thirdly a detailed description is given of the complete experimental procedure from sample preparation to actual testing of the timber. In addition also the test conditions for a ThermoGravimetric Analysis (TGA) are discussed.

The main procedure of the experimental setup is to expose a piece of wood to a controlled heat load, more specifically controlled in terms of imposed external radiative heat flux and exposure time. Once a specific heat load is imposed on the sample all external heating is removed. This way the burning behaviour during and after delivery of an external heat load can be studied. During this whole process both the thermal gradients inside the timber and mass loss rate of the sample are monitored.

The TGA is conducted in order to identify in detail the main oxidation and pyrolysis temperature ranges of the different tested wood species.

4.2.1 Instrument description

The main test equipment used is a standard Mass Loss Calorimeter (MLC) (*ISO 13927 - ISO DIS 17554*). Note that although the test results will be discussed in the context of structural applications, this specific bench scale test does not allow for the sample to be loaded.

The MLC unit is used because it enables samples to be accurately exposed to a controlled heat flux whilst also monitoring the mass loss rate of a sample. The heat flux is controlled by a temperature controller that controls the temperature of an electrical cone heater. In its turn a specific cone heater temperature corresponds to a heat flux to the sample. The mass loss rate of the sample is monitored via a load scale.

The standard procedure for MLC testing (*ISO 13927 - ISO DIS 17554*) is not followed. The exact test procedure that is followed is scrutinized by *Reszka* [96]. In essence the rig is a vertical setup of the MLC unit. A schematic overview of the test setup is given in *Figure 20. Reszka* [96] created this test setup in order to create timber burning tests with well-defined boundary conditions to serve as input for thermal modelling. In these tests high repeatability was achieved. The high level of repeatability can be attributed to the fact that the test setup has well-defined thermal boundary conditions. As demonstrated in *Section 2.2* this is something not achieved in standard fire resistance testing, due to ill-defined boundary conditions.

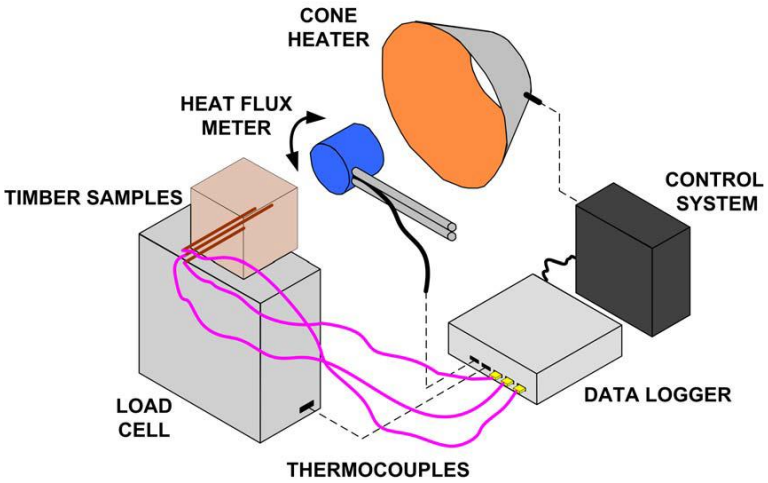

Figure 20: Graphic representation of the test rig based upon a vertical setup of the standard mass loss calorimeter, taken from [96, p. 22]

Temperatures inside the timber element are measured via thermocouple probes. The thermocouple probes are K-type sensors protected with a fibreglass lead and a 100 mm probe piece with a sheath diameter of 3 mm.

Thermocouples can be embedded either from the back surface or the sides of the sample. A concern with placing the thermocouples is that they might have an influence on the temperature field in the wood, since the steel sheet probes have very different thermal properties from the wood itself. Placing thermocouples from the sides of the samples creates the least thermal disturbance in the wood. In this case the probes more or less penetrate a zone with little expected thermal gradients, since the probes are inserted perpendicular to the main heating direction. When the probes are inserted from the back of the sample they penetrate the sample in the direction of heating and thus create greater thermal disturbance. However it was found that when placing the thermocouples from the side the associated errors to temperature measurements are actually larger than placing them from the back of the sample despite the relatively larger thermal disturbance [96]. The main issue with inserting thermocouples from the sides is that the thermal conditions at the sides are not well known.

Temperature measurements are conducted at depths of 5,15,25,35 and 45 mm away from the heated surface. These depths are chosen so the thermal gradients near the pyrolysis front can be monitored. Moreover also the temperature of the back surface of the sample is measured, so in needed the boundary condition at the back of the sample can easily be quantified.

The mass loss of the sample is measured using a load cell. Prior to testing, the load cell is calibrated according to the standard procedure of the manufacturer (Fire Testing Technology Ltd). Before each separate test the load cell is also checked by weighing the sample mass on both a separate scale and the load cell, so to make sure the equipment is still correctly calibrated.

The heat flux meter used is a standard Schmidt-Boelter gauge (Model number GTW-10-32-48-485A).

The incident heat flux from the cone heater is set by adjusting the temperature of the cone in the control system of the MLC unit. In general a specific cone heater temperature corresponds to a certain incident heat flux. Each time a different heat flux or orientation is used the cone heater temperature set-point is re-calibrated with the heat flux metre.

Test data from the load cell, heat flux gauge and thermocouples is collected using an *Agilent Technologies 34890A* data logger unit.

4.2.2 Test conditions and sample characteristics

Besides selecting the actual test samples, defining the test conditions involves setting a range of imposed heat fluxes and selecting a range of exposure times. The selected imposed heat fluxes for heating are 25,40,60 and 80 kW/m^2, exposure times are ranging from 10, 20, 30 to 60 minutes.

Heating is conducted in the direction perpendicular to the grain given this is the dominant configuration that is normally expected during fire exposure of wall and ceiling CLT elements.

The samples used for testing are a selection of two different types of EWP, namely CLT and Glulam, for reference also a few blocks of solid wood were used.

For the CLT samples two commonly available species were used, namely Radiata Pine and Hoop Pine. The Glulam species used is an Australian hardwood, Gympie messmate (*Eucalyptus cloeziana*). All samples have an exposed surface of roughly 100 by 100 mm and variable thicknesses, the specifications of the test samples are given in *Table 4-1*.

Table 4-1: Specifications of the MLC test samples

Species	Type	Bonding agent	Thickness [mm]	MC [%]	Average sample density [kg/m3]
Radiata Pine	3 ply CLT	Polyurethane	72 (20-32-20)	10.7	635
Hoop Pine	3ply CLT	Polyurethane	96 (32-32-32)	11.1	540
Gympie Messmate	Glulam	Phenol Formaldehyde	60	13.4	823
Hoop Pine	Solid Wood	n.a.	70	12.4	560

Before testing of each sample the density was determined, based upon these observations the average density is presented above. Most species showed a fairly constant sample density with a standard deviation around 2%, however the Radiata Pine CLT samples showed a larger spread with a standard deviation of 12%. This relatively large spread on the density of the Radiata pine samples could explained by the fact that the inner ply sometimes contain knots, different moisture contents or other deficiencies which have a large effect on the density of the relatively small sample (100x100x72 mm). As opposed to the Radiata Pine samples the other samples contained a lot less deficiencies.

Prior to the tests two samples of each species were oven-dried during a minimum of 7 days in order to determine the moisture content. All test samples have been conditioned over a long period (minimum of 2 years) moreover the ambient conditions did not dramatically change during testing. The general moisture content should thus be approximated as 11%. However as opposed to the density it was not possible to determine the moisture content for each sample prior to testing.

Two sets of tests were conducted, during one set both mass loss rate and temperatures were measured. These tests will be referred to as test type TC. Especially at lower heat fluxes it was observed that the thermocouples potentially disturbed the mass loss rate measurement. Therefore the experiments were repeated, but only measuring the mass loss rate (so without insertion of any thermocouples). The tests where only mass loss rate is measured are referred to as test type M.

4.2.3 Experimental procedure

4.2.3.1 Sample preparation

The specimens for temperature tests are fitted with 5 thermocouples inserted from the back to different fixed depths from the exposed front surface. One hole is drilled in the exactly in the middle of the sample, four other holes are drilled on a 20 mm radius (see *Figure 21*).

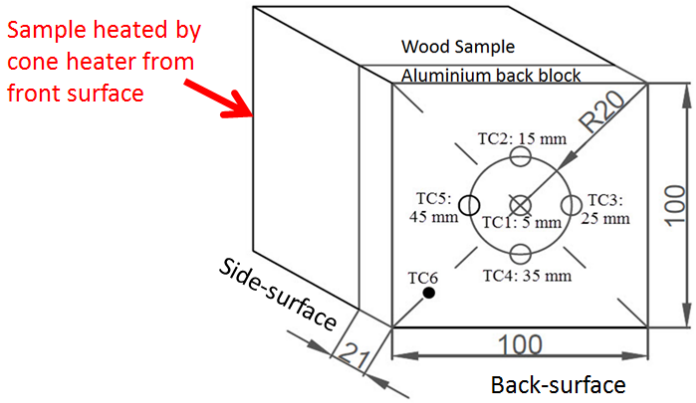

Figure 21: View from the back of the sample with indication of the main heating directions and surfaces. The view includes the aluminium cooling block and indication of the position of the thermocouple probes with their respective depths from the front surface

In each test the thermocouples are placed at the same depths from the exposed surface. In order to provide consistent depths, a drill press is used with a depth stop and feed lever handle. This way the holes can be drilled up to millimetre precision. Because of using a levelled drill table, chances of drilling under an angle are also minimised. Special drill heads are used with a blunt end in order to make sure the thermocouples touch the wood at the end of the drilled hole. Normally wood drills have a sharp drill point; however the thermocouples have a blunt end so when a regular wood drill is used the thermocouples would not fit in perfectly.

The inserted depth of the thermocouples is verified by measuring the protruding part of the steel sheets of the thermocouples, just before and after each test. So the thermocouple depth is controlled within millimetre order. It was found that especially the deeper holes (5 and 15mm) are quite sensitive to deficiencies and expansion of the thermocouple sheets (such as slightly bent thermocouples, soot deposits on thermocouples, collection of saw dust inside the holes, etc.). For this reason thermocouples could potentially get stuck up to 3 mm from the actual drilled depth, any such misalignments were noted per test case.

Before testing each sample is weighed and measured, thus the density of each sample can be determined.

Each sample is also fit with an aluminium block on the back of the sample with dimensions: 100 mm x100 mm x21mm (see *Figure 21*). The purpose of this aluminium block is to keep the back surface temperature as close to ambient temperature as possible. The block basically increases the heat exchange between the back surface and the surroundings. Due to the presence of the block the boundary conditions at the back are well-defined. An overview of the temperature time evolution of the aluminium block can be found in *Figure 22*. The contact between the aluminium and wood is done using a contact cement bond. As can be seen from *Figure 21*, the aluminium block also serves as a frame for the thermocouples to be inserted. Note that the aluminium block was not fitted on the back of any of the Hoop Pine CLT samples. Due to the dimensions of the Hoop Pine sample it was physically impossible to fit the aluminium block without making the sample holder tip over.

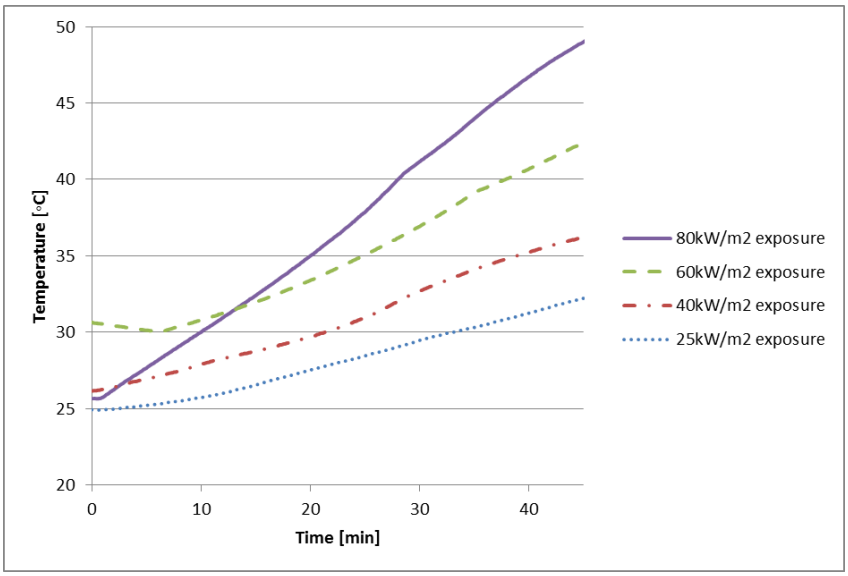

Figure 22: Evolution of the aluminium block temperature for various heat fluxes of Radiata Pine Samples, with a fixed exposure time of 30 min

Note that in *Figure 22* the high starting temperature of the aluminium block in the case of 60 kW/m^2 exposure is probably because the block was not sufficiently cooled between tests.

4.2.3.2 Test procedure

Before testing the heat flux of the cone heater needs to be set by calibrating with a heat flux metre. This calibration is repeated every time the exposure level or orientation is changed.

Prior to testing the load cell is calibrated and the output voltage range is set depending on the sample mass. Because each sample is measured on a different scale before testing the load cell is checked before each test. If readings are incorrect in either the Control Unit or Data Logger the load cell requires recalibration.

The specimens are mounted onto a sample holder and its position is carefully checked prior to each test. First of all the exposed face must be right in the centre of the cone heater. Secondly the distance between the cone heater and the sample is set to 25 mm (the same distance at which the heat flux is calibrated), which is according the standard cone calorimeter procedure (ISO 1993).

An aluminium heat shield is placed on the cone heater once the element is in place. The purpose of the heat shield is twofold. First the cone heater needs to heat up to a certain temperature which corresponds to the desired heat flux. However the heat shield is necessary because the sample cannot be preheated before the cone reaches the desired set-point. At this stage the sample is already on the sample holder but it will only receive an imposed heat flux once the cone is heated up to the desired temperature and the shield is removed. Once the shield is removed the actual time exposure starts to run.

After the desired exposure time (10,20 and 30 min) is reached, the heat shield is put in front of the sample again. This way the burning behaviour of the wood after imposing a controlled heat load (heat flux, exposure time) can be studied. The effectiveness of the Heat Shield is demonstrated in *Figure 23*. For this verification the aluminium block and a thermocouple was placed just behind the heat shield whilst the cone was kept at 920°C for 15 minutes.

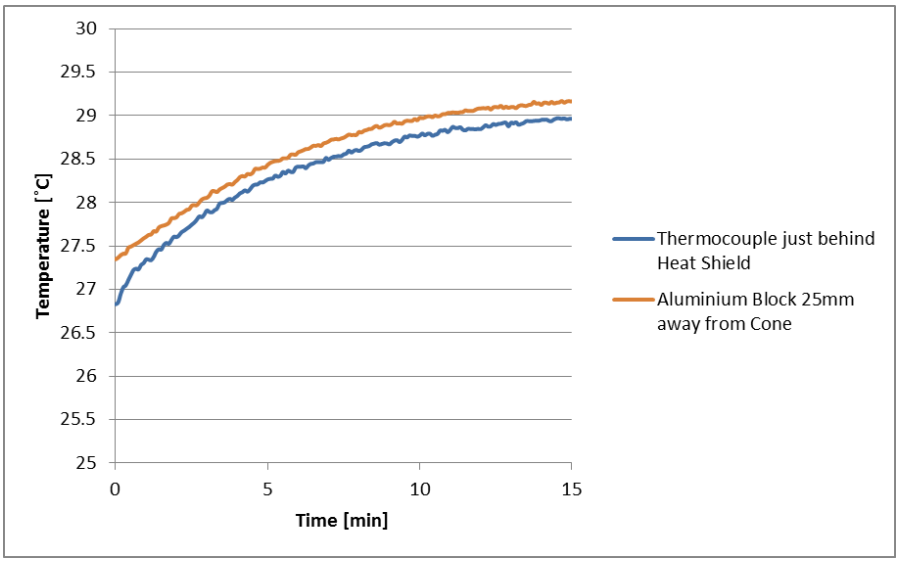

Figure 23: Testing of heat shield effectiveness by measuring temperatures just behind the heat shield with the cone heater on a constant 80 kW/m^2 setting

Test data is logged until mass loss rate data and temperatures were relatively low, so no significant self-sustained charring is expected to occur.

Per setting of heat flux and exposure time, two types of tests are conducted. The first type will be referred to as TC test, during these tests both mass loss rate and temperatures are measured. Due to the potential of interaction between the thermocouple measurements and mass loss measurements a second series of tests is conducted referred to as M test. During test M only the mass loss rate is measured, no embedded thermocouples in the sample are present during this test.

The data acquisition system logged with an interval of 5 seconds. All temperature data presented in the results are directly used as logged in the data files. The load cell data expressed in terms of absolute mass is converted to a mass loss rate. Because the mass loss rate shows very wide scatter the data is further smoothed using a Locally Weighted Polynomial Regression (LOESS) Excel plugin developed by *Hidalgo-Medina* [97]. The number of points used for the moving regression applied to smooth mass loss rata data is set to 34 for most experimental data.

4.2.4 TGA analysis

A TGA analysis is conducted in order to help identify the temperature ranges of pyrolysis and further oxidation of the different species. Determining these ranges will be useful when discussing the temperature gradients obtained in the MLC tests.

In general a TGA is a very accurate mass loss rate measurement of a relatively small size in a well-controlled atmosphere. Milled pieces of each wood species (around 30 mg), were exposed to a temperature range between 30 to and 900°C under a constant heating rate of 10°C/min. Both an inert (N_2) and a regular air atmosphere were applied. Specifically these TGA conditions were adopted after consulting the conditions used in similar research [98].

The results obtained from the TGA analysis are commonly presented in a Derivative ThermoGram (DTG), were the first derivative of the weight loss percentage is plotted against the applied temperature range. With the temperature range being the temperature measured in the control chamber of the TGA analysis, not the sample temperature.

5 Experimental results and discussion

In this chapter an overview is given on the main experimental findings. First a ThermoGravimetric Analysis (TGA) is presented of the different wood species. Secondly four sample cases of the bench-scale MLC tests are elaborately described in order to demonstrate the burning behaviour of the different samples. The discussion is split up into three parts per test case, namely a discussion on the visual observations, a discussion on the collected mass loss rate and a discussion on the temperature data. Thirdly a summary is given on the main experimental findings combined for all MLC tests. This general discussion is again split up into visual observations, mass loss rate data and temperature data. Within the general temperature data discussion a short illustration is given on how extinction conditions can easily be linked to a simple design parameter such as the charring thickness. The fourth part of this chapter presents a brief error analysis.

It is important to indicate that the obtained experimental data could potentially be discussed in the light of many different topics such as ignition, burning under external heating, advanced heat transfer modelling, extinction conditions, moisture migration etc. However the discussion of this chapter is kept limited to three main topics:

1. Analysis of the burning behaviour under external heat flux, with focus on the progression of the pyrolysis front in terms of charring and possible delamination. This analysis will be conducted on the basis of visual observations and mass loss rate data.
2. Analysis of the burning behaviour under external heat flux, with focus on flaming or non-flaming combustion due to auto-ignition of the sample. This analysis will also be conducted on the basis of visual observations and mass loss rate data.
3. Analysis of the burning behaviour after removal of the heat flux, with the focus on post-exposure charring rates and self-extinguishment. Extinguishment will be further discussed in terms of visual observations, critical mass loss rate and also in terms of temperature evolution inside the samples.

A complete overview of all test data is given in *Annex C*.

In total 42 tests were conducted, an overview of all tested MLC configurations in terms of exposure time, heat flux and sample species is given in *Table 5-1*.

Table 5-1: Overview conducted MLC tests

Species	**Heat Flux**			
Exposure time	25 kW/m^2	40 kW/m^2	60 kW/m^2	80 kW/m^2
Radiata Pine CLT				
10 min	*M,TC*	*M,TC*	*M,TC*	*M,TC*
20 min	*M,TC*	*M,TC*	*M,TC*	*M,TC*
30 min	*M,TC*	*M,TC*	*M,TC*	*M,TC*
60 min	*M,TC*	*	*	*
Gympie Messmate Glulam				
30 min			*M,TC*	*M,TC*
60 min	*M,TC*	*M*		
Hoop Pine CLT				
30 min	*M*	*M*	*M,TC*	*M,TC*
Hoop Pine solid wood				
30 min			*TC*	*TC*

M: Mass Loss Rate Measurement without insertion of thermocouple probes in the samples.
TC: Measurements of mass loss rate combined with temperature measurements. So in these case thermocouples

were inserted in the sample.
*: Tests repeatedly failed at time intervals within the previous step of exposure time (failure due to delamination)

5.1 TGA analysis

TGA tests were conducted on Radiata Pine, Hoop Pine and Gympie Messmate samples.

The tests under inert (N_2) atmosphere provide an insight into the main pyrolysis behaviour of the samples. A second series of tests were conducted under regular air atmosphere. Under these conditions both the pyrolysis and further oxidation behaviour of wood can be studied.

As discussed in *Section 3.2* the pyrolysis of timber is mainly subdivided into four stages: moisture migration and decomposition of the three main polymers. *Yang et al.*[98] found that hemicellulose easily decomposes with weight loss mainly occurring in the 220 to 315 ˚C range. Cellulose decomposition occurs at slightly higher temperatures ranging from 315 to 400 ˚C. Lignin was found to be the most difficult to decompose, basically decomposing over the whole tested temperature range (from ambient up to 900 ˚C).

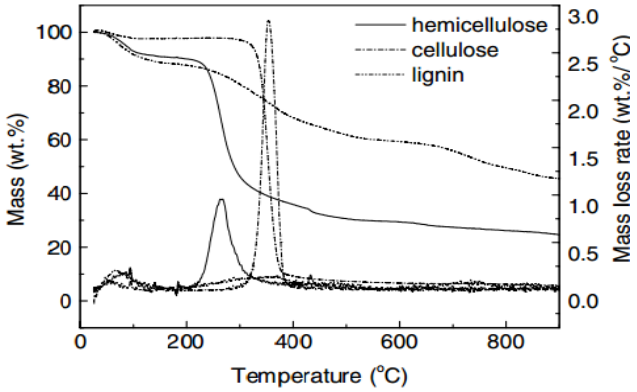

Figure 24: Pyrolysis curves of hemicellulose, cellulose and lignin taken from [98, p. 1783]

The data in *Figure 24* represents the pyrolysis behaviour of the three different wood polymers in isolation [98]. The main pyrolysis behaviour of wood is expected to be represented by the summation of the three individual mass loss rate curves in *Figure 24*. As can be seen from the Nitrogen data in *Figure 25*, the obtained experimental data corresponds well to literature. Note that the peak around 100˚C in *Figure 25* is due to the evaporation of free water.

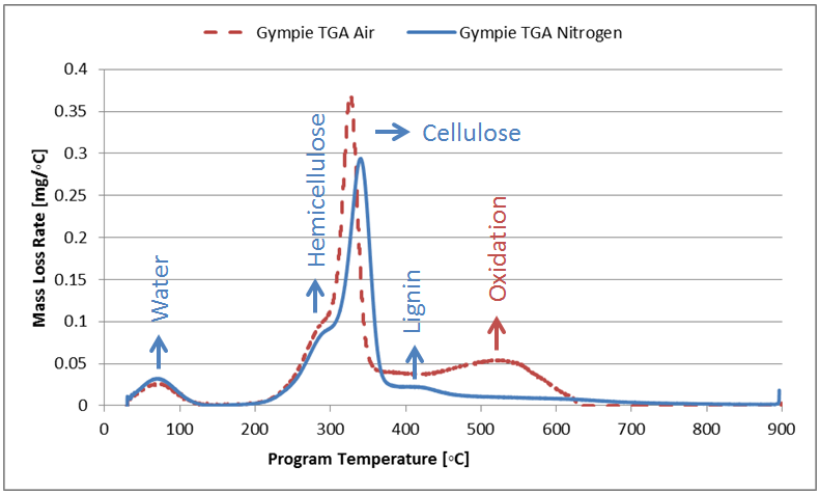

Figure 25: TGA analysis Gympie Messmate for both Nitrogen and Air atmospheres

In all of the TGA results (*Figure 25-27*) a similar mass loss rate trend can be observed. This demonstrates that the burning behaviour of all of the wood samples is mainly determined by the polymer and moisture content. So besides water evaporation no other significant pyrolysis processes take place than the decomposition of cellulose, hemicellulose and lignin.

Slight differences in the curves between species can be attributed to differences in polymer content, moisture content and the possible presence of some impurities in the samples. Moreover the location of the mass loss rate peaks might shift in temperature due to slight heating differences. For each test the sample mass is variable, these differences in mass might be due to small non-uniformities in the heating rates of the samples.

As can be observed from the data, the main pyrolysis temperatures for all tested species are within the same range. This allows for a bound to be placed on the main pyrolysis and oxidation temperatures of the different samples. The temperature bounds obtained in the TGA tests will be further used in the discussion of the MLC tests (i.e. the bounds for Radiata Pine are indicated in *Figure 26*).

Note that these observation also confirm the validity of the commonly assumed 300˚C [51] pyrolysis front temperature, since this temperature is within the experimentally observed bound.

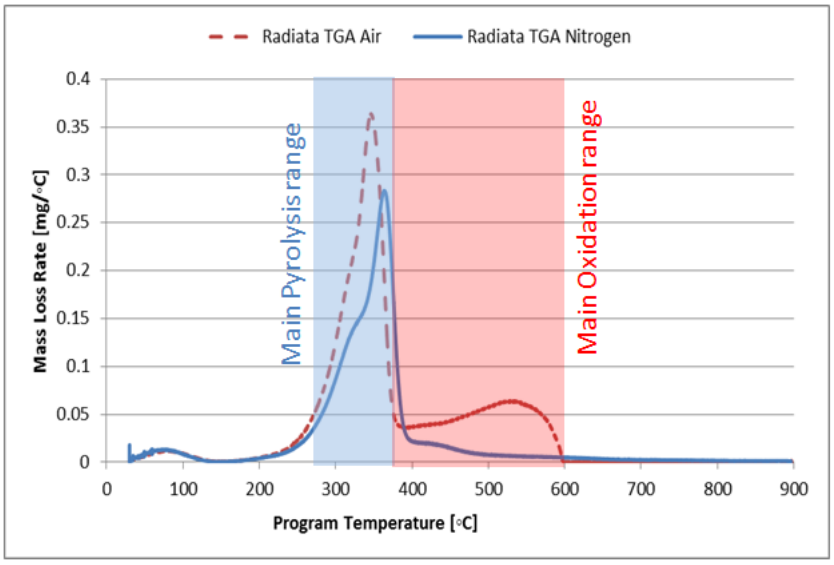

Figure 26: TGA analysis Radiata Pine for both Nitrogen and Air atmospheres

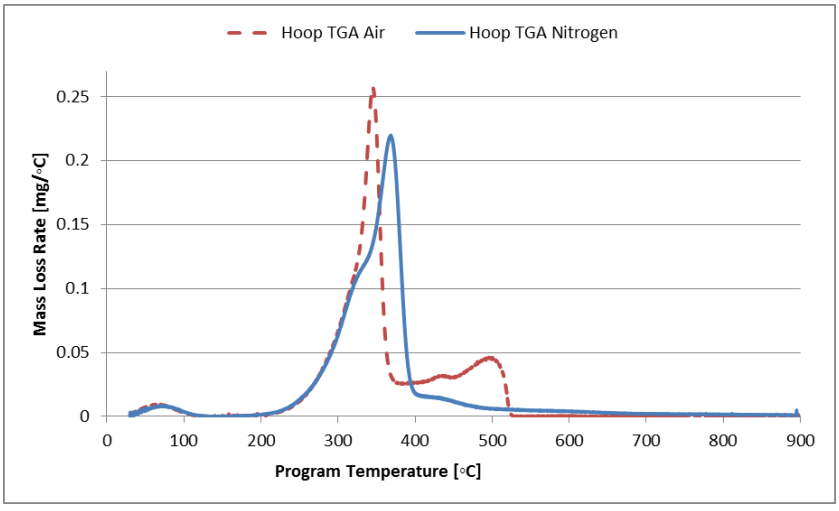

Figure 27: TGA analysis Hoop Pine for both Nitrogen and Air atmospheres

5.2 Detailed analysis of selected MLC test cases

In this section a selection of four MLC tests are elaborately discussed. Per test case an overview of the main visual observations is given followed by a discussion on the mass loss rate and temperature data.

The selected test cases are presented in *Table 5-2*.

Table 5-2: Overview of the selected MLC test cases

Test case	Sample type	Test type	Heat flux level [kW/m^2]	Exposure time [min]
1	Radiata Pine CLT	M	80	10
2	Radiata Pine CLT	TC	25	60
3	Hoop Pine CLT	TC	60	30
4	Gympie Messmate Glulam	TC	80	30

In a way these four test cases can be linked to almost all of the tests conducted for this thesis because specifically these tests cases include:

- The whole range of tested wood species
- Short exposure times combined with high heat flux levels and vice versa
- The visual observations of these tests cases include most of the visually observed phenomena during all MLC tests (e.g. flaming combustion, non-flaming combustion, a distinct moisture migration front, ply delamination, sustained burning and self-extinguishment after removal of the heat flux)

5.2.1 Radiata Pine CLT – 10 minutes exposure at 80 kW/ m² – Test type M

The first test case discussed is a Radiata Pine CLT sample which is exposed for 10 minutes to a heat flux of 80 kW/m^2, the test is of the type M. Sample dimensions: 102x101x72 mm, mass: 573.6 g, density: 773 kg/m^3.

5.2.1.1 Visual observations

Once the cone heater has reached the temperature set-point corresponding to 80 kW/m^2 the heat shield is removed from the cone heater. Already after 2 seconds of exposure, the front surface starts to become black and produces large amounts of white smoke. At 19 seconds of exposure, the white smoke gases ignite (see *Figure 28*). Once ignition occurs most of the produced pyrolysis gases burn, so as opposed to the initial glowing combustion phase very little smoke is produced during the flaming combustion phase. In the minutes after ignition, the average flame height drops down as the char layer builds up. This can be explained, as the char layer builds up less volatiles get released and thus also the average flame height drops down (see mass loss rate discussion further on).

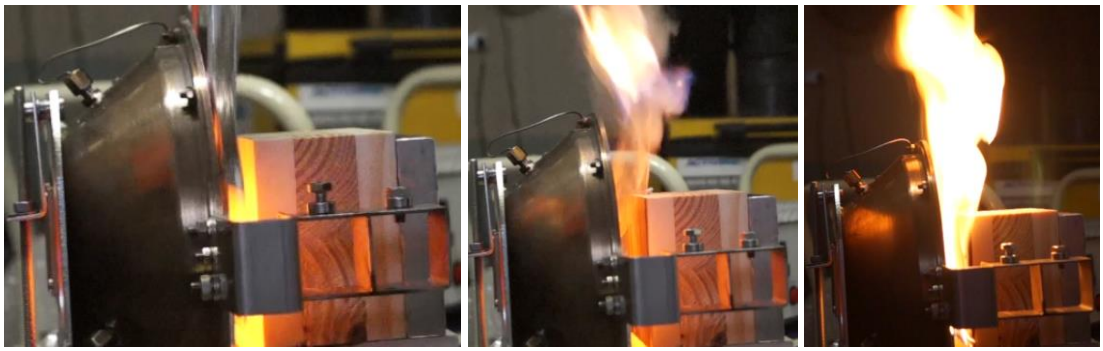

Figure 28: Removal of the heat shield and auto-ignition of the sample

After 10 minutes of exposure time the heat shield is placed back on the cone heater. The heat shield basically ensures that the external heat flux is almost immediately removed from the sample. Once the heat shield is placed over the cone, the flaming combustion does not immediately quench. Small flames on the front surface and side of the sample continue to burn another 2.5 minutes after removal of the heat flux. Once the flames near the front surface are quenched no significant glowing combustion near the surface is observed. Inside some of the cracks of the wood some glowing pieces can be observed but these are very local and quite small in surface area. Moreover distinct cracking sounds could be heard, indicating rapid cooling of the char layer after the flames have quenched.

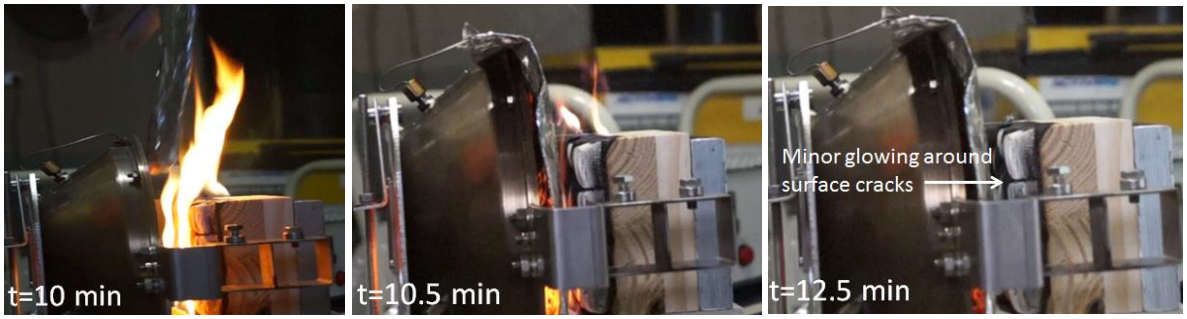

Figure 29: Removal of the external heat flux by placement of the heat shield at 10 minutes, after which most visual flames quench after 30 seconds but minor visual flames sustain for another 2 minutes and 32 seconds

5.2.1.2 Mass loss rate data

After removal of the heat flux data is collected until little temperature increases or mass loss rates are observed. This time interval varied from test to test.

Quite rapidly after removal of the heat flux the flames decay. Only small flames along the front surface sustain up until 2.5 minutes after removal of the heat flux. As can be seen from the Mass Loss rate curve in *Figure 30,* the mass loss rate after removal of the external heat flux immediately drops down. Note that the mass loss rate seems to drop just before rather than on the 10 minute mark, this is not due to a physical phenomenon but simply a consequence of the smoothing process.

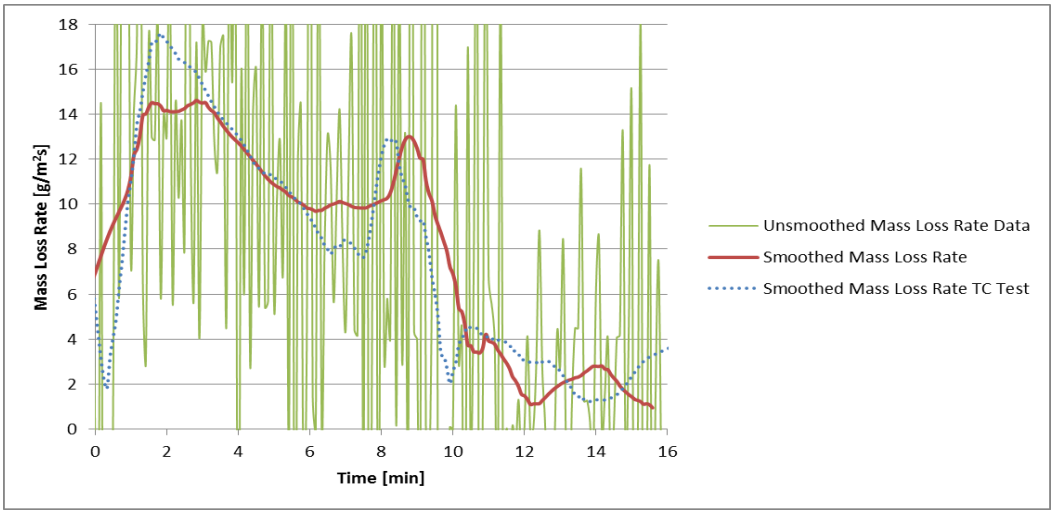

Figure 30: Mass Loss Rate for test case Radiata Pine CLT for 10 min of exposure at 80 kW/m^2

Now in order to obtain the thermal gradients inside the sample during combustion, a test with similar conditions but with thermocouple probes is conducted (test type TC). As can been seen from the data in *Figure 30*, the mass loss rate measurements for both test types (M and TC) are similar. In this case a separate mass loss rate test might not have been necessary. However the repeated M and TC tests do demonstrate the repeatability which can be achieved in this test configuration.

Furthermore the mass loss rate data in *Figure 30* clearly indicates a peak near ignition, after which the mass loss rate gently decays. This behaviour is generally observed in fire testing of wood and is due to the formation of the char layer (see *Section 3.4*). This also supports the visual observation that the flame height steadily decreases as the char layer thickness increases. Just before placement of the heat shield the mass loss rate goes to a second peak. This might be due to contact between the heat shield and sample holder, noise on the data, or indication of a change in the burning behaviour (for example increased burning of the first ply coupled with the onset of delamination).

After the shield has been put in front of the sample, the mass loss rate rapidly decreases to around 4g/(m^2.s). For both the M and TC test, sustained flaming was observed until a few minutes after removal of the heat flux. However this sustained flaming was minor and especially present on the sides and bottom of the sample, whilst most front surface flaming quenched after about 30 seconds. Given that in both test cases a similar mass loss rate near flaming extinction is measured, this would indicate that approximately 4g/(m^2.s) is the critical mass loss rate for flaming extinction (at least under these test conditions).

5.2.2 Radiata Pine CLT – 60 minutes exposure at 25 kW/ m² – Test type TC

The second case considered is a Radiata Pine 3 ply CLT sample exposed for 60 minutes to 25 kW/m^2, test type TC. Sample dimensions: 102x101x72 mm, mass: 405.7 g, density: 547 kg/m^3.

5.2.2.1 Visual observations

Similarly as in the previous case, the sample starts to produce white smoke shortly after exposure. However in this case the surface simple blackens after which it becomes glowing red without any occurrence of flaming auto-ignition.

In this test case a clear moisture front is visible, see *Figure 31*. Moreover it can also been seen that the moisture is front is 'trapped' or obstructed by the CLT bond lines (both in the horizontal and vertical direction). This indicates the adhesive influences/obstructs the moisture migration within the wood. Due to the moisture difference between the top and bottom part of the first ply, the top section chars away considerably faster. After about 40 minutes of exposure the top part of the first ply delaminates (see *Figure 31*).

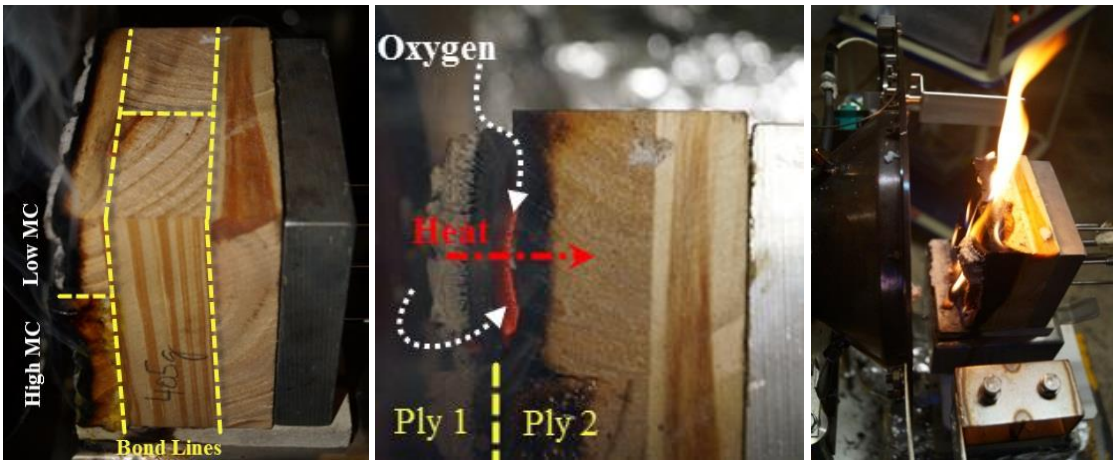

Figure 31: Left: Moisture migration front; Middle: partial delamination of the first ply, Right: complete delamination and flaming combustion

From 46 minutes onwards large parts of the first ply start to delaminate. It can be seen from *Figure 31* that prior to complete delamination the first ply starts to curl. The first ply effectively serves as a heat load to the second ply, whilst allowing oxygen to reach to the surface of the second ply.

In all cases were delamination occurred and the delaminated parts physically hit the cone heater, flaming ignition of the sample occurs. In the cases were delamination only occurred after removal of the heat flux

or if the delaminated layer remained leaning against the second ply, the burning parts of the first ply served as fuel for the second ply, effectively preventing or delaying self-extinguishment.

5.2.2.2 Mass loss rate data

Specifically for this test case ignition and major delamination occurred after 48 minutes of exposure. However this ignition is not to be called auto-ignition since it is more a consequence of failure of the element. These events also explain the peaks in the mass loss rate data (*Figure 32*). Because of delamination the mass loss data becomes invalid beyond 46 minutes (indicated in red in *Figure 32*).

Note that in most test cases data was continued to be collected even after delamination. Be aware that these results should be handled with care. First of all, mass loss rate measurements become invalid after delamination because the delaminated parts mostly fall off the sample holder or create an obstruction between the sample holder and cone heater, preventing sound measurements to be made. Secondly the front surface of the sample becomes very rough and effectively the distance between the cone heater and sample surface becomes unknown. If the distance between sample and cone is unknown, also the imposed heat flux becomes unknown.

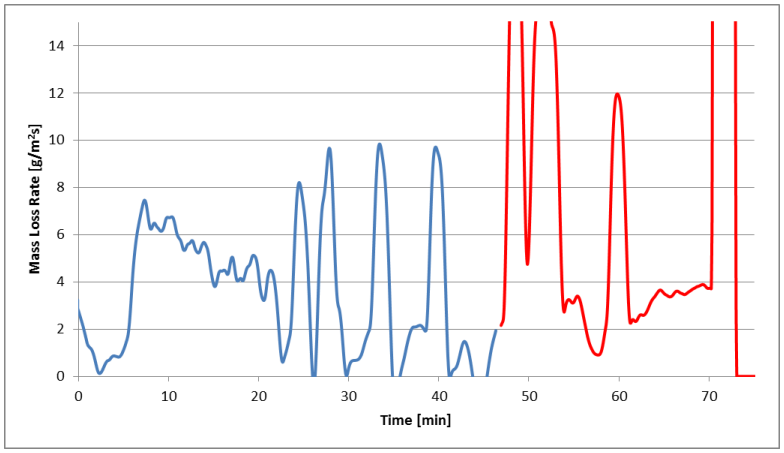

Figure 32: Mass Loss Rate for test case Radiata Pine CLT for 60 min of exposure at 25kW/m^2

From the mass loss rate data the average charring rate can be calculated, as discussed in *Section 3.4*. The average mass loss rate between minute 20-40 is calculated as 4.5g/(m^2.s). Using *Equation 3-17*, the average mass loss between minute 20 and 40 is found to be 0.5 mm/min:

$$w = \frac{\dot{m}_f''}{\rho_w} = \frac{4.5 \cdot 60}{547} = 0.5 mm/min$$

Because of the invalidity of the mass loss rate measurements after delamination it is was impossible to determine a critical mass loss rate for flaming extinction in this test case.

5.2.2.3 *Temperature data*

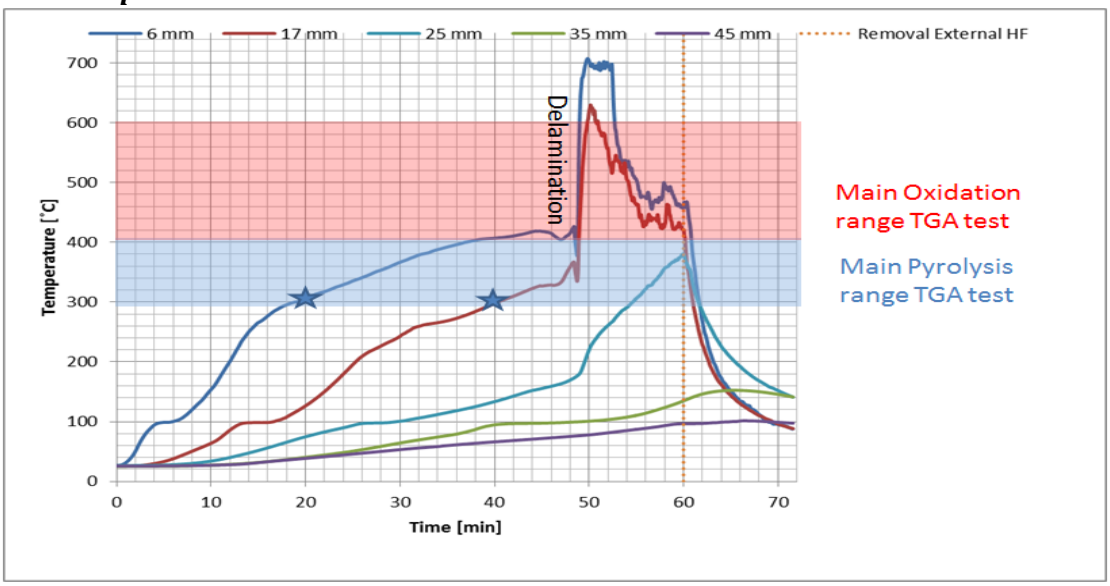

Figure 33: Temperature through time at different depths for test case Radiata Pine CLT for 60 min of exposure at 25kW/m^2

Figure 33 shows the thermocouple readings through time at different depths inside the wood sample. A distinct endothermic plateau near 100°C can be observed in the data. Where the first two thermocouples suddenly peak to their maximum temperature (46-48 min) delamination occurs. Because of this delamination the thermocouples at depths 5 and 15mm become completely exposed. In general once temperature readings have peaked beyond the maximum oxidation temperature of wood, the probes are most likely to have become exposed to the external heat flux or flame. So the temperature readings after they have peaked to around 600°C become irrelevant.

Quickly after removal of the external heat flux (60 min) the temperatures inside the wood drop. Note that the blue coloured range in *Figure 33* indicates the range where the main pyrolysis reactions occur, as derived from the TGA analysis in *Section 5.1*.

After removal of the heat flux all temperatures quickly drop below the pyrolysis range, indicating that self-extinguishment of the element occurs almost immediately after removal of the external heat flux.

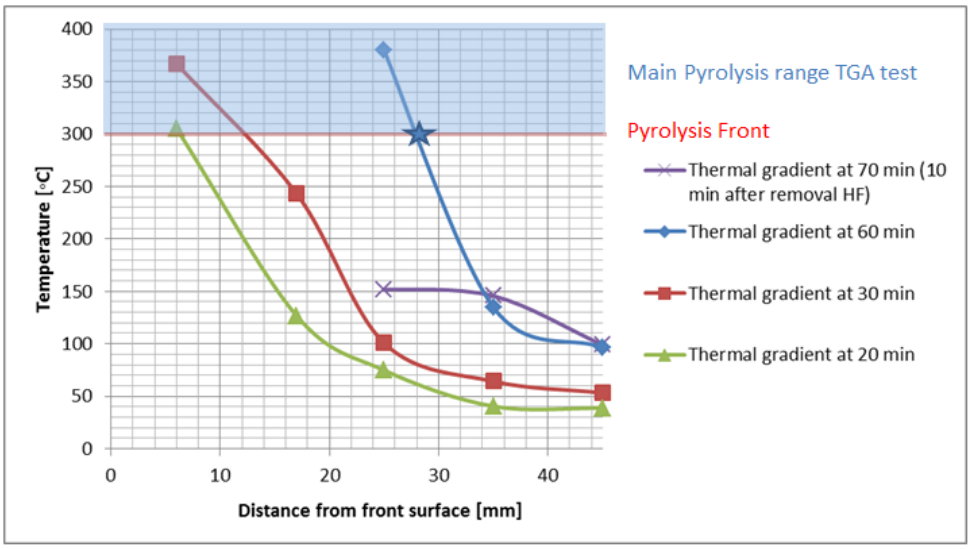

Figure 34: Temperature through thickness profiles at different times for test case Radiata Pine CLT for 60 min of exposure at 25kW/m^2

From the thermocouple data also the thermal gradients inside the timber at different time intervals can be derived (see *Figure 34*). It can be seen that the thermal gradient near the pyrolysis front stay more or less stable through time, indicating a form of steady-state conduction at the pyrolysis interface. Once the heat flux is removed of the sample, the steady state burning condition at the pyrolysis interface does not sustain. After 70 minutes (10 minutes after removal of the external heat flux) the temperature slope flattens as the heat propagates through the material and the front surface is no longer heated due to external heating or flaming.

Note that at depths 35 to 45 mm in both *Figures 33* and *34*, it can be seen that the temperatures continue to increase as the heat propagates through the material even after removal of the heat flux. These post-exposure temperature increases might be significant in the discussion of loss of bond strength. As the glass transition of epoxies occurs at relatively low temperatures, the bonds between different layers of wood might be lost at temperatures that are well below the temperatures that are significant for pyrolysis. For example epoxied steel rods in glulam timber have been found to already lose most of their strength from temperatures beyond 50°C[99].

As per the discussion in *Section 3.3.1*, the thermal gradient near the pyrolysis front will now be approximated. The thermal gradient near the pyrolysis front (indicated by the star in *Figure 34)* at 60 min is approximated by the thermal gradient between the thermocouples at depths 25 and 35 mm:

$$\left|\frac{\Delta T}{\Delta x}\right| = \frac{380 - 135}{0.035 - 0.025} = 24 \cdot 10^3 \; K/m$$

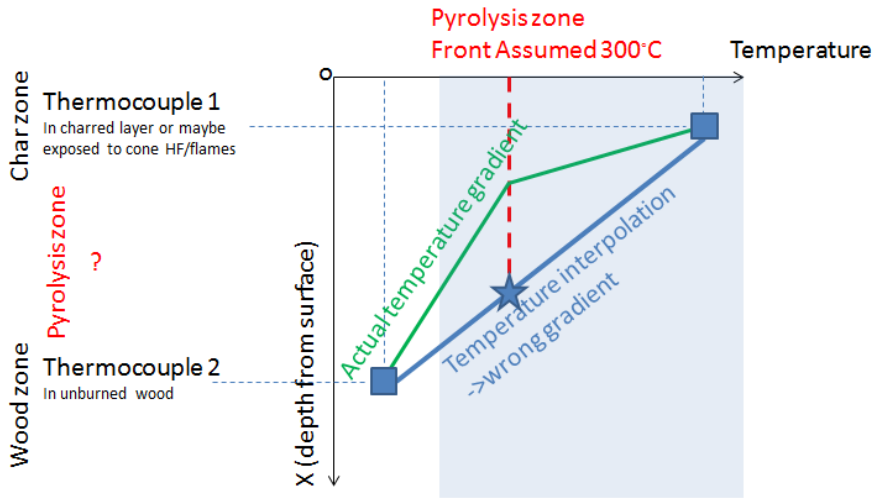

Figure 35: Approximation issues with the thermal gradient near the pyrolysis front

Note that in order to approximate the temperature gradient near the pyrolysis zone some issues need to be highlighted (see *Figure 35)*. Due to the difference in thermal conductivity between the wood and the char layer, there should be a thermal discontinuity at the pyrolysis front. In the data in *Figure* 34 no such discontinuity is observed. This way it is expected that the thermal interpolation obtained between a thermocouple in the char layer and a thermocouple in the wood layer does not accurately represent the thermal profile inside the wood. In reality two different temperature slopes are expected between these two thermocouples (see *Figure 35)*. So exactly determining the real temperature gradient near the pyrolysis zone with only this set of temperature data is fundamentally impossible. However in absence of any better method, the temperature gradient near the pyrolysis zone will be based upon the simple interpolation between the thermocouple readings. So it must be kept in mind whenever this approximation is made in the following this discussion, this implies a source of a major error. In the calculations that follow relatively larger error bars should thus be considered. Further in the text this thermal gradient will be related to extinction conditions and some simple design parameter. The goals is not to represent an accurate calculation, but simply to use the numbers for phenomenological purposes.

Now in order to minimize the associated error to calculating the thermal gradient, following consideration is kept in mind:

- Thermocouple measurement which are used as should be taken as close to the pyrolysis front as possible. Using data from exposed thermocouples in the char layer must be avoided because these probes might drastically increase the temperature slope due to the fact the measurement represent relatively high gas phase temperatures rather than the actual solid phase char temperatures.

Assuming the thermal conductivity k to be approximated by the two equations referred to in Annex D ($k = 0.18\ W/m.K$), the heat absorbed by the wood can be approximated by *Equation 3-13*[6]:

$$\dot{q}''_{in} = -k_{wood}\left.\frac{\partial T}{\partial x}\right|_{x=d^{+}_{char}} = \frac{0.18 \cdot 24 \cdot 10^{3}}{1000} = 4\ \mathrm{kW}/m^{2}$$

5.2.3 Hoop Pine CLT – 30 minutes exposure at 60 kW/ m² – Test type TC

The third case considered is a Hoop Pine 3 ply CLT sample exposed for 30 minutes to 60 kW/m^2, test type TC. Sample dimensions: 102x107x96 mm, mass: 528.0 g, density: 463 kg/m^3

5.2.3.1 Visual observations

Flaming ignition of the sample only occurred after 14min 27s. Note that this is an exceptionally long ignition time, since in most test cases at 60 and 80 kW/m^2 ignition occurred within the 120 sec. This long ignition time might be due to a high moisture content of the first ply, effectively delaying ignition. For example in the corresponding test type M, flaming ignition occurred within 60 sec.

As can be seen from *Figure 36* there is a significant increase in charring along the bond lines between the planks in the first ply. Although this figure was taken from the corresponding M test, this type of burning behaviour was observed in all samples where a bond line was present in the first layer.

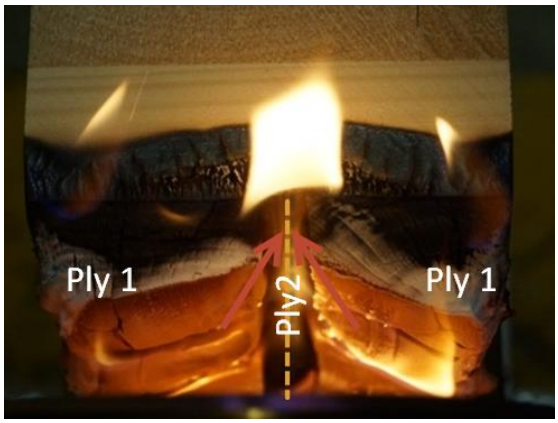

Figure 36: Significantly increased charring along bond line (Test type M)

After removal of the heat flux at 30 min, the sample sustained burning for another11 minutes. In both TC and M type tests, visual delamination occurred just around the 30 minute mark, after which burning sustained due to a contribution effect of the delaminated layer. As can be seen from *Figure 37*, around 10 sec after removal of the heat flux the average flame height significantly decreases. As the front ply completely delaminates (around 2min 26sec), the flame front moves from the front surface of the first

[6] Further justification and explanation on this calculation will be given in *Section 5.3.3*

ply to the front surface of the newly exposed second ply. Flaming extinction occurs around 11 minutes after removal of the heat flux. It must be added though that most flaming at the front surface only sustained about 6 minutes after removal of the heat flux, all further flaming was very localised around the delaminated parts.

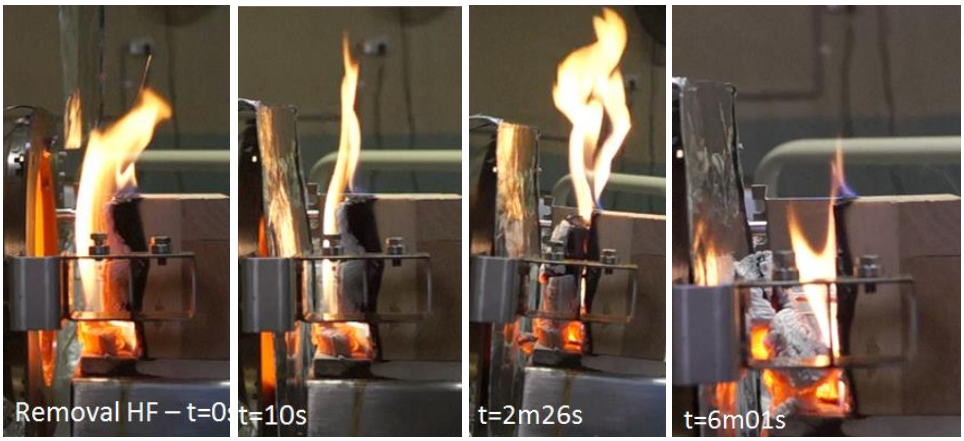

Figure 37: Removal of the heat flux after which ply delamination occurs, causing a movement of the flame front and increased flame height

5.2.3.2 Mass loss rata data

The analysis in *Section 5.3* will demonstrate that the mass loss rate data (under most conditions) is more or less independent from the fact if the samples are flaming or not. This observation can also be made in *Figure 38*, where the mass loss rate data for both the TC and M test are quite similar over the first 14 minutes, even though during that time period test M flamed whilst test TC was non-flaming.

The mass loss rate of flaming (test TC) and non-flaming/glowing (Test M) wood under no external heat flux can be discussed from *Figure 38*. This is possible because for test M flame extinction occurred within the first minutes after removal of the heat flux, whilst in test TC flame quenching only occurred after 11min. Following observations can be made from *Figure 38*:

- When there is no flaming after removal of the heat flux, the mass loss rate quickly drops down. In other words if flame quenching occurs the charring rate drops down.
- As long as flaming combustion sustains the temperatures stay stable or even increase within the pyrolysis range (see star in *Figure 37*). Again from the moment the external flaming stops (even though the sample is still glowing) the temperatures drop and quickly fall outside of the pyrolysis range.

These observations suggest that after removal of the heat flux, visual flaming is basically the key criterion determining if significant charring will sustain or not. Moreover this provides evidence that glowing combustion of timber after removal of the heat flux is not be relevant for charring, at least not within the tested heat flux and exposure time range and in the context of structural applications.

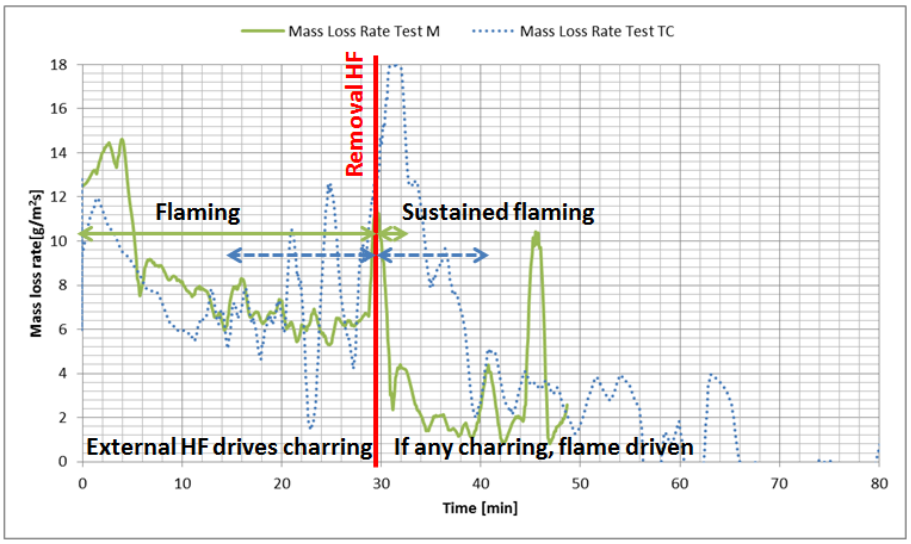

Figure 38: Mass Loss Rate for test case Hoop Pine CLT for 30 min of exposure at 60 kW/m^2

In test case M the mass loss rate for flaming combustion under no external heat flux goes from around 4g/(m^2.s) to below 2g/(m^2.s) when flaming extinction occurs, indicating a critical mass loss rate to be around 4g/(m^2.s). From the TC type test, the critical mass loss rate cannot be properly identified, because of delamination.

With the mass loss rate during exposure evolving towards an asymptotic value of 6g/(m^2.s) the charring rate can be calculated using *Equation 3-17*:

$$w = \frac{\dot{m}_f^{''}}{\rho_w} = \frac{6 \cdot 60}{514} = 0.7\ mm/min$$

5.2.3.3 Temperature data

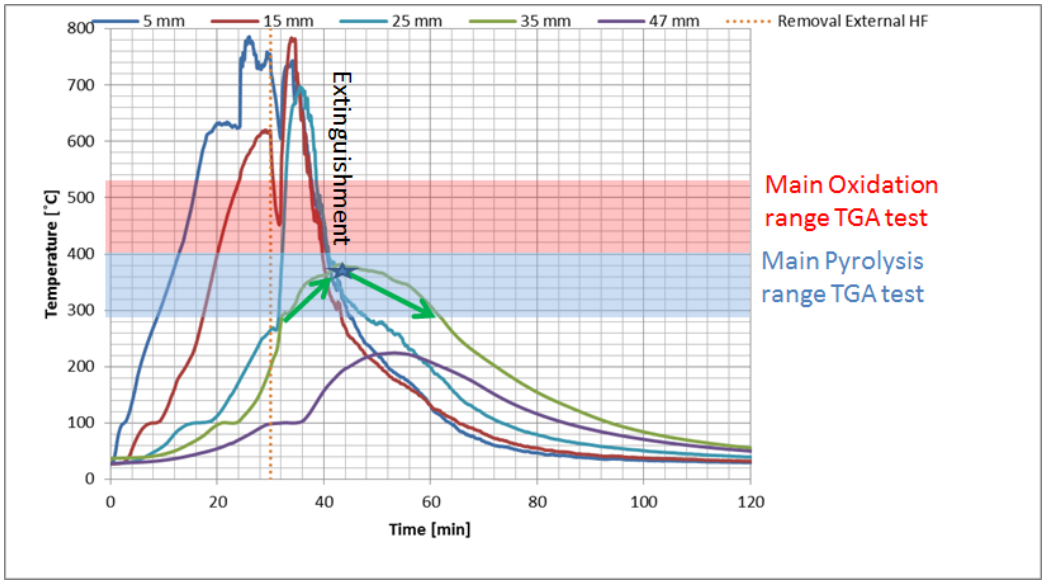

Figure 39: Temperature through time at different depths for test case Hoop Pine CLT for 30 min of exposure at 60 kW/m^2

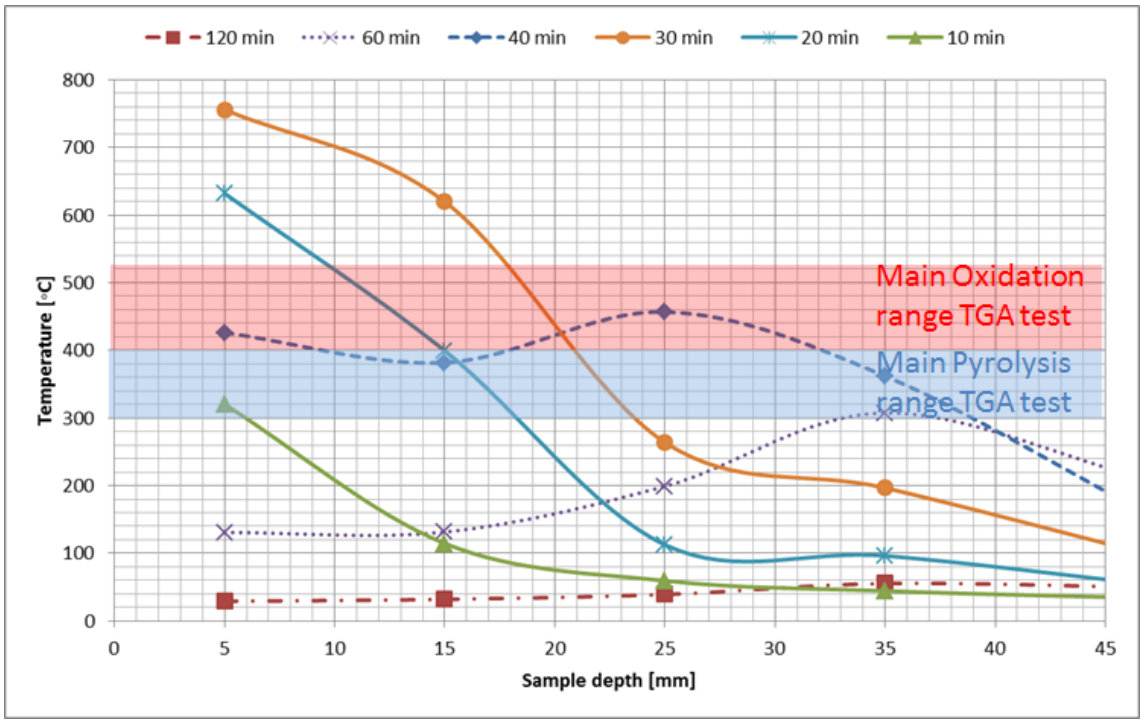

Figure 40: Temperature through thickness profiles at different times for test case Hoop Pine CLT for 30 min of exposure at 60 kW/m^2, dashed lines indicating temperatures measured after removal of the heat flux

Again the absorbed heat flux by the wood near the pyrolysis front is approximated. The thermal gradient near the pyrolysis front is approximated by taking the gradient between the thermocouples at 15 and 25mm from the temperatures measured at min 20 (see *Figure 40*). Also the thermal conductivity is approximated again by the average of the two models referred to in Annex D ($k = 0.18\ W/m.K$), the heat absorbed then becomes (*Equation 3-13)*:

$$\left|\frac{\Delta T}{\Delta x}\right| = \frac{399 - 113}{0.025 - 0.015} = 29 \cdot 10^3\ K/m$$

$$\dot{q}''_{in} = -k_{wood}\left.\frac{\partial T}{\partial x}\right|_{x=d^+_{char}} = \frac{29 \cdot 10^3 \cdot 0.18}{1000} = 5\ \text{kW}/m^2$$

5.2.4 Gympie Messmate Glulam – 30 minutes exposure at 80 kW/ m² – Test type TC

The third case considered is a Gympie Messmate glulam sample exposed for 30 minutes to 80 kW/m^2, test type TC. Sample dimensions: 102x106x60 mm, mass: 509.0 g, density: 785 kg/m^3.

5.2.4.1 Visual observations

Flaming ignition occurred within 10 sec of exposure, the average flame height drops down quite rapidly after ignition. After 10 minutes of exposure visual flaming is still present, but flaming does only occur around the front surface of the sample, so there is very little flame extension compared with the other species.

Almost immediately after ignition the surface of the wood starts to heavily deform. Relatively large pieces of the wood curl up and explosively shoot away from the wood. Glowing pieces of wood were found to be projected more than a metre away. This burning behaviour is only observed for the Gympie Messmate samples and at first sight glance seems to be similar to concrete spalling. This explosive behaviour of Gympie Messmate is also observed in bushfires were ignited trees have been reported to explode [100]. In this reports the explosive behaviour was mainly attributed to the presence of highly flammable Eucalyptus oil.

It is important to mark that in none of the test cases using Gympie Messmate glulam delamination was observed, even though in the glulam pieces all of the bond lines are basically exposed. Providing strong evidence that the fire performance of the bond used for glulam (phenol formaldehyde) has superior fire performance compared to the bond used for CLT (polyurethane glue). This is in line with the research of *Frihart and Hunt* [101] who state that phenol formaldehyde actually more resistant to high temperatures than wood itself, whilst this is not the case for polyurethane glues.

Figure 41: Spalling burning behaviour of Gympie Messmate viewed from the side of the cone and through the cone heater

5.2.4.2 Mass loss rate data

As observed in all of the Gympie Messmate tests, the mass loss rate is highly fluctuating. The mass loss rate starts at relatively high peak values compared to the other species. Shortly after ignition (first 10 min) the mass loss rate trend is quite stable, however near the end of the test the mass loss rate trend starts to heavily fluctuate. After removal of the heat flux the flames almost immediately quench.

The mass loss rate data from the corresponding type M test gives a similar trend as in the TC type test, demonstrating repeatability between both tests (*Figure 42*).

With the mass loss rate during exposure averaging 7g/(m^2.s) (averaged over data from 10 to 30 min) the charring rate through *Equation 3-17* becomes:

$$w = \frac{\dot{m}_f^{"}}{\rho_w} = \frac{7 \cdot 60}{785} = 0.5\ mm/min$$

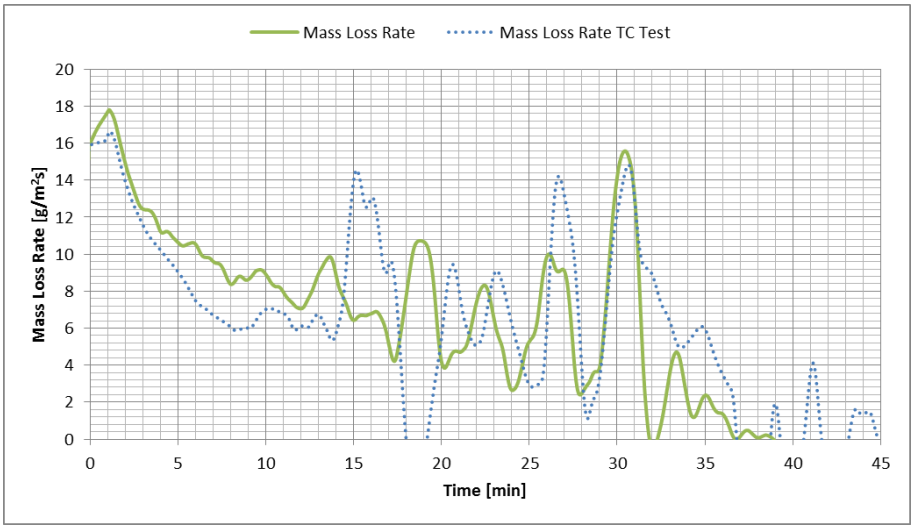

Figure 42: Mass Loss Rate for test case Gympie Messmate Glulam for 30 min of exposure at 80 kW/m^2

5.2.4.3 Temperature data

Again also the absorbed heat flux into the wood can be calculated. The thermal gradient near the pyrolysis front is approximated by taking the gradient between the thermocouples at 5 and 15 mm at minute 20 (see star in *Figure 43*). Also the thermal conductivity is approximated again by the average of the two models referred to in Annex D ($k = 0.20 W/m.K$), the heat absorbed then becomes:

$$\left|\frac{\Delta T}{\Delta x}\right| = \frac{401 - 140}{0.015 - 0.005} = 26 \cdot 10^3 \; K/m$$

$$\dot{q}''_{in} = -k_{wood} \left.\frac{\partial T}{\partial x}\right|_{x=d^+_{char}} = \frac{26 \cdot 10^3 \cdot 0.20}{1000} = 5 \text{ kW}/m^2$$

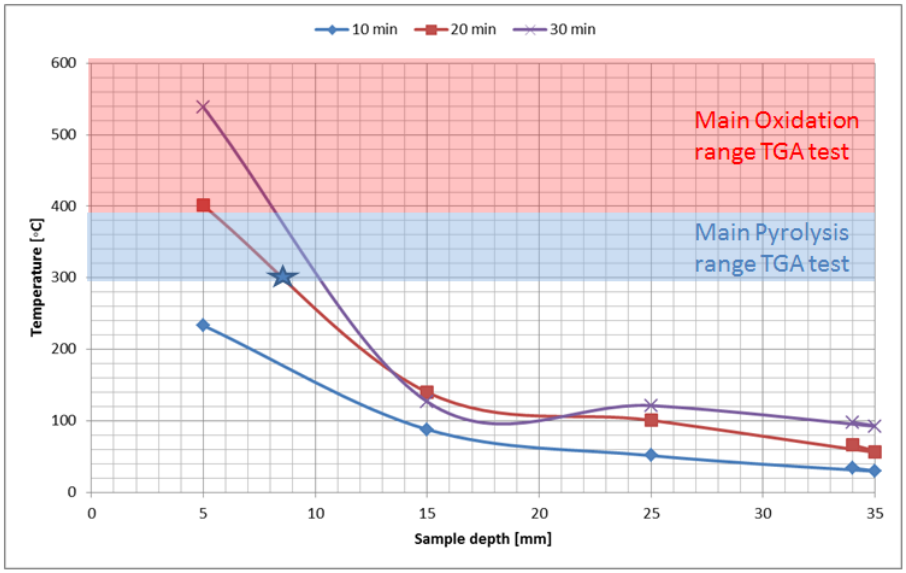

Figure 43: Temperature through thickness profiles at different times for test case Gympie Glulam for 30 min of exposure at 80 kW/m^2

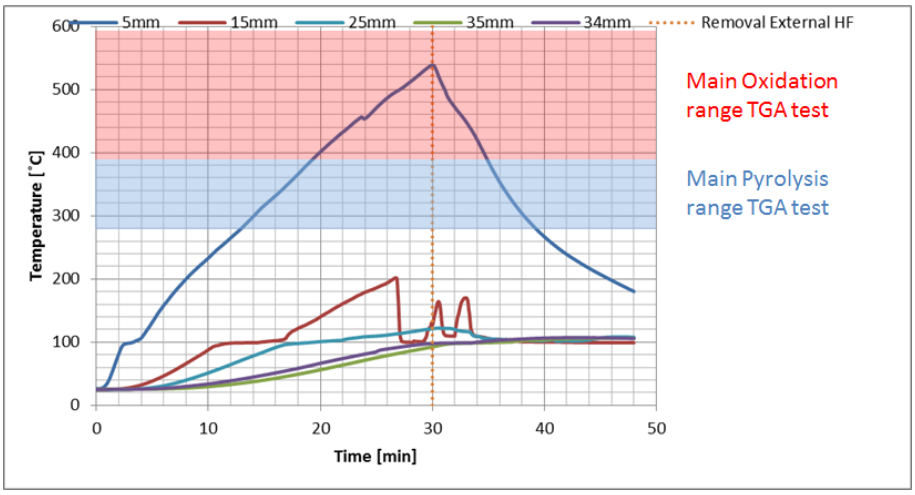

Figure 44: Temperature through time at different depths for test case Gympie Messmate Glulam for 30 min of exposure at 80 kW/m^2

Note that around min 26 the temperature of the thermocouple at 15mm suddenly drops, at this time the sample was still exposed to the external heat flux and consequently sudden temperature drops are not expected. After the experiment is finished the depth of the thermocouples was always checked, so it is unlikely that the thermocouple moved. It is believed that this drop of temperature has to do with moisture migration inside the wood. Water might have condensed inside the thermocouple drill hole. This scenario

is plausible because the holes in the wood are slightly wider than the thermocouple probes themselves and it was observed in some tests that water seeped out of thermocouple holes at the back of the sample.

5.3 General results and discussion MLC tests

In this section the general results of the different MLC tests are discussed. Note that in this discussion all results are obtained from the Radiata Pine CLT samples. Wherever a discussion on the results of the other test samples is appropriate a clear distinction between the species will be made.

5.3.1 Visual observations

In all test cases at exposure levels 60 and 80 kW/m^2 flaming auto-ignition occurred, generally within the first few minutes of exposure. At levels of 25 and 40 kW/m^2 auto-ignition was not normally not observed. In all cases of 25 and 40 kW/m^2 where flaming was observed, except for one case, the flaming was a consequence of ply delamination rather than actual auto-ignition

After removal of the heat flux from the flaming samples, the flames generally quenched within the first few minutes. Whenever flaming was observed beyond the first minutes, flaming was mostly very small and localised near deficiencies such as partly delaminated layers. Whenever flame quenching did not occur, glowing parts of delaminated layers were found to serve as a heat/fuel load for the sample to continue to combust.

Delamination of the Radiata pine CLT samples occurred at all heat flux levels, with only a few samples delamination at lower heat fluxes and consistent delamination at the higher heat fluxes. At 25 kW/m^2 delamination occurred after approximately 35 min of exposure, whilst at 40 kW/m^2 delamination occurred around the 25 minute mark. At heat flux levels of 60 and 80 kW/m^2 delamination occurred more often and from around 16 min of exposure onwards. Note that delamination during tests type M, seemed to consistently occur earlier and more frequent than during the corresponding TC type test. This observation suggests that the thermocouple probes in the sample effectively prevent or postpone ply delamination.

Table 5-3: Main visual observations MLC tests, over all exposure times, heat flux levels and species

Considering all exposure times and species	**Heat flux [kW/m^2]**	
	25/40	**60/80**
Auto-ignition and Flaming combustion?	In general no auto-ignition. Flaming did sometimes occur as consequence of delamination.	Flaming auto-ignition systematically occurred within first few minutes of exposure.
Delamination?	Yes, but very random and only after 25 to 30 min of exposure.	Yes consistent delamination of first ply from around 16 min onwards.
Extinguishment?	Consistent flaming extinction over main front surface within first minute after removal heat flux (only minor flaming occurring for an extended time). Whenever extinction did not occur within first few minutes, sustained flaming was attributed to ply delamination	

5.3.2 Mass loss rate data

Figures 46 to 48 indicate that the mass loss rate more or less strives towards an asymptotic value independent of the imposed heat flux.

Note that in all represented cases in *Figures 46 to 48* with heat fluxes 25 to 40 kW/m^2 no flaming auto-ignition occurred, expect for one case (40 kW/m^2 for 30 min of exposure). In all other cases (60 and 80 kW/m^2) flaming auto-ignition did occur. In other words, during exposure to a heat flux range of 25 to 80

kW/m^2, the mass loss rate goes towards a similar asymptotic value, which seems to be independent from the fact it the sample is flaming or not.

When taking the average mass loss rate during exposure of all cases (Radiata Pine CLT), with exclusion of data points collected after delamination, an asymptotic of 6g/(m^2.s) is obtained.

Using *Equation 3-17* an average charring rate under external heat flux can be calculated:

$$w = \frac{\dot{m}_f^{"}}{\rho_w} = \frac{6 \cdot 60}{635} = 0.6\ mm/min$$

Keeping in mind that the charring rates, near steady state conditions, under relatively high heat fluxes[7] are only slightly dependent on the external heat flux [73]. The experimentally determined charring rates can thus be compared to rates obtained under other heating conditions. For example *EN 1995-1-2* [51], prescribes a charring rate of 0.65 mm/min for softwoods and 0.5 mm/min for hardwoods. These literature values are more or less in line with the experimentally obtained charring rates. For example in *Section 5.2* it was found that the charring rate for Hoop Pine was 0.7 mm/min (softwood) and for Gympie Messmate 0.5 mm/min (hardwood).

Not that the sporadic peaks in the data in *Figures 46-48* are due to delamination of the CLT layers.

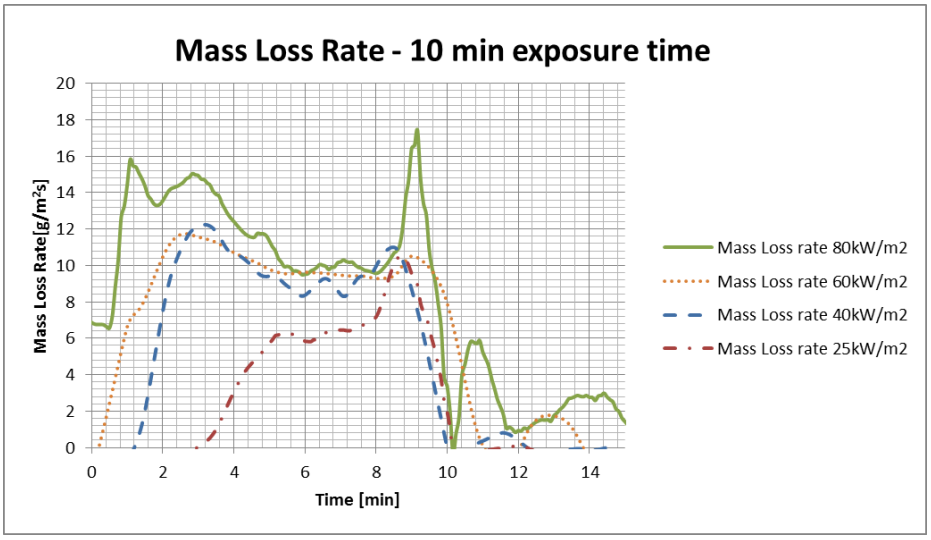

Figure 45: Mass loss rata data 10 minutes of exposure Radiata Pine CLT at different heat flux levels

[7] With relatively high heat fluxes, indicating heat fluxes well beyond the critical radiant heat flux for ignition of wood which is considered to be 12 kW/m^2 [25].

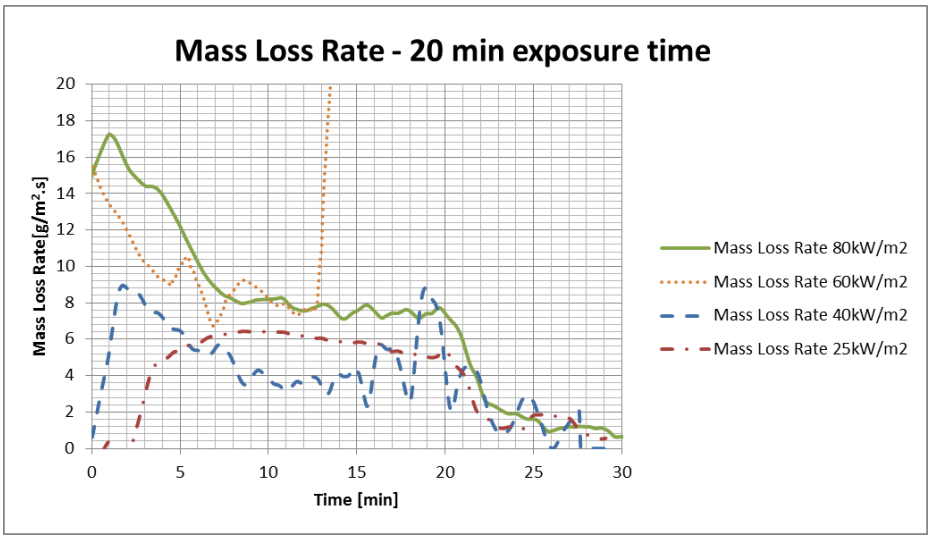

Figure 46: Mass loss rata data 20 minutes of exposure Radiata Pine CLT at different heat flux levels

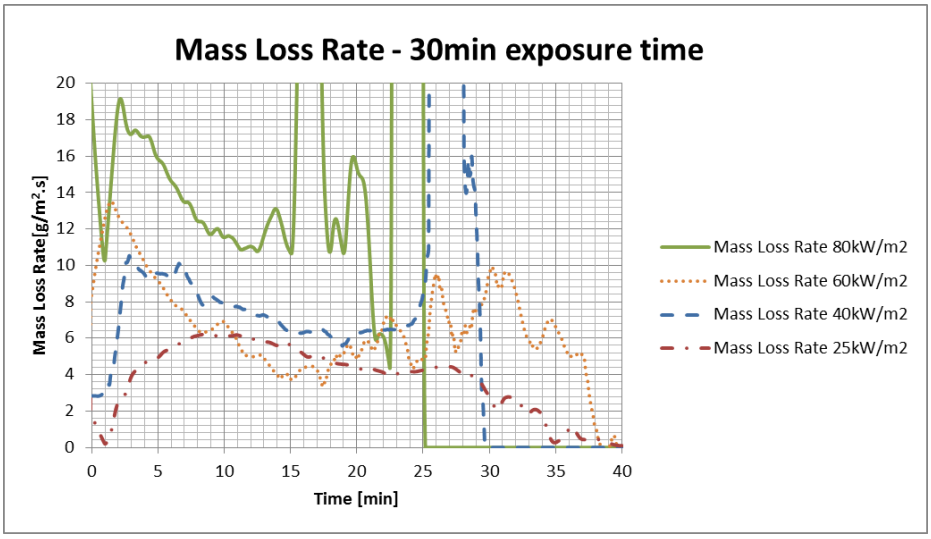

Figure 47: Mass loss rata data 30 minutes of exposure Radiata Pine CLT at different heat flux levels

The lowest mass loss rate which has been repeatedly observed for flaming combustion under no external heat flux, just before flame quenching, is found to be around 4 g/(m^2.s). This indicates the critical mass loss rate for flaming extinction will be roughly 4 g/(m^2.s), this corresponds to the range of 0.5-5.5 g/(m^2.s) which has been reported in literature for an assortment of different materials [90], [91]. Note that in a lot of test cases, where delamination occurred, the mass loss rate measurements after delamination became invalid to use. In all these test cases it was impossible to determine a critical mass loss rate for extinction.

When comparing the mass loss rate data between the different species (see *Figure 48*) it can be seen that for all species a similar moss loss rate trend can be observed. Even more the mass loss rate trend seems to reach an almost similar asymptotic value for the different species. Keeping in mind the density differences of the species and a more or less constant mass loss rate, clearly the denser the wood, the less the char front will advance and vice versa. So the denser the wood, the slower the charring rate will be. This can also be confirmed by previous charring rate calculations.

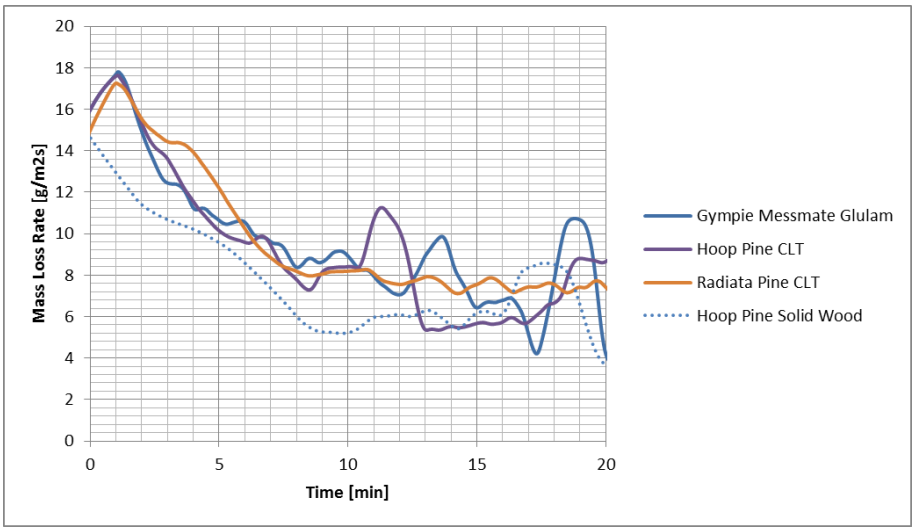

Figure 48: Mass Loss Rate Comparison different species over first 20 min of 80 kW/m^2 exposure

The tests conducted with Hoop Pine CLT for 30 minutes of exposure at 60 and 80 kW/m^2 were repeated with solid blocks of Hoop Pine. Via a comparison of the mass loss rate data (*Figure 49*) it can be demonstrated that CLT behaves almost identical to a corresponding piece of solid wood, at least as long as no delamination occurs. Given that the mass loss rate for both the solid wood and the corresponding CLT product are similar, also the charring rates will be similar.

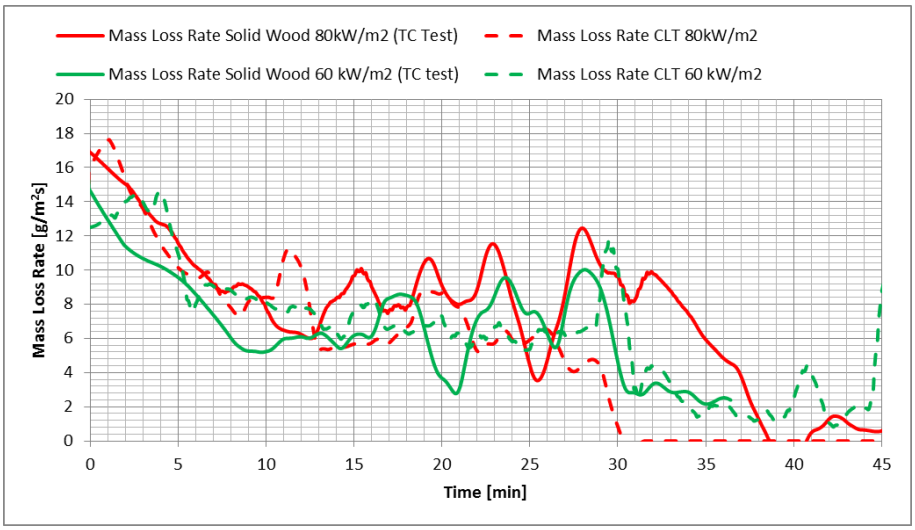

Figure 49: Mass Loss Rate for Hoop Pine solid wood and CLT for 30 min of exposure at different heat flux levels

5.3.3 Temperature data

When comparing the thermal gradients between the different species (see *Figure 50*) it can be seen that the Radiata Pine and Hoop Pine CLT samples show a more or less similar trend near 300˚C. The Gympie samples also demonstrate a similar trend near 300˚C, with the difference that the Gympie samples clearly have a significantly longer endothermic plateau near 100˚C.

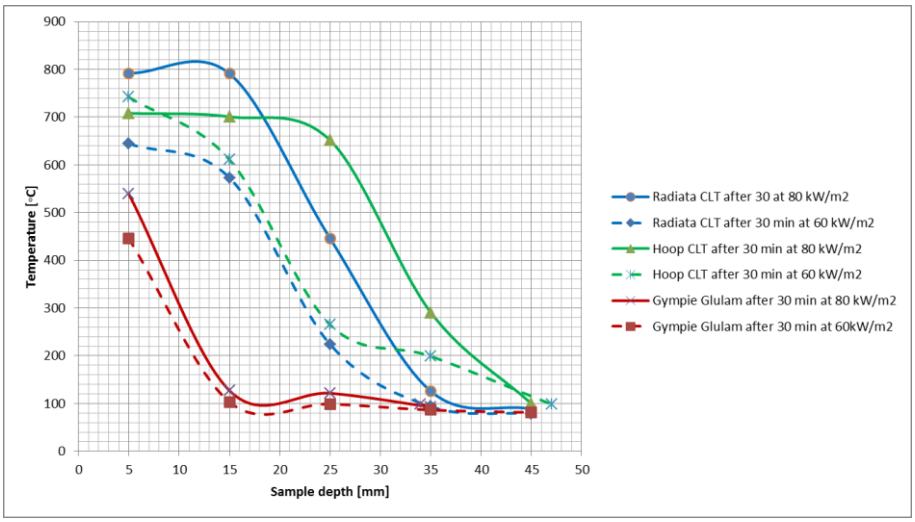

Figure 50: Temperature through thickness profiles at 30 minutes for different species and different heat flux levels

Another interesting observation to make in *Figure 50* is that all of the presented temperature profiles seem exhibit the same slope near the pyrolysis front. *Figure 51* gives another example of temperature profiles which seem to show the same slope near the pyrolysis front at different time intervals. In general the observation of an almost constant slope near the pyrolysis front can be made in most of test cases (so at the different heat flux levels and exposure times) where flaming combustion occurred.

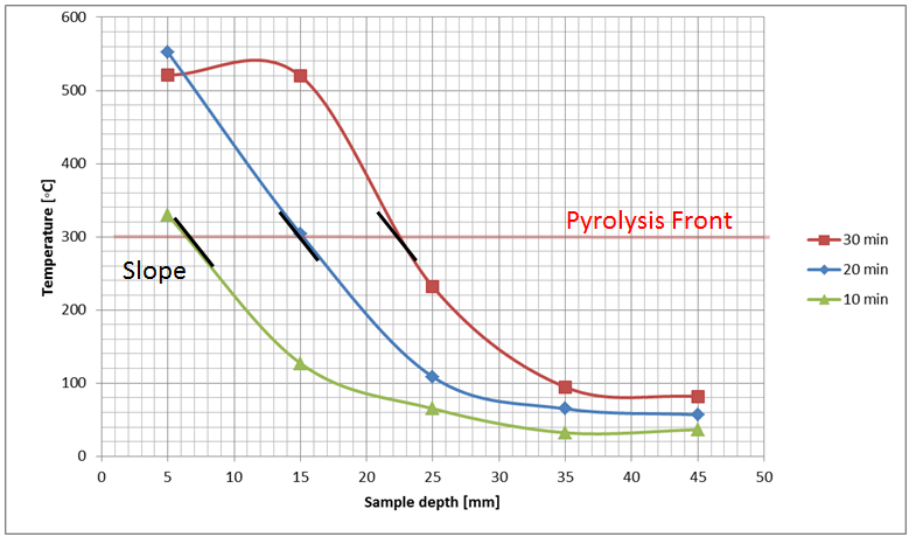

Figure 51: Temperature through thickness profiles at different times for test case Radiata Pine CLT for 30 min of exposure at 60 kW/m^2

For most species the slope of the temperature profile near the pyrolysis front seems to be similar from around 10 minutes onwards till the end of the exposure time.

As per the discussion in *Section 3.3.1*, the steady state thermal gradient will now be calculated in order to discuss the energy equation at the interface.

Table 5-4 gives an overview of the estimated thermal conductivity k of each species at 300°C, derived on the basis of Annex D. Next the average thermal slope near the pyrolysis front is presented per species. This average slope is taken from the slope near the pyrolysis front for all TC test cases. The slope for each case was calculated at the time the heat flux was just removed, so depending on the test case at minute 10, 20 or 30. From this average slope the heat flux absorbed by the virgin wood can be approximated by *Equation 3-13*.

$$\dot{q}''_{in} = -k_{wood} \left.\frac{\partial T}{\partial x}\right|_{x=d^{+}_{char}}$$ **Equation 3-13**

Table 5-4: Calculations of the thermal gradient of each species at the time of removal of the heat flux averaged over all tested cases

Species	$k\ [\frac{W}{m.K}]$	$\left\|\frac{\Delta T}{\Delta x}\right\|_{average}\ [\frac{K}{m}]$	$\left\|\dot{q}''_{in,average}\right\|[\frac{kW}{m^2}]$
Radiata Pine	0.18	$21 \cdot 10^3$	4
Gympie Messmate	0.2	$26 \cdot 10^3$	5
Hoop Pine	0.18	$23 \cdot 10^3$	4

Now keep in mind that it was visually observed that flame quenching occurred for most samples (neglecting delaminated samples) shortly after removal of the external heat flux. Moreover from the discussion in *Section 3.3.1* it can be argued that the just calculated heat flux corresponds to heat losses at the interface when extinction occurs. This leads to the evidence that once the heat flux is removed from the samples, whatever heat flux is conducted through the char layer is not enough to compensate for the losses (approximated to be 4 kW/m^2). When calculating the absorbed heat flux per test case all calculated absorbed heat fluxes were observed to be in a bound between 2 to 6 kW/m^2.

From a practical point of view, calculating this absorbed heat flux might not seem a meaningful concept in this discussion. However it will now be illustrated that this evaluation might actually be very meaning full for structural design. It cannot be emphasised enough that the method used to calculate the thermal gradient and consequently the absorbed heat flux in this discussion is prone to many errors. However these calculations were made to prove a concept, rather than an exact quantification.

In the context of structural fire design one is interested in linking the concept of self-extinguishment to a parameter which can easily be determined by a designer.

For illustration purposes a simple link between extinction and the total charring depth will be elaborated here, this link will be based upon the simple energy balance as described before. The example given below is just to demonstrate the possibilities of future research[8]. The broad aim of this example is that further research will go into developing an easy to use link between extinction conditions and a parameter that can easily linked to structural fire design.

5.3.3.1 Intermezzo: Example calculation of a critical charring depth for extinction

In this example a critical charring depth will be calculated. All following statements consider that the assumptions of the simple 1D heat transfer balance as described in *Section 3.3.1(Equation 3-14)* hold.

By making following simplifications the heat flux conducted through the char layer is approached in a very crude manner:

- Char oxidation happens at the surface of the char layer at a constant temperature, which is assumed to be 600°C. This temperature corresponds to the maximum temperature at which oxidation occurred in the Radiata Pine TGA test.
- Char conduction is quasi steady-state.
- The char conductivity is assumed to be 0.25 W/(m.K). This value is visually derived from *Figure 1* in annex D taking the average conductivity at 600°C.

[8] The example that follows is based upon crude approximations and guesses, not based upon the true physics of the problem. These solutions should thus not be used in any other context than this example.

It is proposed that the critical charring depth corresponds to a thermal gradient inside the char so that the heat transferred through the char at the interface layer just equals the heat absorbed by the wood at the interface. This implies that for similar boundary conditions all larger charring depths will definitely lead to extinction, as the heat gains near the interface will become lower than the heat losses.

Based upon the just calculated heat loses near the pyrolysis front that ranged between 2 to 6 kW/m^2. The critical charring depth can now be easily calculated. Consider *Equation 3-14,* assuming extinction occurs when the heat losses just compensate the gains:

$$Extinction \rightarrow \Delta H_{p,wood}\dot{m}''_{f,wood} \approx 0 \leftrightarrow k_{char}\left.\frac{\partial T}{\partial x}\right|_{x=d^-_{char}} \approx k_{wood}\left.\frac{\partial T}{\partial x}\right|_{x=d^+_{char}}$$

$$0.25 \cdot \left(\frac{600-300}{d_{char,crit}}\right) \approx 2\ to\ 6 \cdot 10^3 \rightarrow d_{char,crit} \approx 40\ to\ 10\ mm$$

5.4 Error treatment

In this section a qualitative error analysis is conducted. The main discussion is focussed on random errors in the data. Systematic errors are expected to be minimised by making sure the test equipment is adequately calibrated and that the test procedures as described in *Section 4.2* are strictly followed.

5.4.1 Mass loss rate data

The noise in the mass loss measurements was smoothed with the help of a Locally Weighted Polynomial Regression [97]. The moving regression for all presented experimental data was kept constant at 34 points.

In order to validate the Mass Loss Rate data the average mass loss rate data at 40 kW/m^2 is compared to the values obtained by *Reszka* [96] in *Figure 52*. Quite good agreement between literature values and the tests can be found. Note that difference exist due to the fact *Reszka* [96] probably averaged over a considerably larger sample group and a different type of species was used (Redwood Pine), most importantly also the type of smoothing applied is different. Besides these small differences, the trend is clearly quite similar.

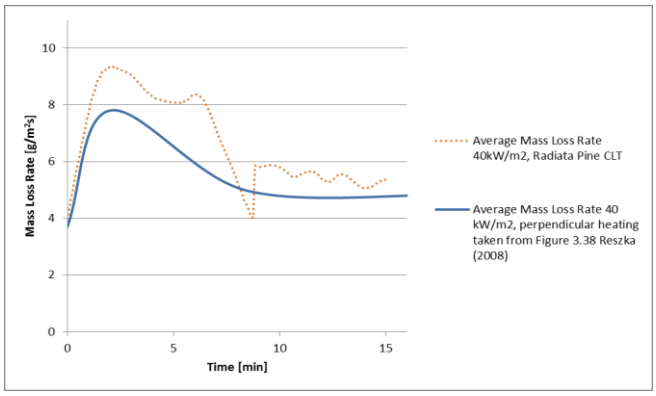

Figure 52: Comparison mass loss rate data to literature values

Repeatability between the different tests has been demonstrated in several instances by comparing the mass loss rate data of the type TC and M test (e.g. mass loss rata charts *Section 5.2*).

It must be noted that throughout the tests it has been found that certain factors had a large influence on the mass loss rate data, where possible these factors were avoided as much as possible:

- Ply delamination

- Externally induced movements of the sample holder and sample through physical contact (e.g. contact of the heat shield), high air flows (e.g. opening doors/windows in the lab), or movement of the embedded thermocouple probes.

5.4.2 Temperature data

Data in *Figure 53* presents temperature profiles over the first 10 minutes of the tests on Radiata Pine CLT samples exposed to 60 kW/m^2. The comparison is made over the first 10 min because this is the minimum exposure time all tests cases received, so in theory within this timeframe all the data should lead to similar results. As can be observed the repeatability of the temperature measurements is not very good. The random errors on the temperatures measurements are thus quite significant. The differences in temperature measurements in *Figure 53* are expected to be mainly due to a difference in burning behaviour between all samples. However there are several factors that might have had a significant impact:

- Errors in thermocouple readings due to misalignments of the drilled thermocouple holes inside the wood. These errors are expected to be a small as possible because of following the correct drilling procedure.
- Accidental movement of thermocouple probes inside the timber element due to external effects, such as accidentally hitting the thermocouple wires. These errors should be minimised because all physical contact with the test rig during actual testing was avoided.
- Movement of the thermocouple positions due to the burning behaviour, e.g. water vapour induced pressure moving the probes backwards or delamination causing thermocouple movement.
- Differences in the burning behaviour of the samples itself because of variations in samples such as MC, position of bond lines, position of localised defects and general density differences.

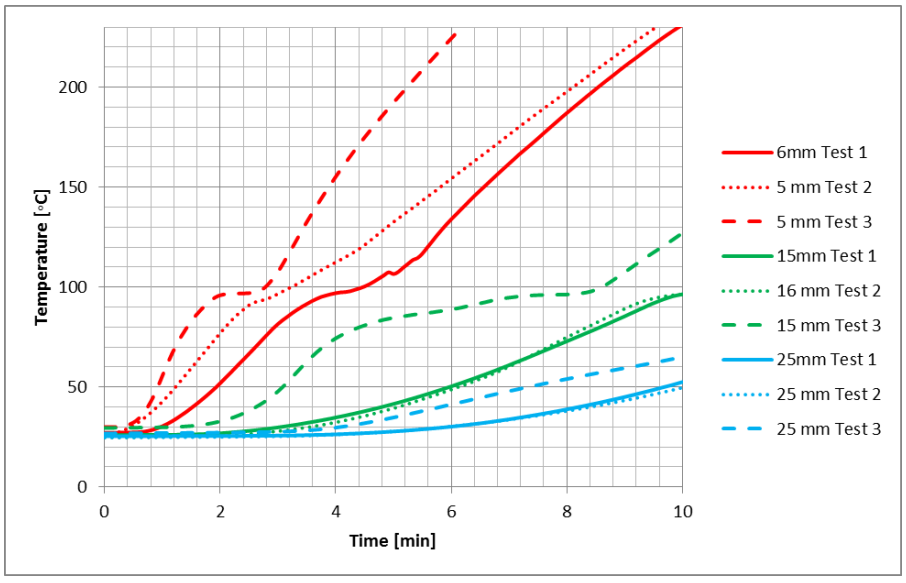

Figure 53: Temperature through thickness profiles at 10 minutes for repeated Radiata Pine CLT samples at 60 kW/m^2

5.4.3 1D Heating Assumption

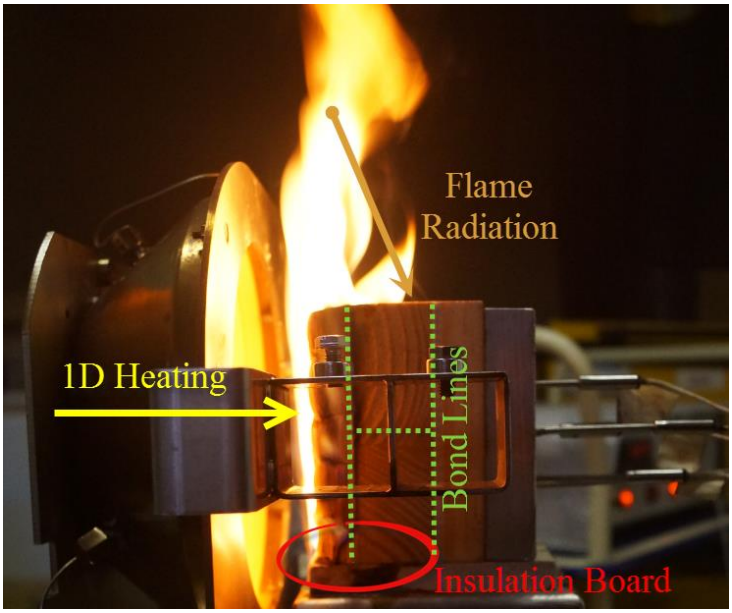

Figure 54: Multi-dimensional heating effects

Making a 1D heat transfer model as proposed in *Section 3.3.1* is possible because during exposure the main and imposed heating direction from the cone is predominantly one-dimensional. However due to a number of burning effects of the wood, a simple 1D may not be without error.

A at lower heat fluxes (25kW/m^2 and 40 kW/m^2) where mostly no flaming combustion is involved the samples seemed to char relatively uniformly in the main heating direction. However there are a number of effects that created non-uniform or multi-dimensional heating (see *Figure 54)*:

- Increased charring along all bond lines, bond lines not only exist between the different plies but also between the planks forming a ply.
- Different MC between timber planks. Due to the bonds the moisture seemed to be mostly trapped between different glue lines, creating non-uniform moisture migration effects.
- Flame spread along top surface because of flames occurring above the sample. A similar but less strong effect is observed along the sides of the sample.
- Thermal effect of the insulating ceramic board at the bottom of the sample.
- Different burning behaviour due to the presence of imperfections (knots) in the samples themselves.
- Delamination or partial delamination of pieces of ply.

Considering that on the temperature measurements there is already a noticeable random error, it is needless to say that all calculations presented before, based on thermal gradients and the simple 1D heat transfer model, contain even bigger errors. It is important to note in all of these calculations two main sources of error are introduced.

- Errors due to the temperature measurements themselves.
- Major errors due to models and assumptions which are not accurately representing the true physical phenomena.

5.5 Conclusions

The pyrolysis and oxidation behaviour of different species has been analysed by a TGA test. For all tested wood products the main pyrolysis behaviour is practically completely determined by the pyrolysis of the three main wood polymers, namely cellulose, hemicellulose and lignin. This way, the pyrolysis reactions for all species occur within a well-defined and almost identical range with pyrolysis reactions occurring from around 300 to 400°C. The TGA results thus justify the use of a pyrolysis temperature independent of wood species, which is commonly assumed to be 300°C [51].

Under the tested conditions the burning behaviour of wood, during exposure to an external heat flux, was found to be more or less independent from the imposed heat flux and if flaming occurred or not. This indicates that within the tested range of 25kW/m^2 to 80 kW/m^2 the charring rate of wood is mainly driven by the external heat flux. Moreover the charring rates were found to be achieving an asymptotic value consistent with literature. These observations justify the use of constant charring rate models, at high heat exposure levels, in the context of structural fire design.

The experiments also showed that the burning behaviour CLT and Glulam products is corresponding quite well to the burning behaviour of solid wood, but only under the condition that no delamination occurs. Specifically for CLT products the failure mode of delamination is occurring well before self-extinguishment even becomes relevant. In order to obtain a sound discussion on the issue of delamination, tests under realistic loading conditions should be conducted[9].

Under no external heat flux it was found that only flaming combustion was able to support significant charring. With significant charring indicated by the temperature profiles which remained increasing within the pyrolysis range. The mass loss rate of glowing samples under no external heat flux did not seem to demonstrate any significant mass loss rate, also the temperature profiles were found to be quickly falling outside of the pyrolysis range. In other words, significant charring will only sustain if also flaming combustion sustains after removal of the heat flux. The critical mass loss rate for flaming combustion under no external heating was found to roughly correspond to 4g/(m^2.s), which is consistent with a range of literature values.

Within the whole tested range of heat fluxes and exposure times, the flames generally quenched within one minute after removal of the heat flux, at least when no delamination occurred. So it can be concluded that wood demonstrates a strong self-extinguishment capacity. Based upon the thermal observations inside the wood element, it is suggested that the thermal conditions obtained near the constantly advancing pyrolysis front are such so that after removal of the heat flux the heat losses are simply too big for any significant self-sustained charring to occur. These observations are also in line with *Tewarson and Pion*[80] and *Petrella*[79] who demonstrated that for several wood species $\dot{Q}_f'' < \dot{Q}_l''$.

The concept of self-extinction might imply that wood elements designed for relatively long standard exposure times are potentially seriously over-dimensioned for what is adequate to meet the performance criteria of preventing structural collapse or fire spread until full burnout. Yet this statement is in need of further supporting evidence. Full scale natural fires test conducted in unprotected and structurally loaded wood compartments need to be further researched.

Moreover also a short example was given in order to demonstrate how further research might explore possibilities to link simple design concepts, such as a critical charring depth, to the concept of self-extinguishment in the context of structural applications.

[9] See *Section 3.4.2* for a more elaborate discussion on delamination.

References

[1] Global Health Observatory, “Urban Population Growth,” 2010. [Online]. Available: http://www.who.int/gho/urban_health/situation_trends/urban_population_growth_text/en/. [Accessed: 05-Sep-2013].

[2] WHO, “Hidden Cities: Unmasking and Overcoming Health Inequities in Urban Settings,” vol. Volume 1: , 2010.

[3] SOM, “Timber Tower Research Project,” vol. Final Report, 2013.

[4] K. Rosenfield, “Michael Green presents: The Case for Tall Wood Buildings,” *Archdaily*, 2012.

[5] Trada, “Stadthaus, 24 Murray Grove, London,” 2009. [Online]. Available: http://eoinc.weebly.com/uploads/3/0/5/1/3051016/murray_grove_case_study.pdf. [Accessed: 21-Feb-2014].

[6] D. Felton, R. Fuller, and R. H. Crawford, “The potential for renewable materials to reduce the embodied energy and associated greenhouse gas emissions of medium-rise buildings,” *Archit. Sci. Rev.*, pp. 1–8, Sep. 2013.

[7] M. Lenzen and G. Treloar, “Embodied energy in buildings: wood versus concrete—reply to Börjesson and Gustavsson,” *Energy Policy*, vol. 30, no. 3, 2002.

[8] J. Köhlen, “Reliability of timber structures,” *Swiss Fed. Inst. Technol. Inst. Struct. Eng.*, no. May, 2007.

[9] Canadian Wood Council, “Mid-rise Construction in British Columbia,” *WoodWorks*, 2011.

[10] S. Thelandersson and D. Honfi, “Behaviour and modelling of timber structures with reference to rubustness,” *Jt. Work. COST Actions TU0601 E55*, vol. Ljubljana,, 2009.

[11] D. Ridley, “A random walk through the forest (or how we guess the strength of wood),” *Napier University*, 2011. [Online]. Available: http://www2.ph.ed.ac.uk/podcasts/Physics/PhysicsGenInt/podcasts.html. [Accessed: 22-Feb-2014].

[12] K. Bryan, “Tall Wood Takes a Stand:Tall wood buildings proven safe and cost effective,” *reThink Wood*, 2012. [Online]. Available: http://continuingeducation.construction.com/article_print.php?L=221&C=960.

[13] I. Smith and A. Frangi, “Overview of Design Issues for Tall Timber Buildings,” *Struct. Eng. Int.*, vol. 18, no. 2, pp. 141–147, May 2008.

[14] The Scottish Building Standards Agency, “International review of fire safety guidance for tall buildings,” no. March, 2007.

[15] SFPE, *Draft Guidelines for Designing Fire Safety in Very Tall Buildings*, Public Rev. Society of Fire Protection Engineers, 2012, p. 154.

[16] B. Östman and B. Källsner, "National building regulations in relation to multi-storey wooden buildings in Europe," no. report 5, pp. 1–26, 2010.

[17] A. H. Buchanan, "Fire performance of timber construction," *Prog. Struct. Eng. Mater.*, vol. 2, no. 3, pp. 278–289, Jul. 2000.

[18] A. Jowsey, "Fire Imposed Heat Fluxes for Structural Analysis," The University of Edinburgh. College of Science and Engineering. School of Engineering and Electronics, 2006.

[19] J. G. Quintiere, *Fundamentals of Fire Phenomena*, University. John Wiley & Sons, Inc., 2006, p. 460.

[20] CEN, *EN 1991-1-2 Eurocode 1 Part 2: Actions on structures exposed to fire*. Brussels, 2002.

[21] T. Tanaka and S. Yamada, "REDUCED SCALE EXPERIMENTS FOR CONVECTIVE HEAT TRANSFER IN THE EARLY STAGE OF FIRES," *Int. J. Eng. Performance-Based Fire Codes*, vol. 1, no. 3, pp. 196–203, 1999.

[22] P. S. Veloo and J. G. Quintiere, "Convective heat transfer coefficient in compartment fires," *J. Fire Sci.*, vol. 31, no. 5, pp. 410–423, Mar. 2013.

[23] A. Jowsey, J. L. Torero, and B. Lane, "The Dalmarnock Fire Tests: Experiments and Modelling, Edited by G. Rein, C. Abecassis Empis and R. Carvel." School of Engineering and Electronics, University of Edinburgh, 14-Nov-2007.

[24] F. P. Incropera and D. P. DeWitt, *Fundametals of Heat and Mass Transfer*. New York: John Wiley & Sons, Inc., 2002.

[25] D. Drysdale, *An introduction to Fire Dynamics*, 3rd Editio. A John Wiley & Sons, Ltd., 2011.

[26] J. Stern-Gottfried, G. Rein, L. A. Bisby, and J. L. Torero, "Experimental review of the homogeneous temperature assumption in post-flashover compartment fires," *Fire Saf. J.*, vol. 45, no. 4, pp. 249–261, Jun. 2010.

[27] J. L. Torero, A. H. Majdalani, C. Abecassis-Empis, and A. Cowlard, "Revisiting the Compartment Fire," *FIRE Saf. Sci. Proc. Elev. Int. Symp.*, p. 18, 2014.

[28] K. Horová, T. Jána, and F. Wald, "Temperature heterogeneity during travelling fire on experimental building," *Adv. Eng. Softw.*, vol. 62–63, pp. 119–130, Aug. 2013.

[29] S. Welch, A. Jowsey, S. Deeny, R. Morgan, and J. L. Torero, "BRE large compartment fire test - characterising post-flashover fires for model validation," *Fire Saf. J.*, no. 42, pp. 548–567, 2007.

[30] G. Rein, C. Abecassis Empis, and R. Carvel, *The Dalmarnock Fire Tests: Experiments and Modelling*. University of Edinburgh, 2007.

[31] A. Frangi and M. Fontana, "Fire Performance Of Timber Structures Under Natural Fire Conditions," *Fire Saf. Sci.*, vol. 8, pp. 279–290, 2005.

[32] V. Babrauskas, "Upholstered Furniture Room Fires--Measurements, Comparison With Furniture Calorimeter Data, and Flashover Predictions," *J. Fire Sci.*, vol. 2, no. 1, pp. 5–19, Jan. 1984.

[33] Z. Chen, "Design fires for motels and hotels," Carelton University, 2008.

[34] A. Frangi, G. Bochicchio, A. Ceccotti, S. M. Alsa, and M. P. Lauriola, "Natural Full-Scale Fire Test on a 3 Storey XLam Timber Building," *Eng. Wood Prod. Assoc.*, 2008.

[35] G. M. E. Cooke, "Tests to determine the behaviour of fully developed natural fires in a large compartment," *BRE, UK*, 1998.

[36] C. Maluk, L. Bisby, G. Terrasi, M. Krajcovic, and J. L. Torero, "Novel Fire Testing Methodology: Why, how and what now?," in *Proceedings of the Mini Symposium on Performance-based Fire Safety Engineering of Structures as part of the 1st International Conference on Performance*, 2012, pp. 448–458.

[37] T. Z. Harmathy and T. T. Lie, "Fire Test Standard in the Light of Fire Research," *ASTM Spec. Tech. Publ. 464*, pp. 85–97, 1970.

[38] K. Ödeen, "Fire Test Standard in the Light of Fire Research," *ASTM Spec. Tech. Publ. 464*, pp. 30–56, 1970.

[39] S. Welch and P. Rubini, "Three-dimensional Simulation of a Fire-Resistance Furnace," *Proc. 5th Int. Symp. Fire Saf. Sci.*, 1997.

[40] M. A. Sultan, "Incident heat flux measurements in floor and wall furnaces of different sizes," *Fire Mater.*, vol. 30, no. 6, pp. 383–396, Nov. 2006.

[41] M. A. Sultan, T. Z. Harmathy, and J. R. Mehaffey, "Heat transmission in fire test furnaces," *Fire Mater.*, vol. 10, no. 2, pp. 47–55, Jun. 1986.

[42] N. Keltner, "What have We Learned about Uncertainty? Are We Still Playing with Fire?," *ASTM J. Test. Eval.*, vol. 40, no. 1, p. 13, 2012.

[43] R. H. White, "Analytical Methods for Determining Fire Resistance of Timber Members," *SFPE Handb. Fire Prot. Eng.*, vol. 3rd Editio, pp. 4–257,4–273, 2008.

[44] F. Kollmann and J. W. Côté, *Principles of wood science and technology*. New York, Springer Verlag;, 1968.

[45] P. Reszka and J. L. Torero, "In-Depth Temperature Measurements of Timber In Fires," *Proc. 4th Int. Work. Struct. Fire*, no. Aveiro, Portugal, pp. 921–930, 2006.

[46] Y. Rogaume, P. D. Moraes, P. Triboulot, and J. F. Bocquet, “Influence of temperature on the embedding strength,” *Holz als Roh- und Werkstoff*, vol. 63, pp. 297–302, 2005.

[47] D. W. Green, J. E. Winandy, and D. E. Kretschmann, “Mechanical Properties of Wood,” in *Wood Handbook - Wood as an engineering material*, U.S. Department of Agriculture, Forest Service, Forest Products Laboratory, 2010, p. 508.

[48] F. L. Browne, “Theories of the combustion of wood and its control: A survey of literature,” *For. Prod. Lab.*, vol. FPL report, 1958.

[49] L. Lowden and T. Hull, “Flammability behaviour of wood and a review of the methods for its reduction,” *Fire Sci. Rev.*, vol. 2, no. 1, p. 4, Sep. 2013.

[50] V. Babrauskas, “Ignition of Wood: a review of the state of the art,” *Interflam 2001*, no. Interscience Communications Ltd., London, pp. 71–88, 2001.

[51] CEN, “EN 1995-1-2:2004 Eurocode 5. Design of timber structures. General. Structural fire design,” 2004.

[52] R. Aseeva, B. Serkov, and A. Sivenkov, *Fire Behavior and Fire Protection in Timber Buildings*. Dordrecht: Springer Netherlands, 2014.

[53] C. Di Blasi, “Modelling and Simulation of Combustion Processes of Charring and Non Charring Solid Fuels,” *Prog. Energy Combust. Sci.*, vol. 19, pp. 71–104, 1993.

[54] L. Shi and M. Y. L. Chew, “A review of fire processes modeling of combustible materials under external heat flux,” *Fuel*, vol. 106, pp. 30–50, Apr. 2013.

[55] C. Di Blasi, “Modeling chemical and physical processes of wood and biomass pyrolysis,” *Prog. Energy Combust. Sci.*, vol. 34, no. 1, pp. 47–90, Feb. 2008.

[56] C. Di Blasi, “Modelling and Simulation of Combustion Processes of Charring and Non Charring Solid Fuels,” *Prog. Energy Combust. Sci.*, vol. 19, pp. 71–104, 1993.

[57] A. G. W. Bradbury, Y. Sakai, and F. Shafizadeh, “A kinetic model for pyrolysis of cellulose,” *J. Appl. Polym. Sci.*, vol. 23, no. 11, pp. 3271–3280, Jun. 1979.

[58] T. Hosoya, H. Kawamoto, and S. Saka, “Pyrolysis behaviors of wood and its constituent polymers at gasification temperature,” *J. Anal. Appl. Pyrolysis*, vol. 78, no. 2, pp. 328–336, Mar. 2007.

[59] G. Várhegyi, M. G. Grønli, and C. Di Blasi, “Effects of Sample Origin, Extraction, and Hot-Water Washing on the Devolatilization Kinetics of Chestnut Wood,” *Ind. Eng. Chem. Res.*, vol. 43, no. 10, pp. 2356–2367, May 2004.

[60] T. Kashiwagi and H. Nambu, “Global Kinetic Constants for Thermal Oxidative Degradation of a Cellulosic Paper,” *Combust. Flame*, vol. 88, no. 3–4, pp. 345–368, 1992.

[61] J. König, “Effective thermal actions and thermal properties of timber members in natural fires,” *Fire Mater.*, vol. 30, no. 1, pp. 51–63, Jan. 2006.

[62] C. H. Bamford, J. Crank, D. H. Malan, and A. H. Wilson, “The combustion of wood. Part I,” *Math. Proc. Cambridge Philos. Soc.*, vol. 42, no. 02, p. 166, Oct. 1946.

[63] S. R. Wasan, P. Rauwoens, J. Vierendeels, and B. Merci, “An enthalpy-based pyrolysis model for charring and non-charring materials in case of fire,” *Combust. Flame*, vol. 157, no. 4, pp. 715–734, Apr. 2010.

[64] M. Janssens, “Fundamental thermophysical characteristics of wood and their role in enclosure fire growth.” Ghent University. Faculty of Engineering, 1991.

[65] A. Atreaya, “Pyrolysis, Ignition and fire spread on horizontal surfaces of Wood,” *Ph. D. Thesis*, vol. Division o, 1983.

[66] W. Parker, “Prediction of the Heat Release Rate of Wood,” *Ph. D. Thesis*, vol. George Was, 1988.

[67] M. . Spearpoint and J. . Quintiere, “Predicting the burning of wood using an integral model,” *Combust. Flame*, vol. 123, no. 3, pp. 308–325, Nov. 2000.

[68] K. Kuan-yun Kuo and R. Acharya, *Fundamentals of Turbulent and Multi-Phase Combustion*. John Wiley & Sons, 2012, p. 864.

[69] R. H. White, “Charring rates of different wood species,” University of Wisconsin-Madison, 1988.

[70] E. L. Schaffer, “Structural Fire Design: Wood,” *U.S. Dep. Agric. For. Serv. For. Prod. Lab.*, p. 16, 1984.

[71] E. L. Schaffer, *Review of information related to the charring rate of wood*. Forest Products Laboratory, 1966, p. 55.

[72] G. S. Hall and Timber Research and Development Association (High Wycombe), *Fire Performance of Timber: A Literature Survey*. Timber Research and Development Association, 1976.

[73] K. L. Friquin, “Material properties and external factors influencing the charring rate of solid wood and glue-laminated timber,” *Fire Mater.*, vol. 35, no. 5, pp. 303–327, Aug. 2011.

[74] L. Shi and M. Y. L. Chew, “Experimental study of woods under external heat flux by autoignition,” *J. Therm. Anal. Calorim.*, vol. 111, no. 2, pp. 1399–1407, Jun. 2012.

[75] J. Vessby, B. Enquist, H. Petersson, and T. Alsmarker, “Experimental study of cross-laminated timber wall panels,” *Eur. J. Wood Wood Prod.*, vol. 67, pp. 211–218, 2009.

[76] S. T. Craft, R. Desjardins, and J. R. Mehaffey, “Investigation of the behaviour of clt panels exposed to fire,” in *Conference Proceedings - Fire and Materials 2011, 12th International Conference and Exhibition*, 2011, pp. 441–454.

[77] A. Frangi, M. Fontana, E. Hugi, and R. Jübstl, “Experimental analysis of cross-laminated timber panels in fire,” *Fire Saf. J.*, vol. 44, pp. 1078–1087, 2009.

[78] C. J. McGregor, “CONTRIBUTION OF CROSS LAMINATED TIMBER PANELS TO ROOM FIRES,” Carleton University, 2013.

[79] R. V. Petrella, “The Mass Burning Rate and Mass Transfer Number of Selected Polymers, Wood, and Organic Liquids,” *Polym. Plast. Technol. Eng.*, vol. 13, no. 1, pp. 83–103, Jan. 1979.

[80] A. Tewarson and R. F. Pion, “Flammability of plastics—I. Burning intensity,” *Combust. Flame*, vol. 26, pp. 85–103, Feb. 1976.

[81] M. A. Delichatsios, M. Gummala, and D. G. Vlachos, “Extinction in solid fuel combustion: Part II Detailed model,” *Fire Saf. J.*, vol. 56, pp. 1–8, Feb. 2013.

[82] C. Law, “Asymptotic theory of ignition and extinction in droplet burning,” *Combust. Flame*, vol. 24, pp. 89–98, 1975.

[83] C. Beyler, “A Unified Model of Fire Suppression,” *J. Fire Prot. Eng.*, vol. 4, pp. 5–16, 1992.

[84] M. . DELICHATSIOS, “Critical Mass Pyrolysis Rates for Extinction of Fires over Solid Materials,” *FIRE Saf. Sci. Proc. FIFTH Int. Symp.*, pp. 153–164, 1996.

[85] D. B. Spalding, “The combustion of liquid fuels,” *4th Symp. Combust.*, pp. 847–864, 1953.

[86] A. Rangwala, “Flame Spread Analysis Using a Variable B-Number,” *Fire Saf. Sci.*, vol. 9, pp. 243–254, 2008.

[87] M. A. Delichatsios, “Piloted ignition times, critical heat fluxes and mass loss rates at reduced oxygen atmospheres,” *Fire Saf. J.*, vol. 40, no. 3, pp. 197–212, Apr. 2005.

[88] D. Rich, C. Lautenberger, J. L. Torero, J. G. Quintiere, and C. Fernandez-Pello, “Mass flux of combustible solids at piloted ignition,” *Proc. Combust. Inst.*, vol. 31 II, pp. 2653–2660, 2007.

[89] A. N. Koohyar, J. R. Welker, and C. M. Sliepcevich, “The irradiation and ignition of wood by flame,” *Fire Technol.*, vol. 4, no. 4, pp. 284–291, Nov. 1968.

[90] D. J. Rasbash, D. D. Drysdale, and D. Deepak, “Critical heat and mass transfer at pilot ignition and extinction of a material,” *Fire Saf. J.*, vol. 10, no. 1, pp. 1–10, Jan. 1986.

[91] M. A. Delichatsios, “Piloted ignition times, critical heat fluxes and mass loss rates at reduced oxygen atmospheres,” *Fire Saf. J.*, vol. 40, no. 3, pp. 197–212, Apr. 2005.

[92] S. McAllister, M. Finney, and J. Cohen, “Critical mass flux for flaming ignition of wood as a function of external radiant heat flux and moisture content,” *7th US Natl. Tech. Meet. Combust. Inst.*, 2011.

[93] C. Beyler and M. Hirschler, “Thermal Decomposition of Polymers,” in *SFPE Handbook of Fire Protection Engineering, 3rd Edition*, 2008, pp. 1–110;1–131.

[94] T. J. Ohlemiller, “Smoldering Combustion,” in *SFPE Handbook of Fire Protection Engineering, 3rd Edition*, 2008, pp. 2–200;2–209.

[95] R. J. McCarter, “Smoldering Combustion of Cotton and Rayon,” *J. Cons. Prod. Flamm.*, vol. 4, p. 346, 1977.

[96] P. Reszka, “In-Depth Temperature Profiles in Pyrolyzing Wood,” The University of Edinburgh, 2008.

[97] J. P. Hidalgo-Medina, “CALORIMETRY CORRELATIONS,” *PhD Proj. “The role Therm. Insul. Prod. fire Behav. energy Effic. Build. – fire growth smoke movement,”* vol. Draft v.3, 2014.

[98] H. Yang, R. Yan, H. Chen, D. H. Lee, and C. Zheng, “Characteristics of hemicellulose, cellulose and lignin pyrolysis,” *Fuel*, vol. 86, no. 12–13, pp. 1781–1788, Aug. 2007.

[99] A. Buchanan and D. Barber, “Fire resistance of epoxied steel rods in glulam timber,” *timberdesign.org.nz*.

[100] R. L. Santos, “The Eucalyptus of California, Section Three: Problems, Cares, Economics, and Species,” 1997. [Online]. Available: http://ivy.csustan.edu/bsantos/section3.htm. [Accessed: 17-Apr-2014].

[101] C. R. Frihart and C. G. Hunt, “Adhesives with Wood Materials, Bond Formation and Performance,” in *Wood Handbook: Wood as an Engineering Material*, FPL-GTR-19th ed., 2010.

Annex A: Structural Fire Resistance Calculations

Delivered in separate document

Annex B: Thermal behaviour and characteristic heating times of a block of wood

Delivered in separate document

Annex C: MLC Test Results

Delivered in separate document

Annex D: Thermal Properties of wood

Delivered in separate document